Morphological Development of the German Wadden Sea from 1996 to 2009 Determined with the Waterline Method and SAR and Landsat Satellite Images

Dissertation zur Erlangung des akademischen Grades

Doktor der Naturwissenschaften (Dr. rer. nat.)

vorgelegt dem Fachbereich 1 Physik der Universität Bremen

Zhen Li

geb. in Qingdao, China

Erstgutachter : Prof. Dr. Justus Notholt

Zweitgutachter: PD Dr. Christian Winter

Datum der Abgabe: 17. 06. 2014

1st Reviewer: Prof. Dr. Justus Notholt,
Institute of Environmental Physics, Universität Bremen

2nd Reviewer: PD Dr. Christian Winter,
Center for Marine Environmental Sciences, Universität Bremen

Anlage zur Dissertation

Eidesstattliche Erklärung

(Gem. § 6(5) Nr. 1-3 PromO)

Hiermit versichere ich, dass ich

1) die vorliegende Arbeit ohne unerlaubte, fremde Hilfe angefertigt habe
2) keine anderen, als die von mir im Text angegebenen Quellen und Hilfsmittel benutzt habe
3) die den benutzen Werken wörtlich oder inhaltlich entnommenen Stellen als solche kenntlich gemacht habe.

Bremen, 17. June, 2014

_____

Zhen Li

Abstract

The Dutch, German, and Danish Wadden Sea contains some of the largest undisturbed tidal flats in the world of about 10,000 km^2. The research areas covered in this thesis are the North Frisian, Neuwerk, and Cuxhaven regions of the German Wadden Sea. The goal of the thesis is to use the waterline method with SAR and optical images to derive topographic maps in order to analyze the morphological development of this valuable ecological system on large spatial and engineering time scales (90 km and 14 years). Compared to earlier applications, the method is improved with respect to the geocoding step and the data coverage of the complete tidal range. The results also allow analyzing smaller scale's developmental details, such as sandbars and estuaries. Topographical maps from 1996 to 1999, and 2004 to 2009 were generated. The largest morphological differences occurred between 2009 and 1996, also observed in the -2 m isobaths map. The Bed Elevation Range of the tidal flats includes all the elevation information from 1996 to 2009 in order to identify the maximum changes during the investigation period. It shows high morphodynamic regions are outer parts of the tidal flat, sandbars, and estuaries. Vertical nodal linear regression gives the direction of the morphological development (erosion or sedimentation). Our result shows that the rate of change is mostly between -0.1 to 0.1 m/yr. Extreme erosion rate reaches over -0.3 m/yr, while extreme sedimentation rate is up to 0.36 m/yr. The absolute amount of elevation change called turnover height has a growth rate of 8.2 mm/yr, indicating the growing morphodynamic activity over the investigation period. The net balance height of the whole investigation region shows an increasing trend of 6.8 mm/yr, demonstrating an overall sedimentation. According to large-scale analyses, the most dynamic areas are the sandbars. Tertiussand, D-Steert, Gelbsand, and Medemgrund/Medemsand are given detailed discussion in this thesis. The west side of the sandbars except for Medemgrund/Medemsand face the high wave and tidal energy arriving from the open North sea, and cause large erosion towards east, while Medemgrund/Medemsand located in the Elbe estuary show migration in the opposite direction. The three cross sections of Tertiussand, Gelbsand and Medemgrund all show clearly increasing elevation if comparing the average elevation over the years 1996-1999 and 2004-2009. Since the areas of Tertiussand and Gelbsand decreased, their increased elevation might relate to internal sediment redistribution. Medemgrund increasead in area, so its increased elevation could be compensated by the adjacent tidal flat Medemsand which has significant erosion towards the north and the sediment brought from Elbe River.

Keywords: SAR, waterline, morphological development, German Wadden Sea, topographic map

Contents

Chapter 1 Introduction

1.1 Overview of the German Tidal Flat, Wadden Sea

The Wadden Sea is located in the south eastern part of the North Sea. It extends from Den Helder (Denmark), through the German Bight to the Dutch coast; it stretches over 450 km, and reaches a width of up to 25 km along the German coast (Zeiler et al., 2008). The total area is about 10,000 km^2 (Figure 1.1). The Wadden Sea has the largest unbroken tidal flat system. Despite the man-made interventions, its natural processes support a whole range of habitats and ensure the maintenance of the ecosystem. UNESO (United Nations Educational, Scientific and Cultural Organization) inscribed it into the world heritage sites in 2009 (UNESO world heritage list, http://whc.unesco.org/en/list/1314) for its outstanding geomorphological and ecological values.

The Wadden Sea area formed during the post glacial period. It is a relatively young ecosystem on the geomorphological and evolutionary scale, being about 8000 years old. The genesis differs from the North to the South (Kohlus, 1998). It features many unique dynamics: its ecosystem is composed of tidal flats and a barrier island system with extensive salt marshes. It is part on an intertidal region with minor river influences which enhance its morphdynamics. The unique properties of the Wadden Sea tidal flats are that they are the only tidal flats and barrier island depositional system of this scale and diversity in the world; as well, they also are one of the last remaining large-scale intertidal ecosystems in Europe with functional natural processes.

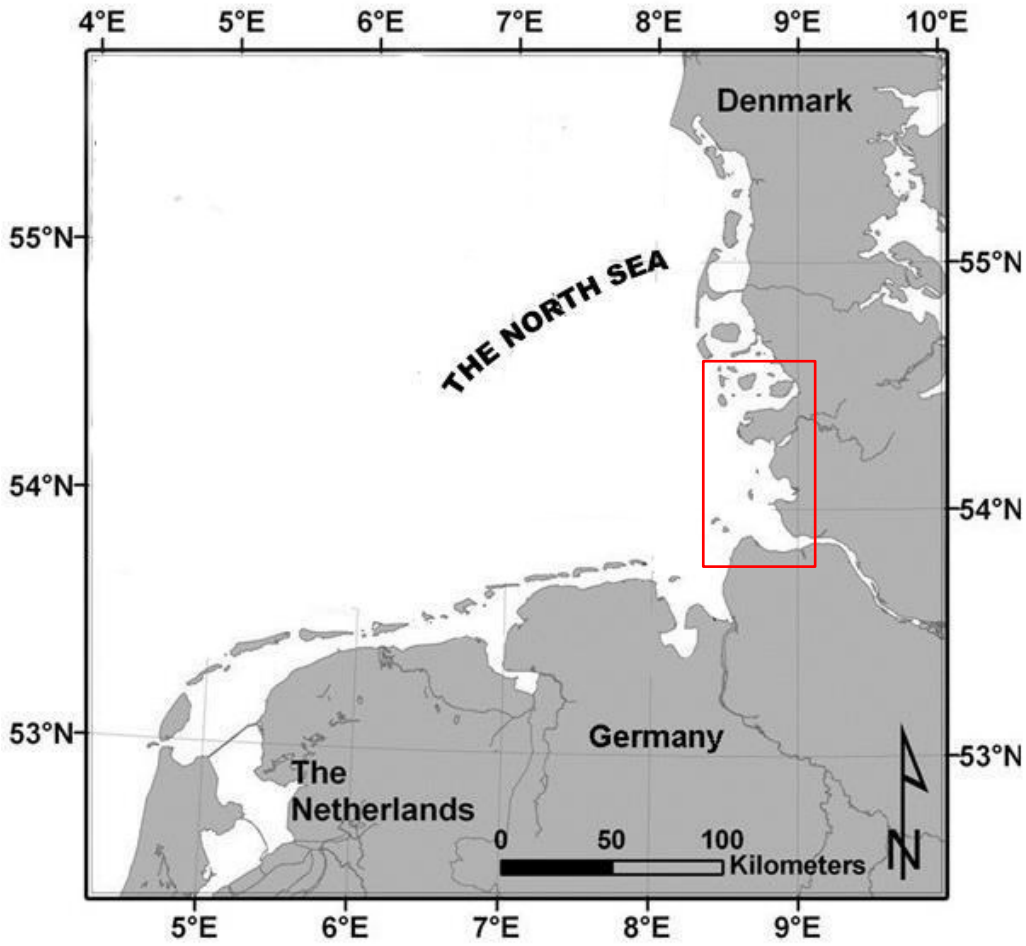

Figure 1.1: Wadden Sea (Chu et al., 2013) (Research area marked with red frame).

1.2 Tidal Flat and Oceanographic System

Tidal flats, also known as mud flats, are coastal wetlands that form when mud is deposited by tides or rivers. They can often be found in bays, bayous, lagoons, and estuaries (http://en.wikipedia.org/wiki/Mudflat). It is a transitional environment between land and sea with constantly changing water from floods and ebb tides. The Wadden Sea tidal flat submerges and exposes approximately twice a day (Figure 1.2 intertidal area). The sediment body thickness of the tidal flat can reach about 40m (Ahrendt, 2006).

The development of the tidal flat Wadden Sea is constantly changing. All kinds of developmental phases can be found in this area. The tidal flat of the Wadden Sea supports a large variety of plants and animals which grow, live, breed, molt and rest throughout its area, and is especially important to migrating birds – up to 12 million birds use this region every year. The Wadden Sea is a very valuable ecological system and it needs to be protected. The maintenance of tidal flats is also important for preventing coastal erosion. However, tidal flats are under risk by rising sea levels, land claiming, dredging, and pollution. Accurate monitoring is fundamental to protect their systems, and is required for a variety of purposes such as salt marshe protection, shipping, fishing, tourism and emergencies.

The North Sea is a shallow shelf with a wide-open northern boundary to the Northeast Atlantic Ocean. The geomorphological processes in the Wadden Sea are almost exclusively associated with flowing water. North Sea currents are composed of semi-diurnal tidal currents, as well as wind-driven and density-driven currents (Klein and Frohse, 2008). The ebb and flood currents in the open North Sea occur in almost the opposite directions. The ebb current flows northwest, and the flood current flows southeast. The residual currents are determined by averaging one or more tidal periods (12.5 hours). They measure the net transport of an individual water particle at a particular point within the observational period. They aslo represents the current circulation pattern. The German Bight has nine typical

circulation patterns. They are reproduced by the operational circulation model 'BSHcmod' of the German Federal Maritime and Hydrographic Agency (BSH, Bundesamt fuer Seeschifffahrt und Hydrographie, German Federal Maritime and Hydrographic Agency). The dominating patterns are cyclonic (anti-clockwise, 43%) and anti-cyclonic (13%) (Figure 1.3a, b). The other six types (Figure 1.3c) are mostly related to strong wind events with a minor overall importance (Klein and Frohse, 2008). In addition to the tidal currents, the wind-dependent 'drift currents' (Goehren, 1968) are quite important in coastal areas. The drift currents are influenced by water depth and wind speed, and are more pronounced as water depth decreases. They move considerable amounts of water and sediment through the tidal flats (Ehlers, 1988).

The development of sediments and geomorphological development (morphodynamics) is ruled by waves and tides. Phases of storm induced high water levels often lead to severe changes of the coastal geomorphological environment within a short term of time. A storm surge can be defined as a "period of time during which water levels on the coasts and in estuaries are high, due primarily to strong winds" (Petersen and Rohde, 1977). These extreme events have strong effect on morphological development within one tidal cycle.

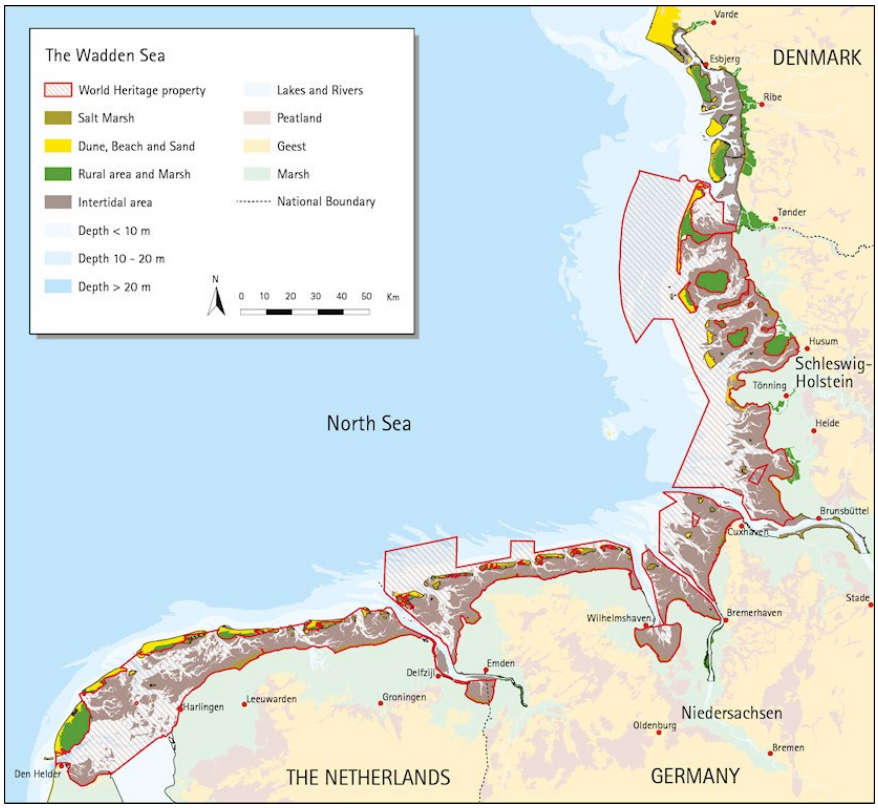

Figure 1.2: Tidal flat of the Wadden Sea (marked as grey color) (Wadden Sea World Heritage Site).

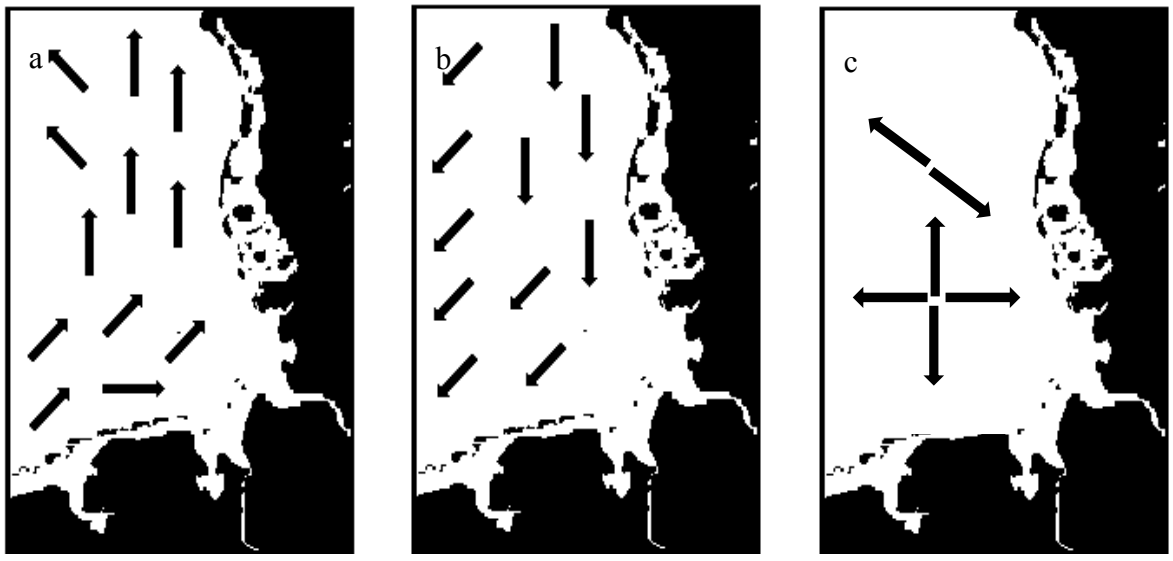

Figure 1.3: Daily averaged residual currents of the upper model layer, circulation pattern (BSH). a) cyclonic pattern, b) anti-cyclonic pattern, c) other less important patterns.

1.3 Historical development of Wadden Sea area

In order to understand the changing of the landscape it is necessary to have some knowledge of the historical development of Wadden Sea area.

Trade started to have a major role in the Wadden Sea area during the early middle ages. Fishing and whaling started from about 1425 and 1610 respectively. Commercial shipping played a major role in the islands. Later on, first tourism business began at Norderney in 1797. The development of tourism industry led to the construction of coastal protection. Both of them had a great impact on the morphological development of the islands. After the Second World War, tourism began anew. The explosion of the tourism brought an expanding economy and population growth. However, it also had a negative impact on the state of the natural resources (Ehlers, 1988).

The first Government Conference on the Protection of the Wadden Sea was held in 1978 in the Hague, Netherlands. The trilateral cooperation was established at the third conference in Copenhagen, and included three countries: Denmark, Germany and the Netherlands. The cooperation covered all kinds of areas such as landscape and culture, water and sediments, tidal areas, salt marshes, estuaries etc. Three ‘Reference area’ were introduced in 1991 (Marencic Ed., 2009), designated as ‘sufficiently large areas, spread evenly over the Wadden Sea, where all exploitation and all disturbing activities were banned and which can serve as reference areas for scientific purposes’ (Esbjerg Declaration, 1991). They were able to serve monitoring and research undertaking in the Wadden Sea (Figure 1.4).

Figure 1.4: Reference areas in the Wadden Sea (Marencic H. (Ed.), 2009).

1.4 Overview of the Research

1.4.1 Existing Methods

Topographic maps of the tidal flats in the Wadden Sea are the fundamental data bases used to monitor and manage the tidal flats area. There are several methods to measure the topography of the tidal flats in the Wadden Sea, and range from classical ways to modern surveying methods. Below is a brief summary of the methods.

Classical land surveying methods:

This is the oldest way to derive topographic maps. Observers record data with ground-based equipment. The accuracy of this method is up to centimeters, but it cannot be done regularly every year, and is not suitable for tidal flats due to the expensive cost and inaccessibility of flooded areas and estuaries.

Hydrographic survey:

The BSH carries a regular hydrographic survey for the German North Sea and Baltic Sea. The definition of the hydrographic survey is topographic mapping of the sea bottom and tidal mudflats as well as the determination of the positions of stationary objects at sea, both above and below the water surface. It uses single beam echosounders operating at a frequency of 210 kHz (Figure 1.5). The error range is up to 20 cm, which is satisfactory for most of the applications. However, only the water channels are covered by frequent surveys. It takes up to six or more years to complete the whole Wadden Sea survey (Figure 1.6), and only navigable areas can be measured.

Airborne survey:

Airborne technology makes possible the accurate surveying of large areas. It can also access tidal flats located in low water levels, which cannot traditionaly be covered by classic land or hydrographic survey (WSA Cuxhaven, 2002; Brzank et al., 2008). However, the high operating and associated cost of airborne surveys make it difficult to apply this method on a regular, long term basis.

Remote sensing method:

It will be explained in detail in Chapter 1.4.2.

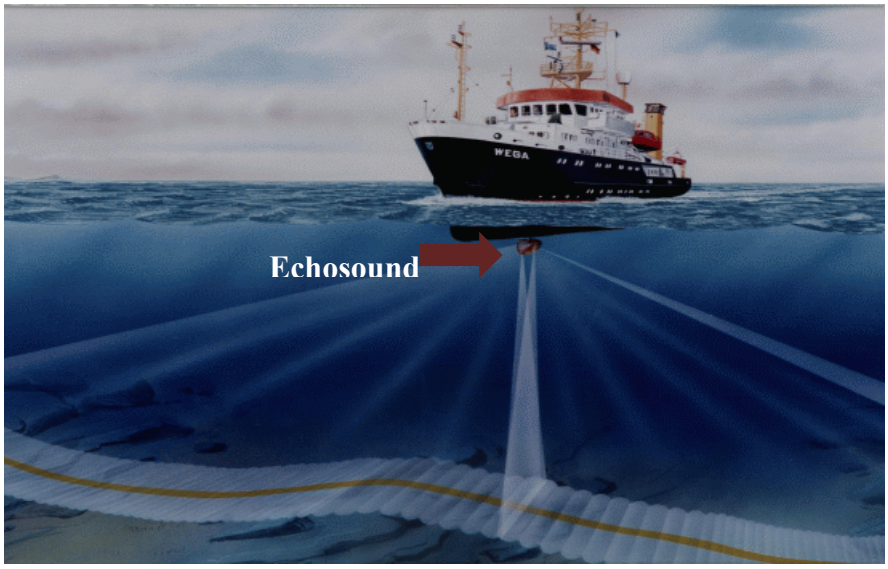

Figure 1.5: Illustration of hydrographic survey (BSH).

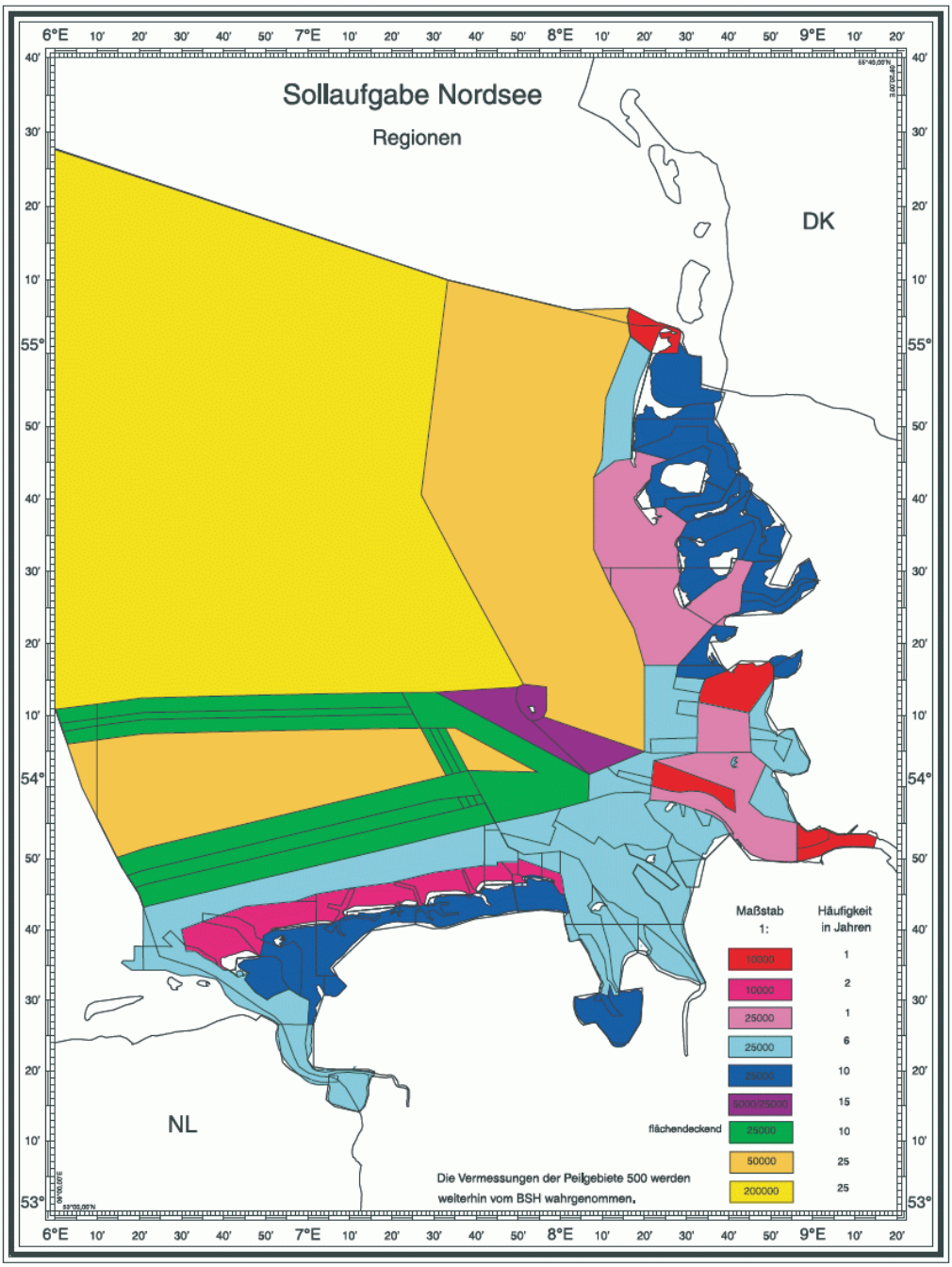

Figure 1.6: The survey areas, survey intervals and survey scales (BSH).

1.4.2 State of the Art and Research Goals

First tests of the waterline method to derive the topographic maps of the tidal flats were concluded in 1990s' (Wang and Koopmans, 1993, 1995). This method measured the height of the tidal flats by using aerial photos and water level data. The water line method was composed of several parts. First, the remote sensing images were acquired during different stages of the tidal cycle. After the ever-shifting border between the tidal flats and adjacent water parts (water lines) were detected, they were assigned water level data at the time of image captured. The water lines from all acquired images composed the data basis for the topography of the tidal flat. The missing points of the topographic map were generated by interpolation based on the water line points. However, the first test failed due to the limited aerial photos and the changing tidal water during one flight mission (Zee, 1980). Afterward, Wang and Koopmans (1993) established the working procedure for water line method with spectral Landsat data, but the lack of cloudless images available to represent different tidal stages was still a problem.

Synthetic Aperture Radar (SAR) images taken from space are independent of daylight and capable for all weather conditions. However, waterlines extraction suffers from speckle noise and wind roughened, wave modulated sea. The lack of contrast makes waterline detection difficult when used with the former method due to gray level threshold and segmentation by edge magnitude. Lee (1980, 1981, 1983) developed an algorithm to effectively reduce the adaptive speckle noise of SAR images, and applied it to coastline detection of SAR images in 1990 (Lee, 1990). A case study was performed on the Western Wadden Sea, the Netherlands (Wang and Koopmans, 1995). This method was also used to monitor the flood on 30th January, 1995 in the Netherlands (Wang and Koopmans, 1995).

The researches above were mainly testing their researches through the case study method. Mason et al. (1995, 1996) applied the waterline method to construct an inter-tidal digital elevation model (DEM). A case study used to generate topographic map with this method was derived on the Western Wash (Mason et al.,

1997). The application for sediment volume measurement (Mason et al., 1999) and morphological change (Mason et al., 2010) were then successfully applied. Later on, an on-screen digitization method to extract waterlines in order to construct tidal flat digital elevation models with MODIS and medium resolution satellite images has been suggested (Liu et al., 2012 and 2013). All of these studies helped to develop the waterline method into a reliable operational approach to generate topographic map of tidal flats.

In addition to SAR images, other sensors such as Light Detection and Ranging (LiDAR) and airborne radar interferometry (InSAR) are also used to retrieve topographic maps for tidal flat with very high horizontal (1 to 2 m) and vertical resolutions (20 cm) (Flood et al., 1997; Stockdon et al., 2002; Deronde et al., 2006; Wimmer et al., 2000; Brzank et al., 2008). While the high entrance fee limits them to small region and temporary observation, they may be well suited to validate results of the water line method.

There were a few attempts to get topographic maps of the tidal flats in the Wadden Sea (Niedermeier et al., 2000 and 2005; Wimmer et al., 2000; Brzank et al., 2008), but the researches were mainly focused on relatively small regions, and there were no long-time series morphological development studies based on satellite data done to date.

Heygster et al. (2010) established an operational waterline method and applied it over the German Wadden Sea (North Frisian and Cuxhaven, Neuwerk area). They managed to generate the topographic maps from 1996 to 1999. Our research is based on their research and has the following goals:

1. Improve the waterline method (Heygster et al., 2010) to derive topographic maps of tidal flats in the German Wadden Sea;
2. Extend the data coverage by adding Envisat ASAR and Landsat TM5 datasets, and extend the former study until 2009 (1996 to 1999, 2004 to 2009);
3. Focus on the study of its morphological development and morphodynamics of

the German Wadden Sea at decade timescale (14 years). This study enables to analyze the tidal flats at larger spatial scale and smaller local spatial scale.

4. Build up data bases for monitoring the tidal flat topography.

Chapter 2 Data Sources

There are four different datasets used in current thesis. They are SAR (Synthetic Aperture Radar) images, Landsat 5 TM images, water level model data and gauge data.

2.1 SAR (Synthetic Aperture Radar) Images

Synthetic Aperture Radar (SAR) is formed as advanced side-looking airborne radar. Radar is an active system that transmits a beam of electromagnetic radiation in the microwave region of the EM spectrum and measures the signal scattered back by the target. This instrument extends our ability to observe properties of the earth's surface that previously were not detectable. SAR overcomes the limit of conventional beam scanning instruments, which is poor spatial resolution. SAR is an instrument with capabilities of all-weather, independent on solar illumination, generally unaffected by cloud and fine resolution. These make SAR an ideal remote sensing instrument for many applications in target detection mapping, as well as the earth resources management, especially suitable for oceanic observations due to the large scale geography and always changing subjects. The first civilian SAR satellite was launched in 1978 as SEASAT, and operated for 106 days until 10 October 1978, when a massive short circuit in the satellite's electrical system ended the mission. Since then Canada, Europe, Japan and Russia have launched SAR satellites. They provide rich information on diverse ocean phenomena such as surface waves, currents, shoals, sea ice, wind, rainfall and the anthropogenic influence on nature.

2.1.1 SAR History

Fine resolution remote sensing images of the earth surface were first achieved by National Aeronautics and Space Administration (NASA) for military purposes in the 1960s. They were made by passive radiometers and recorded the electromagnetic energy in the visible or infrared spectra. Optical images with 10s of meters resolution were produced. These radiometers provided fine spatial and spectral resolution, but they were limited by cloud and darkness. Only during the cloudless day time, the good quality images could have been provided. In order to solve this problem, microwave sensors which were able to penetrate cloud were introduced. However, it was impossible for passive radiometer to get the same fine resolution images by the instrument operating at visible or infrared wavelength. The 10s of meters resolution at visible or infrared wavelength can be achieved by a camera aperture of a few 10s of centimeters on the satellite. The angular resolution of an optical system is proportional to wavelength and inversely proportional to aperture dimension ($R = \lambda/D$). When the wavelength increases from visible and infrared to microwave, in order to get the same resolution, the antenna apertures have to increase proportional to the wavelength. That leads to the order of 10s of kilometers of an antenna aperture dimension on a satellite, which is impossible.

SAR was developed to overcome this problem. Radar beam is directed orthogonal to its moving direction. It can be considered as a long antenna synthesized by combining reflected signals from one object. Thus, it equals to a huge antenna aperture. The synthesized aperture enables to produce images with a few meters resolution.

Evolution started from 90s and Europe launched ERS-1/2 in the 90s. Table 2.1 shows the highlights of the SAR history. Table 2.2 gives a list of SAR sensors on satellites. Carl A. Wiley of Goodyear Aircraft Corp. invented the use of Doppler frequency analysis as applied to coherent moving radar in June 1951 (Wiley, 1954). He concluded that a frequency analysis of the reflected signals from the target could allow better along track resolution than that permitted by the actual physical antenna

beam itself. It was called ‘Doppler beam-sharpening’, which is the origin of synthetic aperture radar as known today. This concept was studied independently by Goodyear and a group at the University of Illinois directed by C. W. Sherwin. In 1952, The Illinois group demonstrated the concept with an X-band pulsed radar fixed on an airborne. After the first demonstration, Project Wolverine was established with University of Michigan (Cutrona et al., 1961). They developed operational airborne SAR system. In the following years, there were other activities which advanced the development of early SAR system (Table 2.1). In 1974, Jet Propulsion Laboratory (JPL) formed an alliance with National Oceanic and Atmospheric Administration (NOAA) to determine if an ocean application SAR satellite could be established. Until that time, the major satellite remote sensing was on land applications using visible and infrared sensors. First SAR satellite SEASAT was launched in 1978. There were more SAR satellites launched afterward with more advanced features (Table 2.1 and Table 2.2) (Curlander et al., 1991). After launch of Envisat in 2002, Cosmo-SkyMed and TerraSAR-X with X-band were launched in 2007 and SeoSAR was expected launched in 2013. They can produce SAR images with 1m resolution.

Table 2.1: Highlights of SAR History (McCandless and Jackson, 2004).

Date	Development
1951	Carl Wiley of Goodyear postulates the Doppler beam-sharpening concept.
1952	University of Illinois demonstrates the beam-sharpening concept.
1957	University of Michigan produces the first SAR imagery using an optical correlator.
1964	Analog electronic SAR correlation demonstrated in non-real time (University of Michigan).
1969	Digital electronic SAR correlation demonstrated in non-real time (Hughes, Goodyear, Westinghouse).
1972	Real-time digital SAR demonstrated with motion compensation (for aircraft system).
1978	First space-borne SAR NASA/JPL SEASAT satellite. Analog downlink; optical and non-real-time digital processing.
1981	Shuttle Imaging Radar series starts – SIR-A. Non-real-time optical processing on ground.
1984	SIR-B. Digital downlink; non-real-time digital processing on ground.
1986	Space-borne SAR Real-time processing demonstration using JPL Advanced Digital SAR processor (ADSP).
1987	Soviet 1870 SAR is placed in earth orbit.
1990	Magellan SAR images Venus.
1990	Evolution of SAR begins in space; Soviet ALMAZ (1991), European ERS-1 (1991), Japanese JERS-1 (1992), SIR-C (1994), ERS-2 (1995), Canadian RADARSAT-1 (1995).
2000	SRTM (2000), ENVISAT(2002), COSMO-SkyMed (2007), Radarsat-2 (2007), TerraSAR-X (2007), TanDEM-X (2010), Sentinel (2014).

Table 2.2: Characteristics of some Earth orbital SAR systems (McCandless and Jackson, 2004). *Based on 0.1 μs uncoded pulse length.

Satellite	Country	Year	Band	Frequency (GHz)	Wavelength (cm)	Incident Angle (deg)	Polarization	Pluse Bandwith (MHz)/(Range Resolution(m))	Azimuth Resolution (m) / (Looks)
SEASAT	USA	1978	L-band	1.275	23.5	23	HH	19 / (7.9)	6 / (1)
SIR-A	USA	1981	L-band	1.275	23.5	50	HH	6 / (24.9)	6.5 / (1)
SIR-B	USA	1984	L-band	1.275	23.5	15-65	HH	12 / (12.5)	6 / (1)
ERS-1/2	Europe	1991/95	C-band	5.25	5.7	23	VV	15.5 / (9.7)	25 / (3)
ALMAZ	USSR	1991	S-band	3.0	10	30-60	HH	- / 15*	15 / (2)
JERS-1	Japan	1992	L-band	1.275	23.5	39	HH	15 / (10)	30 / (4)
SIR-C / X-SAR	USA Germany	1994	L-band C-band X-band	1.25 5.3 9.6	23.5 5.7 3	15 - 55 15 - 55 54	HH, HV, VH, VV VV	10 / (15) 20 / (7.5)	7.5 / (1) 6 / (1)
RADASAT-1	Canada	1995	C-band	5.3	5.7	20 - 50	HH	11.6 / (12.9) 17.3 / (8.6) 30 / (5)	28 / (4) 50 / (2-4) 100 / (4-8)
SRTM	USA Germany	2000	C-band X-band	5.25 9.6	5.7 3	54 54	HH, VV VV	20 / (7.5) 8 / (18.7)	15 / (1) 8-12 / (1)
ENVISAT	Europe	2002	C-band	5.25	5.7	15 - 45	HH, HV, VH, VV	9 / (16.6)	6 / (1) 150 / (12) 1000 / (18-21)

2.1.2 SAR Theory

Figure 2.1 is the simplified illustration of SAR geometry. Radar is carried by a spacecraft moving at a constant altitude (satellite orbital path). The radar beam is directed perpendicular to the flight path. η is the incidence angle, which is the same as pointing looking angle γ. The incidence angle η is the angle between the radar beam and the normal of the specific point on the ground. The ground swath width is the range extent of the radar beam. The radar illuminates an area by transmitting a coherent pulse of microwave frequency. The pulses are reflected from the illuminated area and collected by the radar. The distance between the radar and the illuminated object is calculated, it is called as slant range (Figure 2.1). The spatial resolution contains two directions. One is the range direction (range resolution); the other is the azimuth direction (azimuth resolution) (Figure 2.1). The range resolution is the minimum range separation of two points that can be distinguished as separate by the system (Curlander et al., 1991). The range resolution is defined as

$$\delta_R = \frac{c}{2\beta} \ ,$$

β is the pulse bandwidth, c is the light speed (McCandless and Jackson, 2004). This range resolution can be arbitrarily fine (with practical limits) by increasing the pulse bandwidth.

All radar systems solve targets in the range dimension in the same way. The azimuth resolution distinguishes SAR from other radar system. Assume the length of the radar antenna is L_a along the azimuth direction. The radar beam has an angular spread in that dimension, $\theta_H = \lambda/L_a$, where λ is the wavelength of the transmitted pulse. The azimuth resolution $\delta_{AT} = R\lambda/L_a$, R is the slant range (Curlander et al., 1991). For conventional side-looking aperture radar (SLAR), there are three ways to have fine azimuth resolution. First is to increase the frequency (reduce the wavelength); second is to increase the along track antenna length; the last one is to decrease the slant range. However, none of these options can be used in the space. Therefore, the Synthetic Aperture Radar (SAR) was developed.

A SAR takes advantage of the Doppler history of the radar echoes generated by the forward motion of the spacecraft to synthesize a large antenna. This enables high azimuthal resolution image despite a physically small antenna. The SAR antenna transmits hundreds of pulses and collects all backscattered responses while its spacecraft passes over an object. The distance between the positions where the SAR sees the object for the first and the last time is the synthetic aperture. This means synthetic aperture equals to the distance SAR traveled while object is in view (Figure 2.2). All the backscattered responses collected during this period are manipulated into the resulting image. For example, the spacecraft moves four km when the object is still in the view, which means that the radar antenna can be synthesized into a four km long antenna.

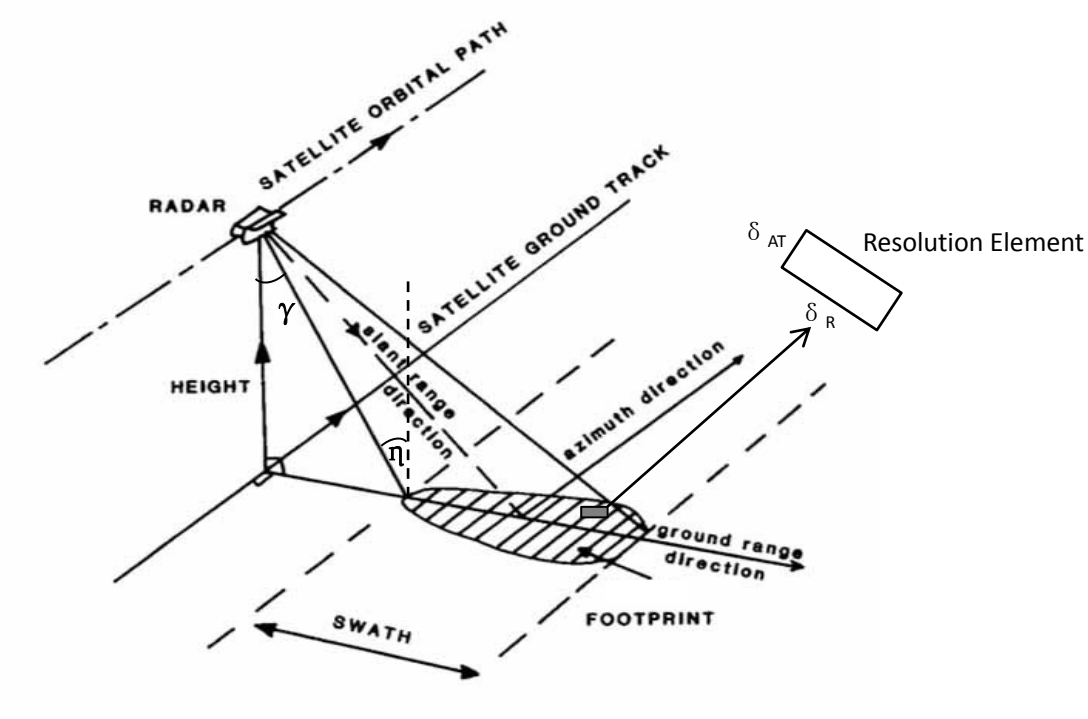

Figure 2.1: SAR Geometry (modified from https://www.eeb.ucla.edu/test/faculty/nezlin/RemoteSensingOfTheSea.htm).

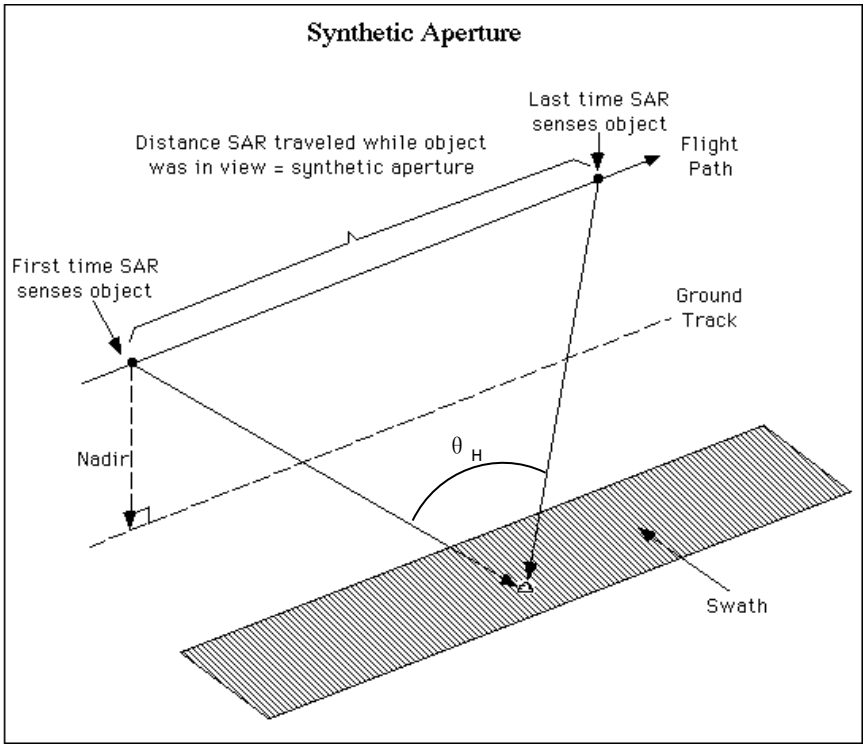

Figure 2.2: Synthetic Aperture
(http://www.eosnap.com/earth-observation/asar-image-orthorectification/).

Along with the high resolution image, noise is inevitable. Speckle is in general considered as a noise-like characteristic produced by a coherent system such as SAR. The coherent interference between the objects is the basis for the speckle in the SAR images. Speckle is assumed as a random multiplicative noise, caused by the interference of electromagnetic waves scattered from surfaces or objects and appears itself conspicuously bright or dark. When transforming SAR signals into imagery, multi-look processing is applied to reduce the speckle noise. Multi-look processing generates SAR images by averaging over the range and azimuth resolution cells. It reduces the speckle noise, but some important information is also deemed in this process. The remaining speckle can be reduced further by filtering. However, unlike system noise, speckle is a real electromagnetic measurement with useful information, which can also be studied in SAR interferometry (InSAR).

There are various applications supported by SAR. SAR was used for military purpose at the beginning and further on developed exponentially for scientific usage,

mostly focusing on oceans and ice monitoring. Nowadays, the SAR applications cover not only scientific purpose, but also commercial intents. The applications include measurements of ocean surface features (currents, fronts, eddies, internal waves), directional ocean wave spectra, sea floor topography, snow cover and ice sheet dynamics. Operational systems have been developed for mapping sea ice, oil slick monitoring and ship detection. The aim of our research is to operationalize topographic mapping of tidal flat, and monitor the long-term morphological development. The SAR instruments allow continuity and improvement of the ocean, coastal zone and land monitoring. Such data is required to initiate or validate models and long term monitoring over various scales. The main three groups of users of SAR data are remote sensing science community, earth science community and commercial applications.

2.1.3 Characteristics of ERS-2 and Envisat ASAR

The European Remote sensing Satellite (ERS) was the European Space Agency's first Earth-observing satellite program. The first satellite ERS-1 was launched in July 1991 and ended its operation in March 2000. ERS-2 was launched into the same orbit in July 1995 and retired in July 2011. ERS-2 is the parallel satellite to ERS-1. Envisat was launched in March 2002. The Advanced Synthetic Aperture Radar (ASAR) instrument onboard the Envisat satellite extended the SAR mission of the satellite ERS-1 and ERS-2. ERS-2 and Envisat ASAR have the same repeat cycle of 35 days; they are also using the same wave band, which is C-band 5.3 GHz with around 30 m spatial resolution and 100 km swath width. Figure 2.3 is the illustration of the Wadden Sea with the SAR scenes. Table 2.3 is the characteristics overview of ERS-2 and Envisat ASAR. Figure 2.4 is an example SAR image of the Wadden Sea (Envisat ASAR, Feb 19th, 2009).

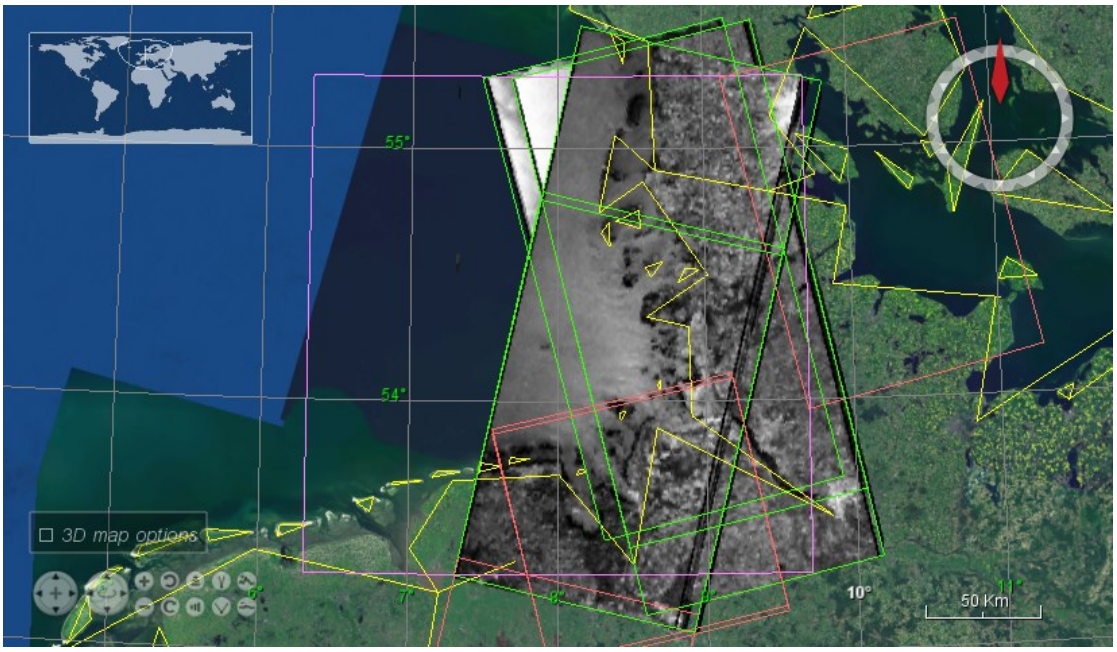

Figure 2.3: SAR scenes covering the Wadden Sea (Eolisa, the ESA order catalogue).

Table 2.3: Characteristics overview of ERS-2 and Envisat ASAR.

	ERS-2	Envisat ASAR
Operation time	April, 1995 – July, 2011	March, 2002 – April, 2012
Waveband	5.3 GHz, C-band	5.3 GHz, C-band
Polarization	VV	VV (used here)
Spatial resolution	30 m	30 m
Swath width	100 km	100 km
Image size (pixel) (km)	approx. 8080×8900 approx. 100×110	approx. 8450×8840 approx. 105×110
Pixel size	12.5 m	12.5 m
Repeat cycle	35 days	35 days

Figure 2.4: Example SAR image of the Wadden Sea, from Envisat ASAR, Feb 19th, 2009 (09:45, UTC time).

2.2 Landsat data

The Landsat program offers the world's longest continuous Earth's surface observation record. It collects space based moderate resolution land remote sensing data. This program started in 1972 (Figure 2.5), and works over four decades to provide data resource for agriculture, geology, forestry, regional planning, education, mapping, and global change research. It works also for emergency response and disaster relief.

Landsat 5 was launched on 1st March, 1984. As a continuation of the Landsat program, Landsat 5 was partly managed by the USGS (U.S. Geological Survey) and the NASA. It ended its mission on 5th June, 2013. Landsat 5 has already outlived its original three-year design life. It was substituted for most applications by Landsat 7

and Landsat 8.

Landsat 5 needs 99 minutes to complete one orbit and thus it can complete about 14 full orbits every day. The repeat cycle is 16 days at an altitude of 705.3 km with a maximum transmission bandwidth of 85 Mbit/s. The Landsat images used here are from Landsat 5 Thematic Mapper (TM). Figure 2.6 is an example of Landsat 5 TM image from 7th Jan, 2004. Thematic Mapper is a multispectral scanner radiometer carried on board of Landsat 5. There are seven bands with the TM sensor (blue-green, green, red, near infrared (near-IR), mid-infrared, thermal infrared and min-infrared). The TM sensor has spatial resolution of 30 meters for the visible, near-IR bands; and in addition a 120-meter thermal-IR band (Landsat Project Factsheet, 2012). Different bands have their own advantages for detecting different surface types. The goal of our work is to detect the shifting water lines between water and the tidal flat. We need a band which can distinguish water and land best. Since water absorbs nearly all light at near infrared band, water bodies appear dark. This contrasts with bright reflectance for soil and vegetation so this band is a good choice for defining the water/land interface (Figure 2.7).

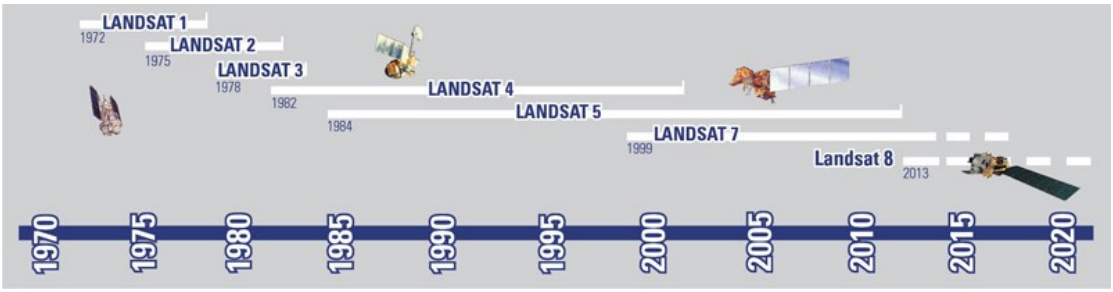

Figure 2.5: Historic timetable of Landsat satellite
(https://landsat.usgs.gov/images/squares/timeline.jpg).

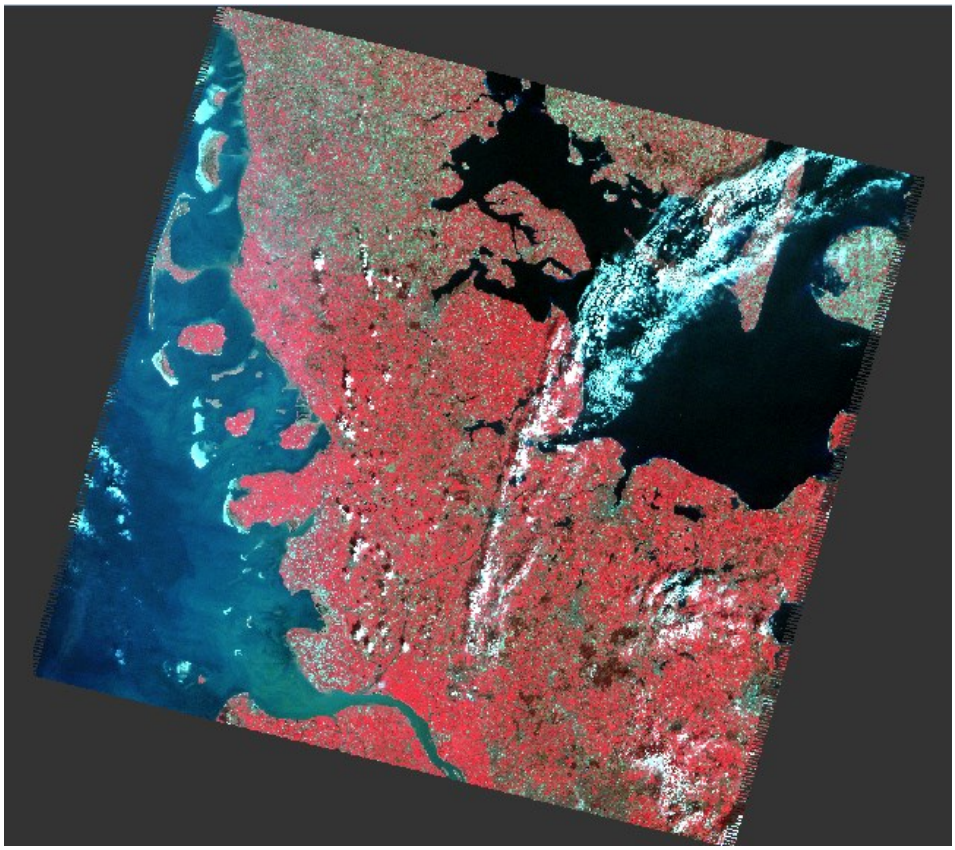

Figure 2.6: Landsat 5 TM image from 7th Jan, 2004.

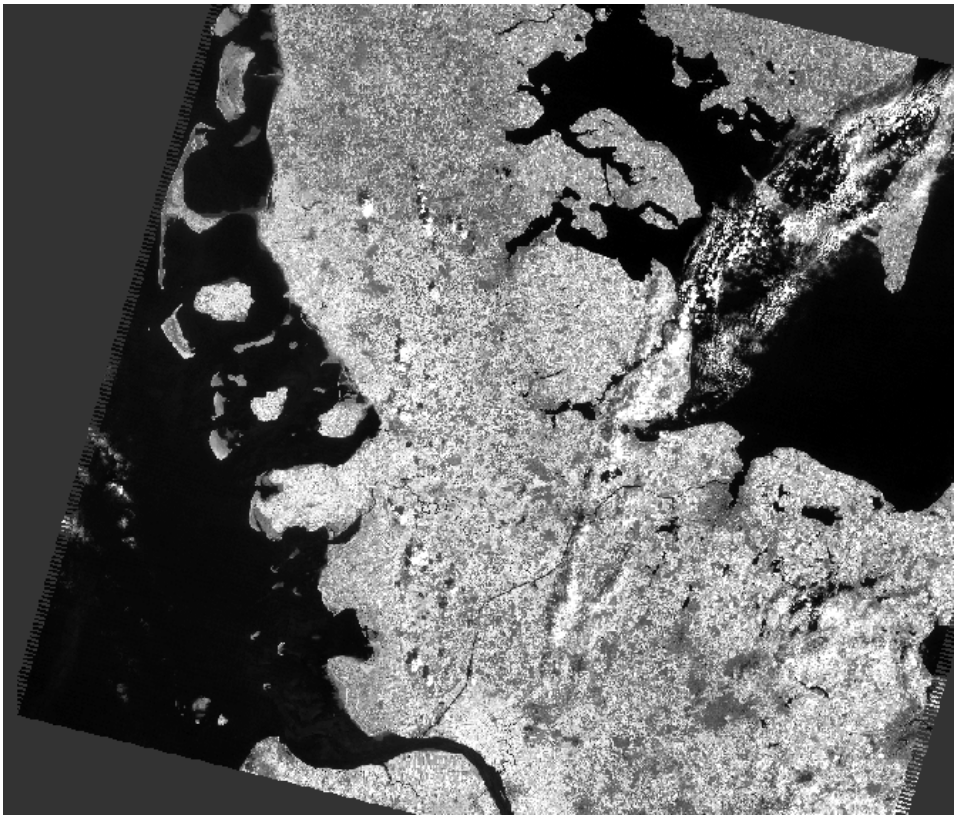

Figure 2.7: Landsat 5 TM image, near infrared band, 0.76-0.90 μm (7th Jan, 2004).

2.3 Model Data

The waterlines can be detected from SAR images and need to be assigned with water level in order to yield topographic maps. Water level data is provided from BSH's ocean circulation model. This model (BSHcmod) is a three-dimensional hydrostatic primitive-equation circulation model formulated in spherical, horizontal and generalized vertical coordinates, with mixing length formulation for horizontal and vertical turbulence (Kleine, 1994; Dick, 1997; Dick et al., 2001; Kleine, 2003). In the North Sea, the model covers the region from 4°W to 30.5°E and from 48.5°N to 60.5°N.

The horizontal grid size is 1.8 km (1 nautical mile) in the German Bight and 10 km in the other part of the North Sea. There are 44 layers in the vertical dimension and the layer thickness varies from 2 m near the surface to 3 m close to the bottom. The operational version of BSHcmod used here adopts a two-way nested high resolution grid to cover the German Bight. A sponge layer closes the northern open boundary in the North Sea. Another sponge layer is included at the entrance to the English Channel. External surges entering to the North Sea from Atlantic are calculated by a two-dimensional BSH model for the North East Atlantic with resolution of 40 km. This coarser model and the operational version BSHcmod are both forced by meteorological data from the DWD (German Weather Service). DWD data is meteorological forecast data with hourly values of air temperature and humidity, air pressure, wind velocity and total cloud cover. Rivers are also considered in the model as fresh water fluxes. The harmonic constants of 14 tidal constituents are used to implement tidal forcing at the open boundaries of the North Sea. The model also simulates the flooding and falling dry of tidal flats, allowing the complex processes in the highly structured German coastal waters (tidal flats, sandbars, and tidal channels, barrier islands) to be modeled realistically. Figure 2.8 is an example of the water level model data taken on 10:15am, March 6th, 2009.

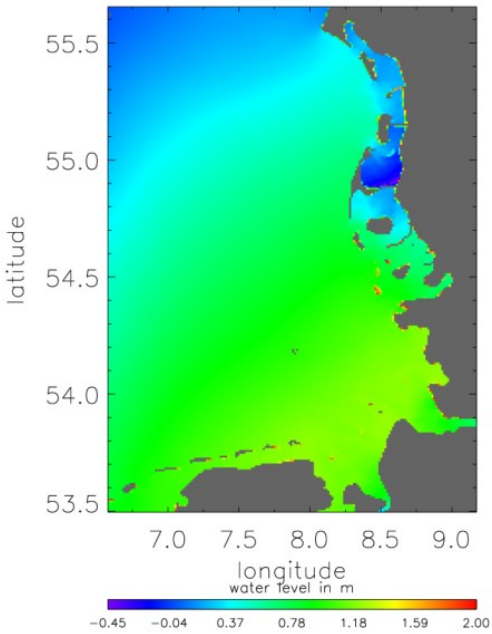

Figure 2.8: Water level model data from BSHcmod on 10:15am, March 6th, 2009 (UTM).

2.4 Gauge Data

Gauge data are provided by WSV (Wasser- und Schifffahrtsverwaltung des Bundes, the Waterways and Shipping Administration in Germany). One of the main error sources of water level model data from BSH is the error of the wind velocity from the DWD weather prediction model. In order to compensate for the water level errors, water level data are corrected by gauge data. Gauge data is recorded at the tide gauge stations near by the coast or islands. A tide gauge is a device for measuring the change in sea level relative to a datum. Sensors continuously record the height of the water level with respect to MSL (Mean Sea Level). Figure 2.9 shows the examples of the different tide gauges WSV is using.

Figure 2.9: Different tide gauge stations (www.wsa-emden.de).

The tide gauge records local water level every second all day long. It also gives MSL value at the tide gauge station. The water level used here is calculated by the sum of the gauge water level and MSL. For example, recorded water level at Bake A gauge station on Jan 15th, 2009 10:25 is 324.50 cm. The MSL at Bake A gauge station is -5 m.

The water level = 3.245 – 5 = -1.755 m

The gauge data is recorded with local time, CET (Central European Time). However, SAR data is recorded with UTC (Coordinated Universal Time), which is one hour earlier than CET. The time difference is considered by UTC = CET -1.

Figure 2.10 shows the distribution of the gauge stations in the Wadden Sea.

There are 10 gauge stations data used in this study. Table 2.4 gives the locations and MSL values for these 10 gauge stations.

Figure 2.10: Gauge stations' distribution in Wadden Sea (http://www.pegelonline.wsv.de/gast/karte/standard).

Table 2.4: Location and MSL of chosen gauge stations.

Gauge sations	Gauss-Krüger Coordinates		MSL (m) (Mean Sea Level)
	Easting (m)	Northing (m)	
Pellworm Anleger	3480765.00	6041274.00	-5.00
Husum	3501676.00	6038046.00	-5.00
Eider-Sperrwerk BP	3490261.00	6015078.00	-5.00
Büsum	3490858.00	5999038.00	-5.00
Zehnerloch	3477635.00	5980578.00	-5.00
Cuxhaven Streubenhöft	3481482.00	5970786.00	-5.02
Hookspielplate	3443798.00	5948990.00	-5.02
Mellumplate	3440237.00	5960449.00	-5.02
Leuchtturm Alte Weser	3442674.00	5970610.00	-4.96
Bake A	3455144.00	5983959.00	-5.00

2.5 Bathymetry Data

The bathymetry data used later in validation and morphological parameter calculation is from AufMod (Aufbau integrierter Modellsysteme zur Analyse der langfristigen Morphodynamik in der Deutschen Bucht; Development of integrated model systems for the analysis of long-term morphodynamics in the German Bight) project. The bathymetry module in this project is a two-dimensional measurement data-based model which describes the terrain surface of the seabed. It takes account all available survey data from 1982 to 2012 and chooses 1st Jan, 1900 as a timestamp for the time-invariant basis of the model. If there were no surveys on a location, the

depth was referred to the time-invariant basis. The annual topography was derived by interpolating spatiotemporally on 1st of June every year with 50×50 m grid size and a spatial extent from the coastline to the seaward 20 m isobaths. The accuracy of the data based on the modeling and the temporal and local distance to the survey point was measured by a parameter called Confidence [m]. It increases with temporal and spatial distance to the survey point. 0.2 m indicates the average accuracy. Lower values represent a higher level of reliability of the model data; high values represent a low level of reliability (Valerius et al., 2013).

Chapter 3 Generation of Topographic Maps

This chapter describes edge detection, geocoding, model data processing, data coverage, map (DEMs) generation, and validation. The methodology is based on Dannenberg (2004). Since the main focus of our study is the morphological development of the German Wadden Sea (the application of the method), we only present a brief summary of the edge detection theory and the method. The improvements in geocoding, data coverage, and the results will be discussed in detail.

3.1 Edge Detection Theory

Lee (1980, 1981, 1983, 1990) developed a method to detect edges in digital images including a reduction of multiplicative speckle noise by approximating the multiplicative noise model to a linear model with Maximum Mean Square Error (MMSE) criteria, and an edge-tracing algorithm based on the Robert's operator (Roberts 1963). With the enhanced Lee filter, Touzi et al. (1988) developed a constant false alarm rate (CFAR) edge detector based on the ratio between pixel values instead of the conventional methods, which consider the difference between pixel values (Davis, 1975). It is able to detect edges of the image with multiplicative noises. When compared to the other CFAR edge detectors, the coefficient of variation detector (Ulaby et al., 1986) and the Frost et al. (1982) edge detector, the Touzi edge detector showed better results and lower computing time. It has been

previously used by Mason and Davenport (1996), and Klocke (2001) in order to detect waterlines in satellite SAR images. Niedermeier (2000, 2005) tried a wavelet-transform based edge detection to track over the scale accurately. However, this process is too time consuming and the quality does not justify the effort. Dannenberg (2004) also applied a wavelet-transform based edge detector to derive topographic map of the German Wadden Sea, but instead of tracking all scales accurately, he used the coarser scales to confine the area of interest.

The edge detection used here is with multi-scale edge detection WTMM (Wavelet Transform Modulus Maxima) in combination with a region growing segmentation procedure.

3.1.1 Multi-scale edge detection

The waterlines (edges) are the ever shifting borderlines between the sea and the tidal flat. In order to reduce the computational burden, only the coastal areas are considered. First, the SAR image (approx. 8000×8000 pixels) is split into small patches (512×512 pixels) and then the VMR (Variance to Mean Ratio) of each patch is calculated. Sea surfaces have relatively low VMR value due to the homogeneous texture, but the areas containing waterlines show a high value due to the transition from the homogeneous texture to rough texture. According to this, the patches with lower VMR value are excluded from this step. Logarithm of the original SAR backscatter values is taken before the edge detection in order to transform the multiplicative speckle noise into additive noise, thus to reduce the influence of the background noise.

The modulus maxima of the wavelet transform are used to extract the edges. A wavelet is a function $\psi \in \boldsymbol{L}^2(\mathbb{R})$ with a zero average: $\int_{-\infty}^{\infty} \psi(t)dt = 0$. It is normalized $\|\psi\| = 1$ and centered in the neighborhood of $t = 0$. This is the basic function (mother wavelet). The wavelet transform of a function *f(t)* scaled by a factor *s* and shifted by *u,* can be presented as (Mallat, 1997):

$$Wf(u, s) = \langle f, \psi_{u,s} \rangle = \int_{-\infty}^{+\infty} f(t) \frac{1}{\sqrt{s}} \psi^*(\frac{t-u}{s}) dt \quad (3.1)$$

$$\psi_{u,s}(t) = \frac{1}{\sqrt{s}} \psi(\frac{t-u}{s}). \quad (3.2)$$

$\psi_{u,s}(t)$ is a dictionary of time-frequency atoms that is obtained by scaling ψ by $s \in \mathbb{R}^+$, and translating it by $u \in \mathbb{R}$, $||\psi_{u,s}|| = 1$. $\psi^*_{u,s}$ is the complex conjugate of $\psi_{u,s}$.

If ψ has exactly n vanishing moments and a compact support, then there is a θ of compact support such that $\psi = (-1)^n \theta^{(n)}$ with $\int_{-\infty}^{+\infty} \theta(t) dt \neq 0$. A wavelet ψ with n vanishing moments can be expressed as the n^{th} order derivative of a fast decaying function θ (Mallat, 1997):

$$\psi(t) = (-1)^n \frac{d^n \theta(t)}{dt^n} \quad (3.3)$$

As a consequence, the wavelet transform can be presented as

$$Wf(u, s) = s^n \frac{d^u}{du^n} (f * \theta_s)(u) \quad (3.4)$$

where

$$\theta_s(t) = s^{-1/2} \theta(-t/s). \quad (3.5)$$

(3.4) shows that $Wf(u, s)$ using a wavelet with n vanishing moments can be applied as a multi-scale differential operator θ_s with order n. If the wavelet has only one vanishing moment, local maxima of the wavelet transform are the maxima of the first order derivative of the function f smoothed by the function θ_s. $W_1 f(u, s)$ has modulus maxima at the sharp variation points of the convolution, where are the irregular jump (edges) in the signal (Figure 3.1).

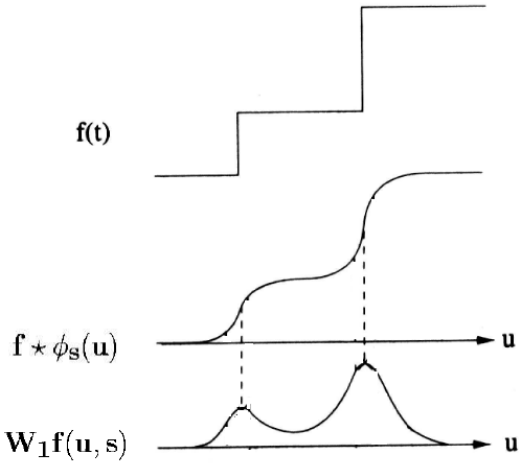

Figure 3.1: Illustration of the wavelet transform with the first order derivative. *f(t)*: signal function; $f * \theta_s$: convolution between the signal and the multi-scale differential operator; $W_1 f(u, s)$: the first order derivative of the wavelet transform (Mallat, 1997).

Therefore, the quadratic spline wavelet with one vanishing moment is selected. For fast numerical computation, dyadic scales $s = 2^j$(j = 1, 2, 3, 4, 5) are chosen. The location u_0 of an edge in scale s_0 in the image is given by

$$\frac{\partial W f(u_0, s_0)}{\partial u} = 0 \qquad (3.6)$$

and the strength of the edges is estimated by the modulus

$$Mf(u, s) = \sqrt{|W^H f(u_H, s)|^2 + |W^V f(u_V, s)|^2} \qquad (3.7)$$

The idea of this multi-scale edge detection is to detect the edges from the scales 2, 2^2, 2^3, 2^4, and to track the edges containing in all the scales. The noise has less influence when the scale increases, but the location accuracy reduces due to the smoothed image. The finest scale (s=2) has the most accurate location of the edges; however, it also contains the strongest noise. Several steps are taken in order to compensate these disadvantages. First, stronger edges are selected by applying different threshold on $Mf(u_0, s_0)$ at each scale; Second, since the accuracy of the edges' location is low at the coarser scales (s = 2^3, 2^4), the edges' locations are broadened to define the areas containing edges; Third, only the edges located in the areas of

interest through all the scales are defined as the resulting edges candidates. Most of the noise at the fine scales is removed because it does not locate within the broadened areas at the coarser scales and the locations of the edges are preserved by the finer scales.

The edges in the interior of the tidal flat and the open sea are removed by a region growing segmentation procedure. This procedure combines the regions with same averaged brightness and starts with randomly distributed seeds. Edges that are at a distance away from the segment borders more than 5 pixels are removed. Manual inspection is needed in the end to clean the image of unclassified edges.

3.2 Summary of the Waterline Method

Figure 3.2 describes the whole procedure of this method. For each detected waterline (edge) pixel, its geographical coordinates are determined in the geocoding step. A polynomial transform is applied according to a set of points with known geographic coordinates (GCPs, Ground Control Points) (Schowengerdt, 1997), and used to transform all detected waterlines into Gauss-Krueger coordinates (Olbrich et al., 1996). The geocoded waterlines are assigned with water level data, provided by the BSH and corrected by gauge data provided by the WSV. The correction is performed by adding the averaged water level correction at the gauge stations to the water level model result. It is a constant correction. The dataset of all waterlines from one year, attached with water levels, is interpolated into a 20 m grid size topographic map using the map generating software TASH (Kruse, 2003) which employs Delaunay triangulation. Delaunay triangulation has two criteria: there is no other point located in the triangle; for the third point of a triangle, only the one with largest crown angle is selected (Buziek, 1990). The version of TASH used in (Dannenberg, 2004) was not capable of processing an entire year's worth of waterline dataset at one time. The data needed to be subdivided into several parts, and later recomposed together again after the interpolation. The new version of TASH is adapted for large datasets. It is able to process one year's dataset at one time in around three to four hours of processing time.

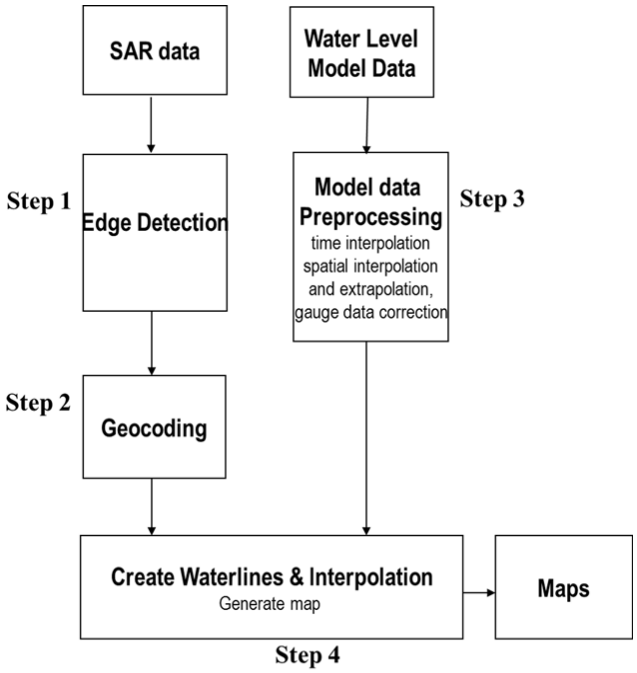

Figure 3.2: Flowchart of waterline method.

3.3 Improvement of Geocoding

The maximum error of the edge detection is about 2 pixels, resulting in a total uncertainty of about 50 m. The tidal flat has weak gradients; the uncertainty in the edge location only causes less than 10 cm error at the usual gradients of 0.002 (Dannenberg, 2004). The additional GCPs on Helgoland (Figure 3.3 arrow) increase the accuracy of the geocoding (the images are able to cover Helgoland). These are chosen interactively from the 'Amtliche Topographische Karten, Top 25' (Official Topographic Maps of Schleswig-Holstein/Hamburg, 2009). In order to calculate the accuracy of the geocoding before and after adding the extra GCPs on Heligoland, eight testing GCPs are chosen (Figure 3.3 white frames) from the digital map. Their Gauss-Krueger coordinates are known. The error of the geocoding is estimated by determining the distance between the calculated coordinates and the actual coordinates of the testing GCPs. Figure 3.3 shows that adding GCPs on Heligoland reduces the error at North and Southeast of the research area. Details show in Table 3.1. On average, the error is reduced from 34.95 m to 24.43 m, which is 30%. The largest improvements (more than 10 m error reduction) are found at points 1, 2, 4, and 7 which are all located within the area of interest (the red frame).

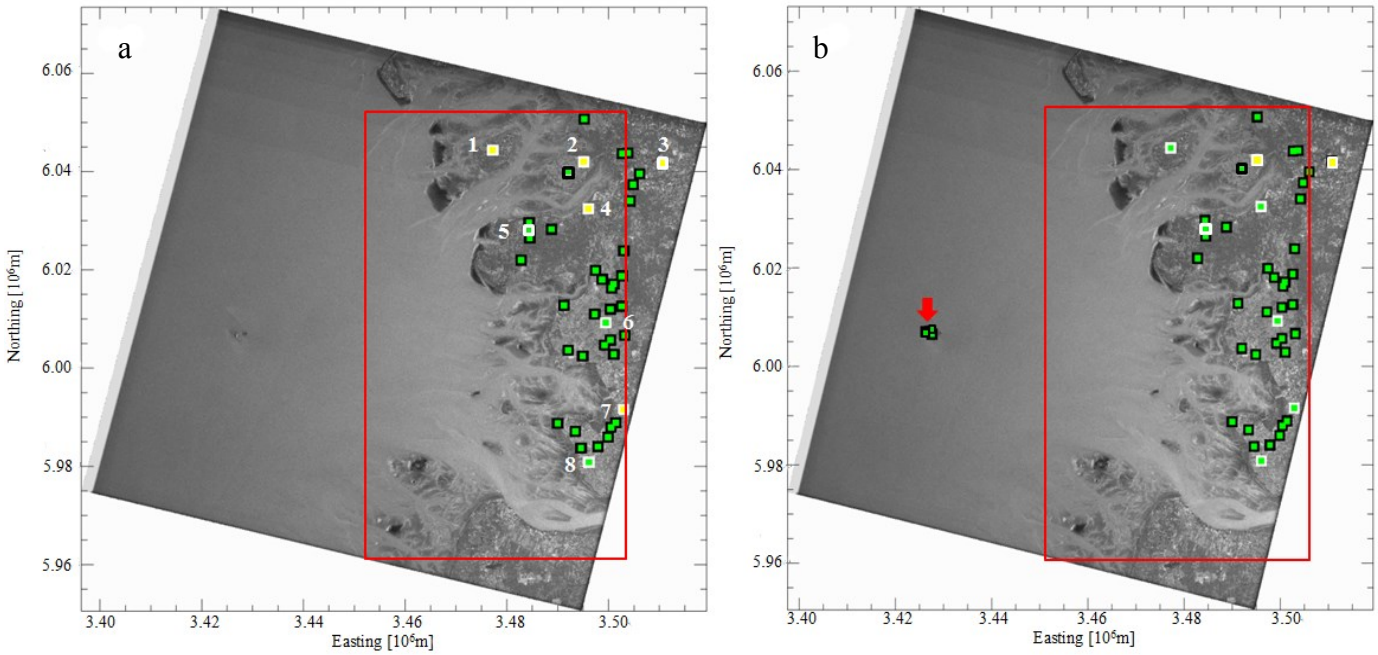

Figure 3.3: Geocoding result before (a) and after (b) add GCPs on Helgoland. Green means error is up to 25 m, yellow means error is up to 50 m. White frame points are testing GCPs, black frame points are GCPs.

Table 3.1 Geocoding error before and after adding GCPs on Helgoland
(For location of points see numbers in Figure 3.3)

Number	Error before adding GCPs on Heligoland (m)	Error after adding GCPs on Heligoland (m)
1	44.7	24.2
2	46.2	29.0
3	46.5	45.4
4	42.0	19.7
5	22.1	17.6
6	17.8	17.6
7	41.6	23.7
8	18.7	18.2
Average	34.95	24.43

3.3 Topographic Map Results

The topographic maps from 1996 to 1999 were reproduced and the maps from 2004 to 2009 were generated (Figure 3.4). Land and deep water areas were set to gray and white, respectively. The maps from all years reflected the large scale topography correctly, and properly locate the important features like sandbars and tidal channels. The locations of the large structures, such as Neuwerk, Trischen, Medemsand, Medemgrund, Tertiussand, Gelbsand, Südsand and Norderoogsand (Figure 3.4a) can be found in the maps of each year at relatively stable position (Figure 3.4). Although the larger structures are present at similar locations in every map, their height and shape gradually changes from year to year. Larger changes can be found between year group A (1996 – 1999) and year group B (2004 – 2009). The most dynamic regions are the outer parts of the tidal flat, tidal channels, sandbars and estuaries.

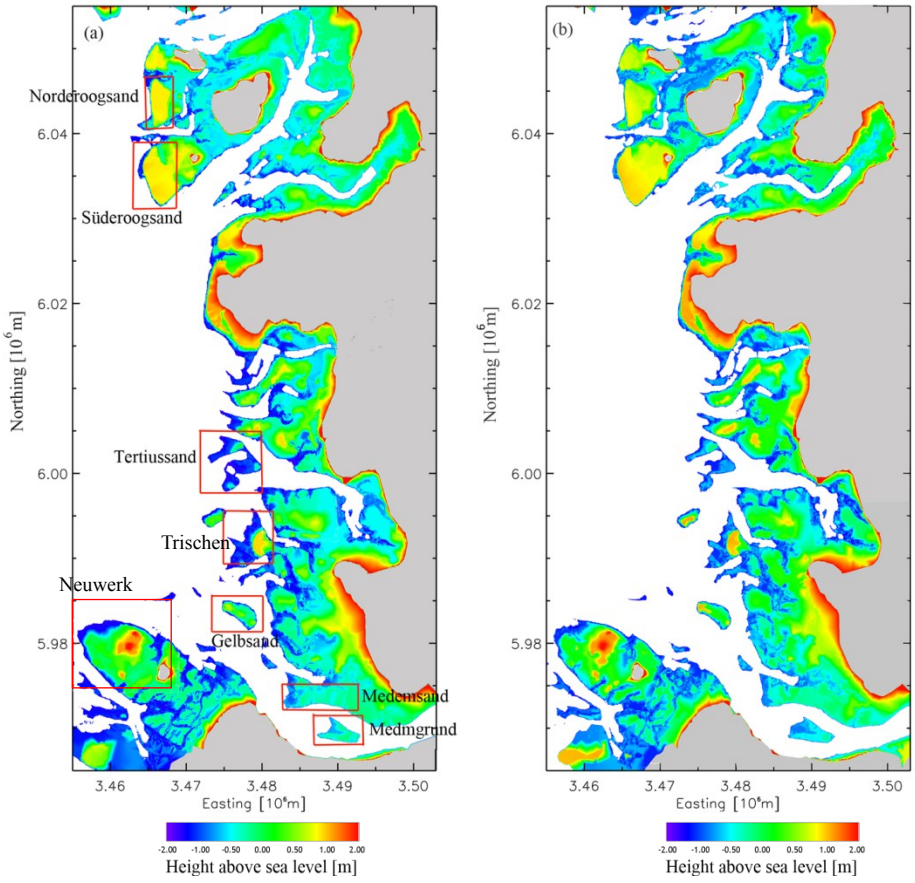

Figure 3.4: Topographic maps (a, 1996; b, 1997; c, 1998; d, 1999; e, 2004; f, 2005; g, 2006; h, 2007; i, 2008; j, 2009).

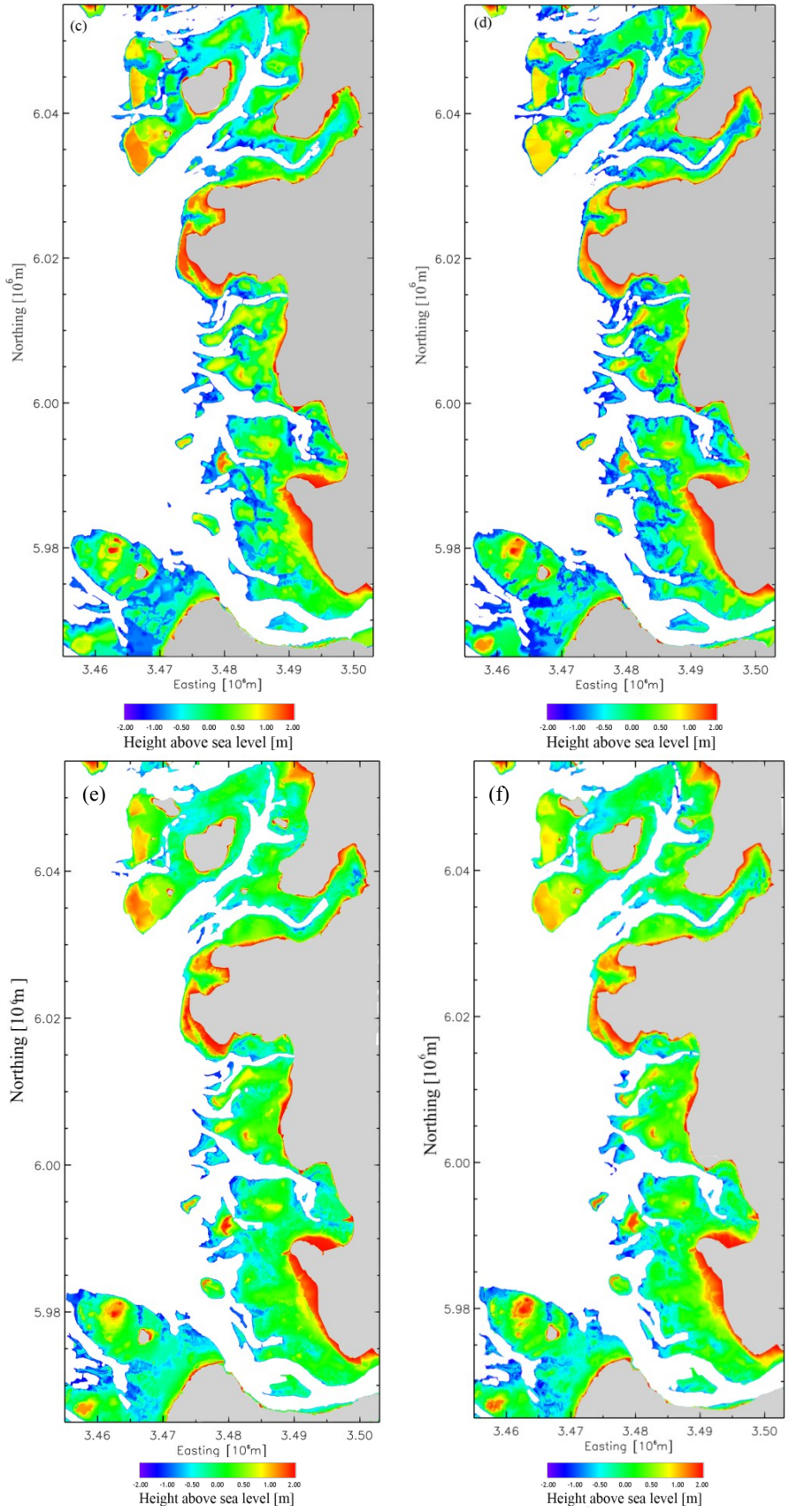

Figure 3.4: (Continued)

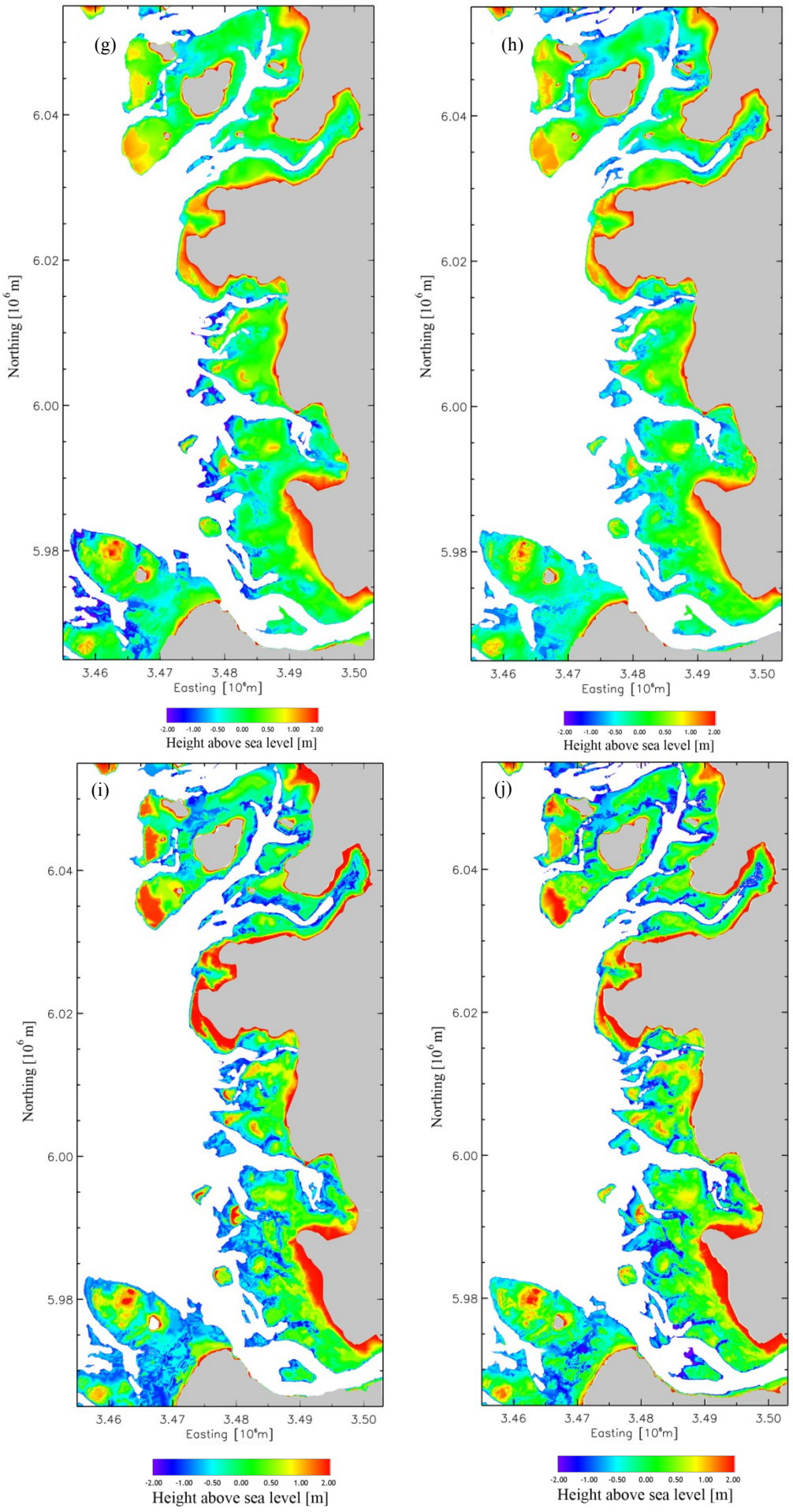

Figure 3.4: (Continued)

3.4 Data Coverage and Validation

The vertical data coverage of the satellite images of all years can be read from Figure 3.5, where the water levels of the tidal gauge in Cuxhaven at the time of data captured is shown. The representation allows easily assessing the height range covered by the satellite scenes for each single year, which of the same time is the height range of the resulting topographic maps. Similarly, height range gaps not covered by the satellite scenes can be identified. Diagram Figure 3.5 is exactly valid for the tidal levels of Cuxhaven. However, the horizontal change of the tidal level within the region of the generated maps is small, so that Figure 3.5 with the water levels of Cuxhaven may serve to estimate the height coverage of the satellite scenes of one year in the whole mapped region.

We extended the vertical data coverage by adding Envisat ASAR images and Landsat TM5 optical images, depicted in Figure 3.5 in red and green. We also tried to avoid the time of strong topography changes caused by extreme weather condition due to the difficulty of edge detection. The data from 1996 to 1999 only contained ERS-1/2 images. Since Envisat was launched in 2002, we were able to include the Envisat ASAR images of the German Wadden Sea in the map generation process from 2004 onward. They filled the tidal level gaps where ERS images could not cover the height range homogeneously. Landsat TM5 images were not available through all years, but only for 2004, 2005, 2006, and 2009. The lowest tidal levels of the years 2004, 2005, and 2006 were extended by the Landsat TM5 images. The tidal level coverage is an important factor of the waterline method. Better coverage represents better quality. The two extra datasets give a much better coverage comparing to the years from 1996 to 1999.

We take the year 2005 as an example to demonstrate how the data coverage improves the topographic map. Figure 3.6a is the topographic map only with ERS SAR dataset and Figure 3.6b is the topographic map with ERS SAR, Envisat ASAR, and Landsat TM5 datasets. Overall, they show a similar topography, but Figure 3.6b contains lower tidal level data and shows more details. Especially for the marked

areas (Figure 3.6, red frames), the tail of Tertiussand could not be detected using only ERS data and the tidal flat area of Medemgrund also is reduced due to the data limitation.

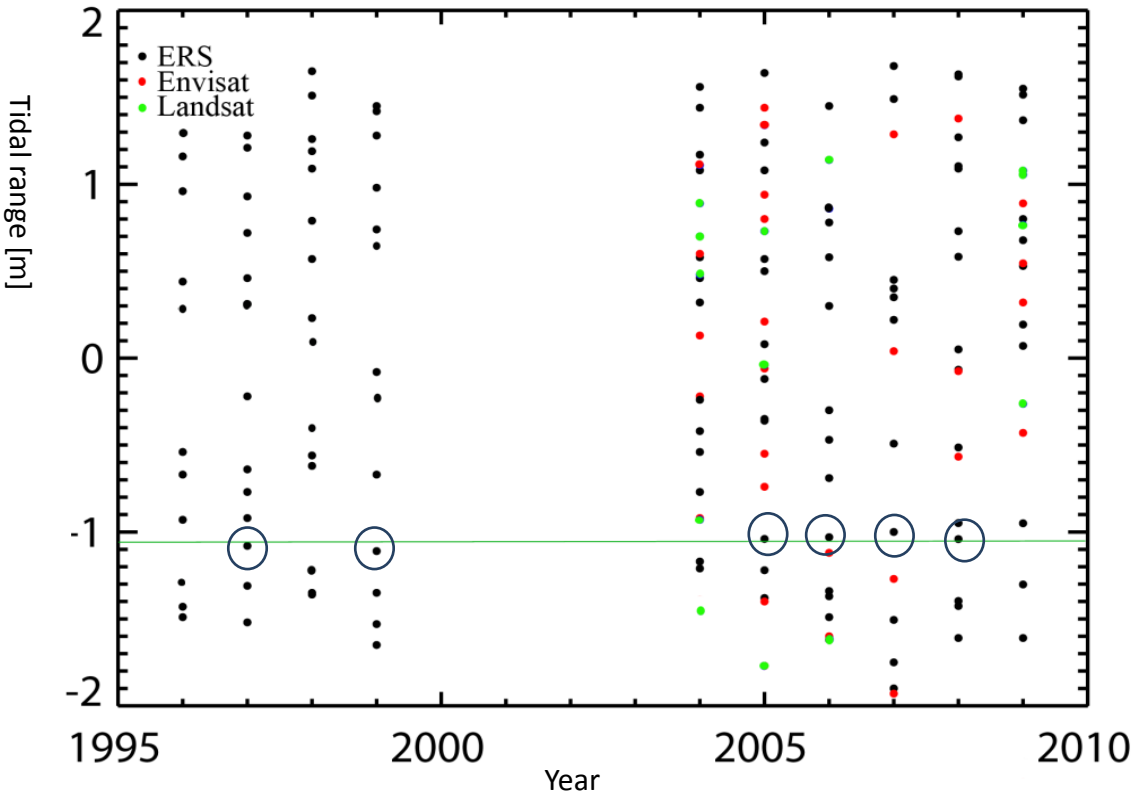

Figure 3.5: The tidal range coverage of the images
(Tidal range data is from Cuxhaven gauge station; the dots marked by green circles mean the images were taken at nearly the same tidal level).

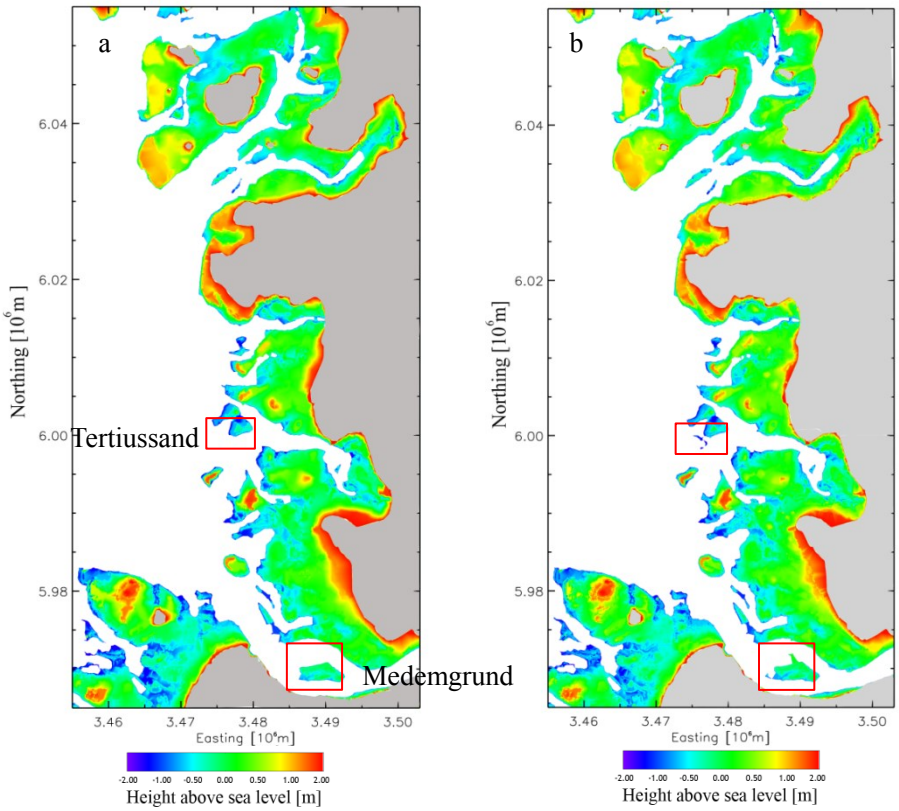

Figure 3.6: Topographic maps of the year 2005 (a, with only ERS SAR images; b, with ERS, Envisat ASAR, and Landsat images).

The first step of validation is to check the reliability of the maps. The method is as follows: we selected a set of images taken at nearly the same tidal level. Second, chose two locations, one of significant change during the study period, and another one which stayed relatively stable. If the detection results of these two locations at the same tidal level show the same development as in reality confirmed from an independent source, it indicates the reliability of this method.

We selected six SAR images taken at nearly identical tidal level at 12th June 1997, 30th Sep 1999, 2nd April 2005, 14th Oct 2006, 21st July 2007, and 6th Nov 2008 (Figure 3.5, green line – the tidal level, and green circles – the images). The range of the tidal levels of the scenes is from -1.10 m to -1.00 m (with respect to mean sea level). Here, we chose Gelbsand and Bielshövensand. Gelbsand is a sandbar in the Wadden Sea; its shape had great change according to the historical study (Ulrich

1990). Bielshövensand remained relatively stable, only at the western tip it expanded pronouncedly towards the north-west (Ricklefs and Neto 2005). The detection results (Figure 3.7) of this method fit to the description mentioned above. It confirms the reliability of this method.

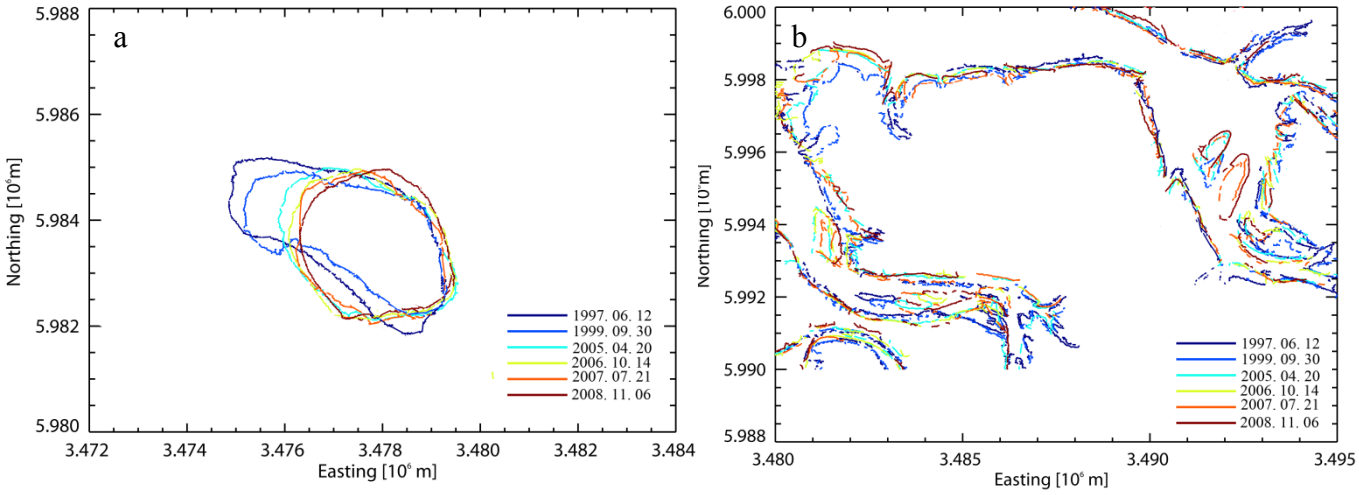

Figure 3.7: Gelbsand (a) as example for mobile sand, and Bielshövensand (b) as example for stable sand. The waterlines detected at the same tidal level from different years (the corresponding images are marked with green circle in Figure 3.5).

The second step of validation is to compare the results with in situ bathymetric data from BSH. As introduced in Chapter 2.5, this dataset has a confidence parameter and the value of 0.2 m represents the average accuracy of the bathymetry measurements. The range of this parameter is from 0 m to 61.04 m. There is another parameter called 'minimum dt', it describes the minimum temporal distance to the next temporally located field campaign in the database (Figure 3.8). It gives a quick assessment of the reliability of the temporal interpolation. We chose for validation data with confidence parameter less than 0.2 m. In the area selected for validation, the minimum dt parameter is below one year. Figure 3.9a shows the distribution of the confidence parameter from 0 m to 1 m in 2008, and Figure 3.9b shows it from 0 m to 0.2 m in the same year. Medemgrund/Medemsand, Trischen, and part of Neuwerk (Figure 3.9b, marked) are covered by the data with confidence parameter below 0.2 m. These regions are chosen for validation. Figure 3.10 illustrates the

difference map between waterline method and bathymetric data (waterline method minus bathymetry data) in 2008. The other years (2004, 2006, 2007, and 2009) are also validated using the same procedure. Because the confidence parameter less than 0.2 m covers only a small area in 2005 (Figure 3.11a), we chose the area covered by confidence parameter less than 0.3 m as the validation area, which is mostly the Tertiussand area (Figure 3.11b, validation area is marked). The validation results are shown in Table 3.2. All the years' results of the waterline method are higher than the bathymetric data results, but they are all within their standard deviation. The average difference and standard deviation are both reduced in our results compared to the validation results in 1996 and 1999 at the same region. The validation results from Heygster et al. (2010) in 1996 and 1999 were validated at Neuwerk region and they had higher difference value and standard deviation.

Table 3.2 also gives the involved number of scenes and maximum height difference between two scenes. The minimum number of scenes in year group B (2007) is the maximum number in year group A (1998). The increased number of scenes reduces the maximum difference between two scenes from 0.67 m to 0.51 m on average, which is 30 %. While the height range covered by the used satellite images is similar in the years 1999 and 2009 (Figure 3.5), the number of available scenes is in 2009 higher (19 scenes) than in 1999 (13 scenes), leading to a reduction the maximum height difference between two scenes from 0.73 m in 1999 to 0.51 m in 2009.

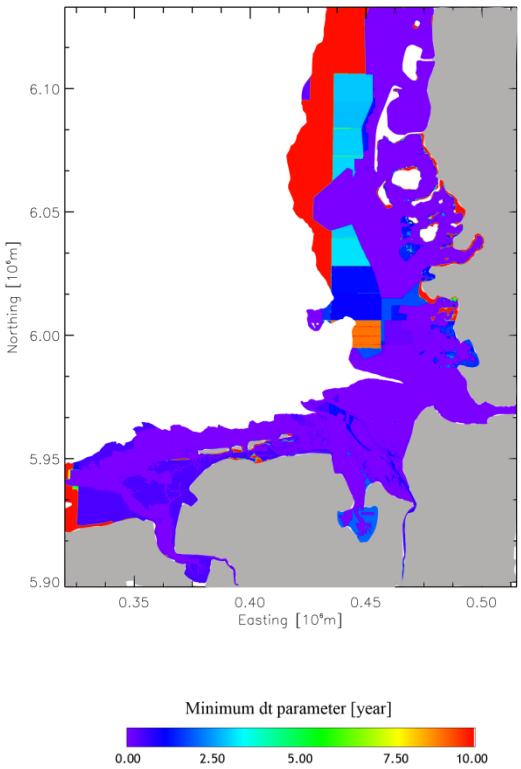

Figure 3.8: Minimum dt parameter distribution.

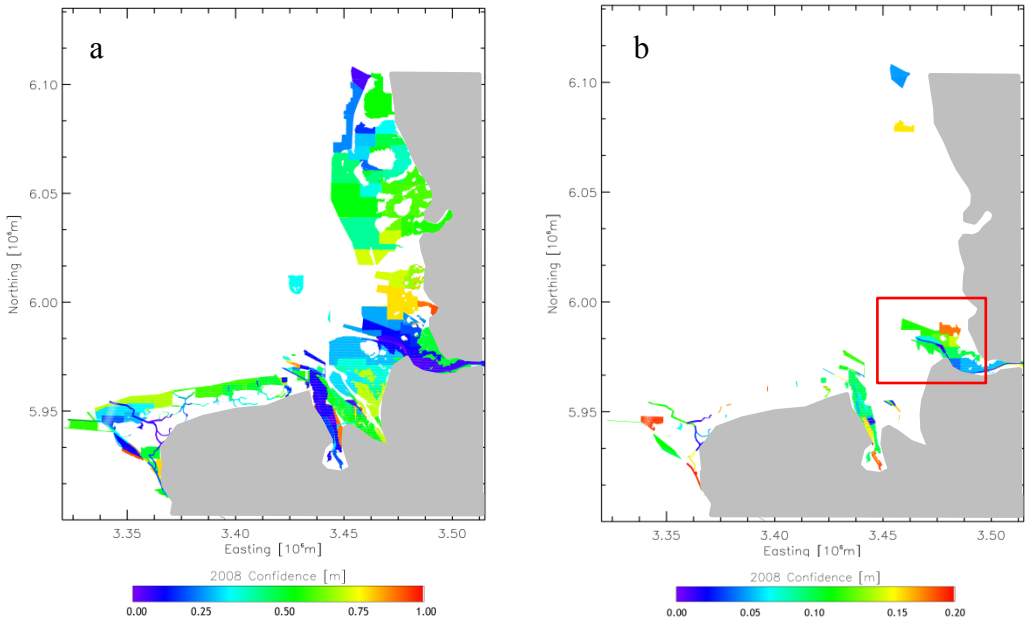

Figure 3.9: Confidence parameter distribution (a, from 0 to 1m; b, from 0 to 0.2 m).

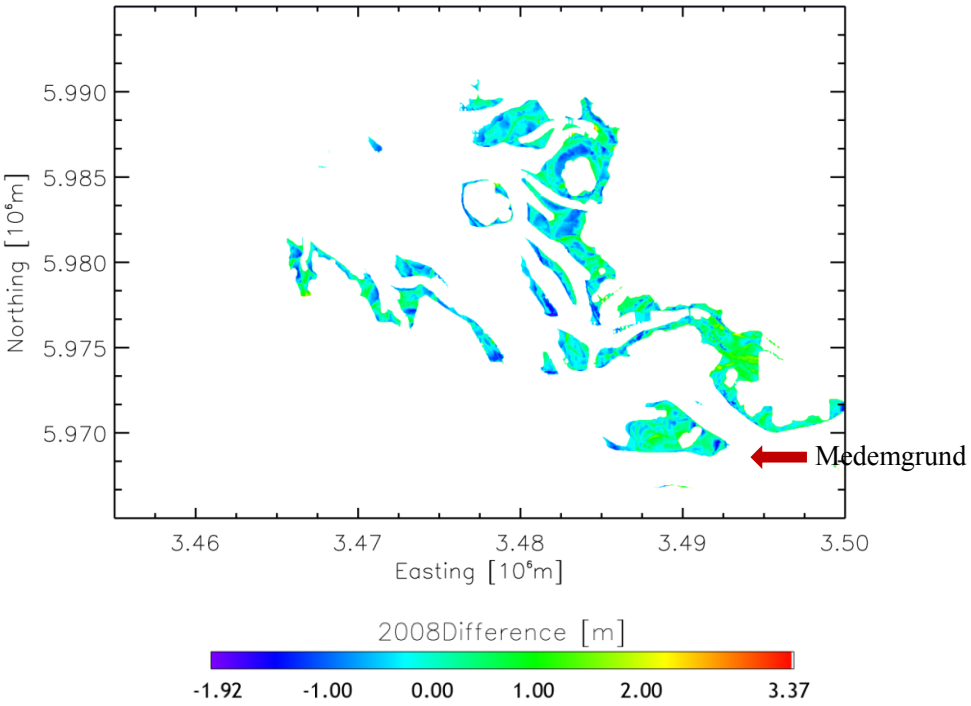

Figure 3.10: Difference map of waterline method and bathymetry data (2008).

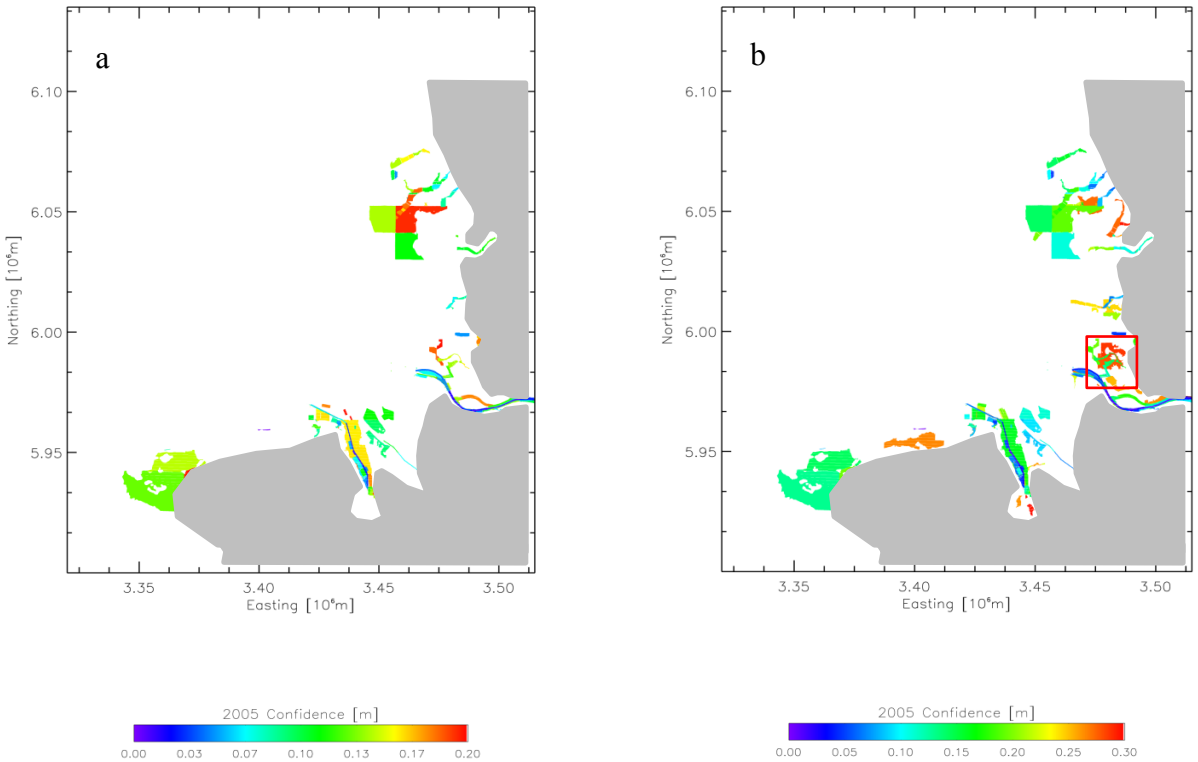

Figure 3.11: Confidence parameter distribution in 2005 (a, from 0 to 0.2 m; b, from 0 to 0.3 m), marked in b is the validation area.

Table 3.2 Validation results

Year group A	Number of involved scenes	Max height difference between two scenes (m)	Average difference with bathymetric data (m)		Standard deviation (m)	
			Result 1*	Result 2*	Result 1*	Result 2*
1996	11	0.82	0.20	0.12	0.37	0.27
1997	13	0.53				
1998	15	0.61				
1999	13	0.73	0.21	0.14	0.45	0.30
Average	**13**	**0.67**	**0.21**	**0.13**	**0.41**	**0.29**
Year group B						
2004	23	0.32	0.020		0.15	
2005	23	0.35	0.119		0.34	
2006	16	0.64	0.013		0.13	
2007	15	0.71	0.061		0.27	
2008	17	0.52	0.006		0.14	
2009	19	0.51	0.011		0.13	
Average	**17**	**0.51**	**0.04**		**0.19**	

* Result 1: validation results from Heygster et al. (2010) at Neuwerk.
* Result 2: validation results at Trischen, Gelbsand, and Medemgrund with current bathymetric data from AufMod, the same regions as year group B.

Chapter 4 Morphological Development of the German Wadden Sea

Morphological development of the coastal system is mainly controlled by erosion and deposition. Time series of topographic maps of the tidal flat will enable a better understanding of how morphological changes.

4.1 Coastal System

A tidal flat is part of a dynamic coastal system, whereby the coast is represented by a line where the land meets the sea at a given point in time. The spatial coastal system boundary follows the definition set by Inman and Brush (1973), which includes the coastal plain, the continental shelf, and the waters that cover the shelf. Other major features include large bays, estuaries, lagoons, coastal dune fields, river estuaries, and deltas, which are illustrated as elements of a coastal system (Masselink et al., 2011) in Figure 4.1.

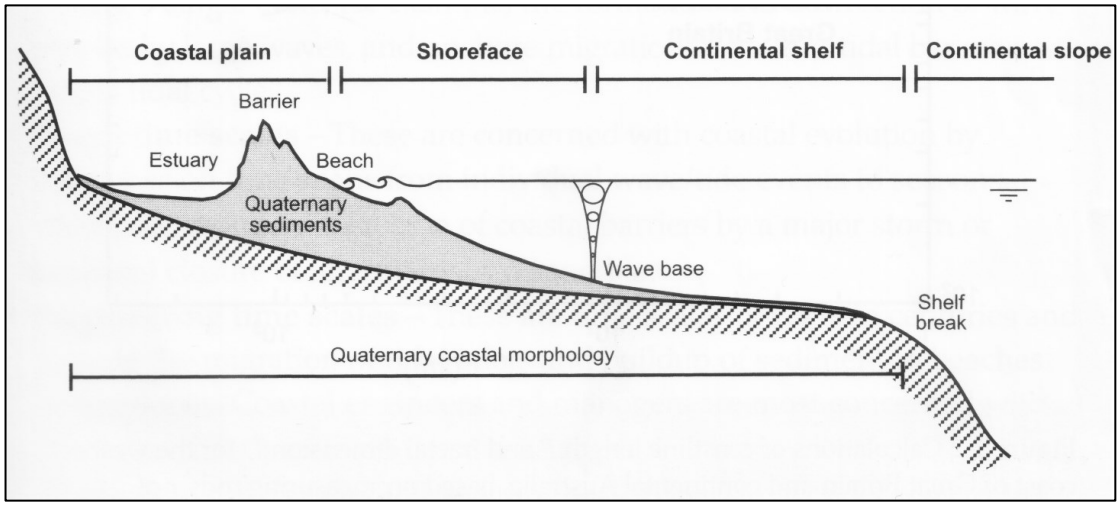

Figure 4.1: Spatial boundaries of the coastal system (Masselink et al., 2011).

Many previous studies attempted to classify coasts (Inman and Nordstrom, 1971; Davies, 1972; Cotton, 1995; Tanner, 1960; Rhodes, 2004) that can be divided into three categories: genetic classification, descriptive classification or combinations of both. In this chapter, two classifications that reflect the nature of costal environments and the effect of plate tectonics on the coastal development are presented: the morphogenic classification and the geotectonic classification (Trenhaile, 1997). They will be used to specifically illustrate the role of the Wadden Sea in the global coastal system.

4.1.1 The Morphogenic Classification

The morphogenic classification is based on wave height and tidal range proposed by Davies (1972). A wave is generated by wind, so the distribution of wave environments varies with latitude and global climate zone (Figure 4.2). Storm wave environments are located at higher temperate and Arctic latitudes; swell dominated coastal areas are located at lower temperate latitudes; and cyclones are concentrated at tropical latitudes. The Wadden Sea is located in the storm wave dominated area (Figure 4.2, red frame).

The global tidal range distribution is shown in Figure 4.3, where tidal range is the vertical difference between high tide and the succeeding low tide. Tidal range is very low in the middle of the ocean and increases towards the coast. The tidal range depends on the shape of the continental shelf where water approaches the coast, the geography of the continent, and the number and size of large embayments. The macro-tidal range (more than 4 m) occurs in the semi-closed seas and at the entrance of tunnel-shaped estuaries, while micro-tidal range (less than 2 m) occurs mostly along the open sea coast or in almost fully enclosed areas. The Wadden Sea is located in between these two extremes, with a meso-tidal range of 2 – 4 m (Figure 4.3, red frame).

Distributions of the wave environment and the tidal range are related to the dominance of waves and tides of the coastal morphology, and are important factors for shaping the coast. A particular coast area can be dominated by wave, or tide, or both and can span to cover several fields as illustrated in Figure 4.4.

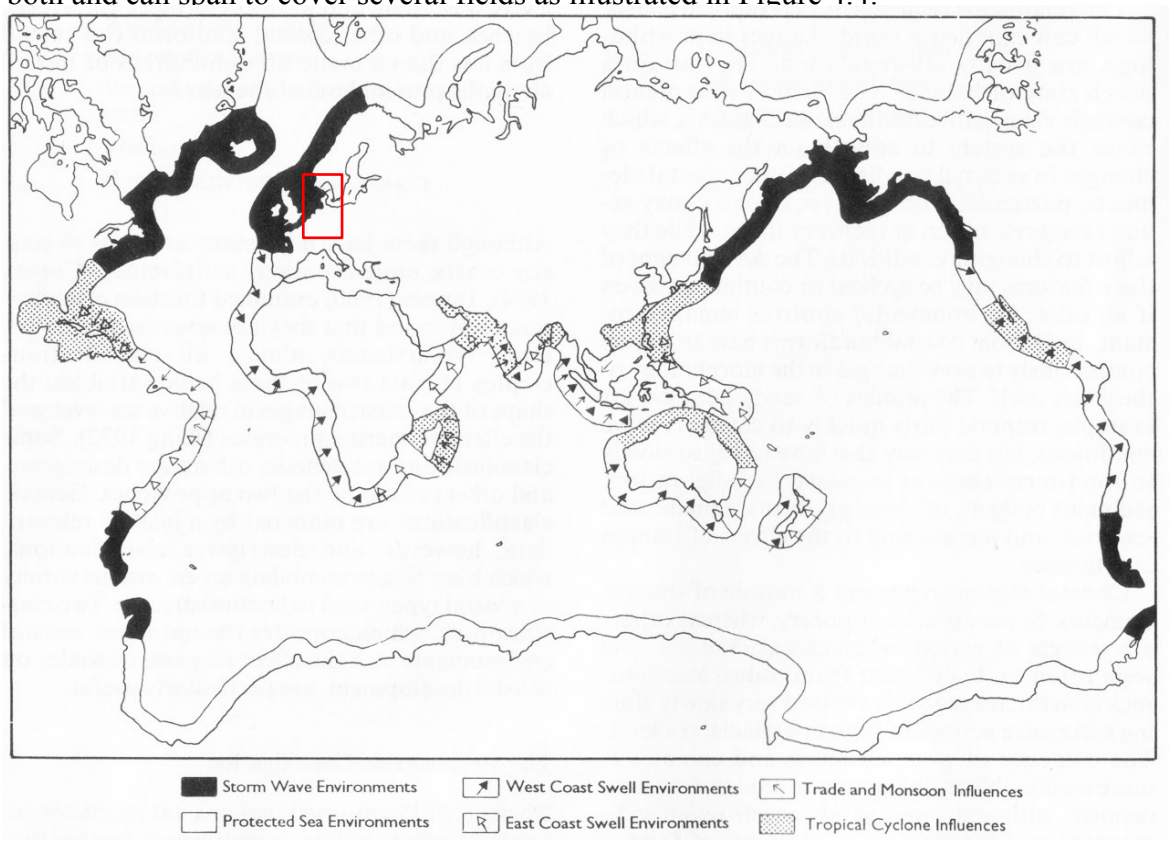

Figure 4.2: Global distribution of wave environments (modified from Davies, 1972), red frame is the Wadden Sea.

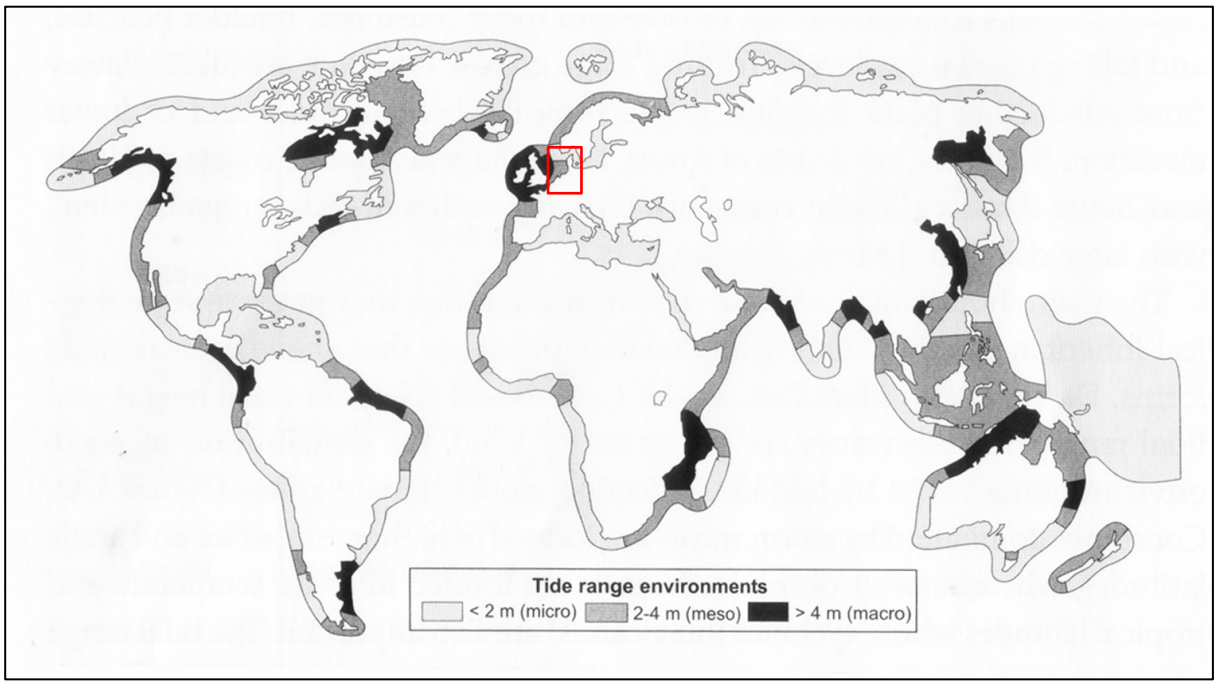

Figure 4.3: Global distribution of mean spring tidal range (Masselink et al., 2003, modified from Davies, 1980).

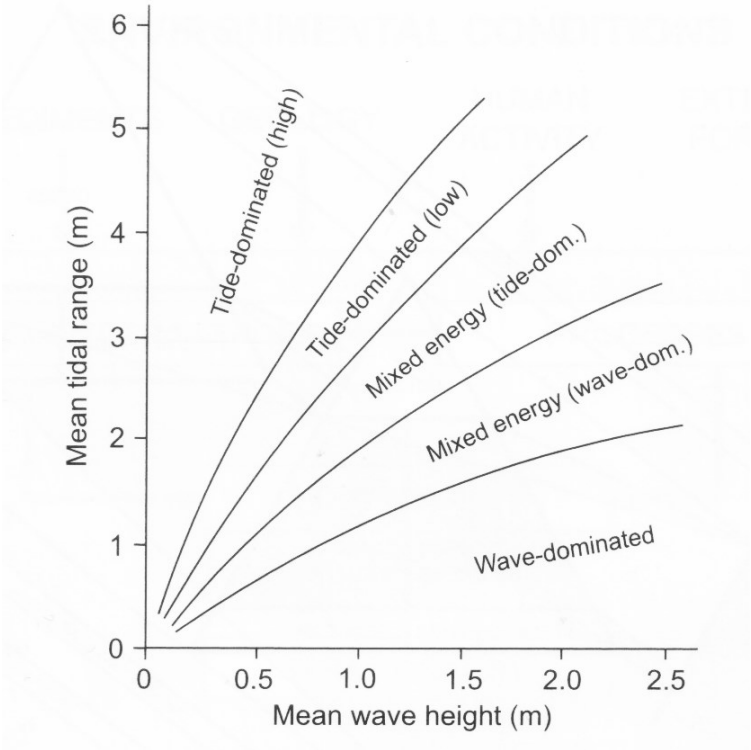

Figure 4.4: Relationship between tidal range and wave height as to wave/tide dominated coastal morphology (modified from Davis and Hayes, 1984).

4.1.2 The Geotectonic Classification

The geotectonic classification was proposed by Inman and Nordstrom (1971). There are three size scales associated with coast in terms of coastal forms globally. They are called as first-, second- and third-order features. The geotectonic classification is according to the first-order feature and three major classes and some subclasses of the coasts. The first-order features are those associated with the moving tectonic plates and of about 1000 km along the coastline, on-off-shore dimensions of about 100 km, and vertical dimensions from sea floor to coastal mountains of about 10 km. The three major classes and subclasses are (Figure 4.5):

1. Collision coasts, on the collision edge of continents and island arcs. They are formed by convergence.

2. Trailing-edge coasts, on the trailing edge or noncollision side of a continent. It has three main types:
   a. Neo-trailing edge coasts are new trailing edge coasts formed near beginning separation centers and rifts. Volcanism and earthquake activities are common along these coasts. Their topography is typically rugged (cliffs and mountains).
   b. Afro-trailing edge coasts are where the opposite coast of the continent is also trailing.
   c. Amero-trailing edge coasts are where the opposite coast of the continent is a collision coast.

3. Marginal sea coasts are the coasts fronting on marginal seas and protected by island arcs from the open sea.

The Wadden Sea belongs to the typical Amero-trailing edge coasts (Figure 4.5, red frame). Amero-trailing edge coasts have large drainage systems with high sediment

supplies. These relatively old coastlines usually possess wide depositional continental shelves. A relatively wide, flat coastal plain occurs landward of these coastlines. Depositional features such as barrier islands, deltas, marshes, mangrove swamps, and tidal flats are common.

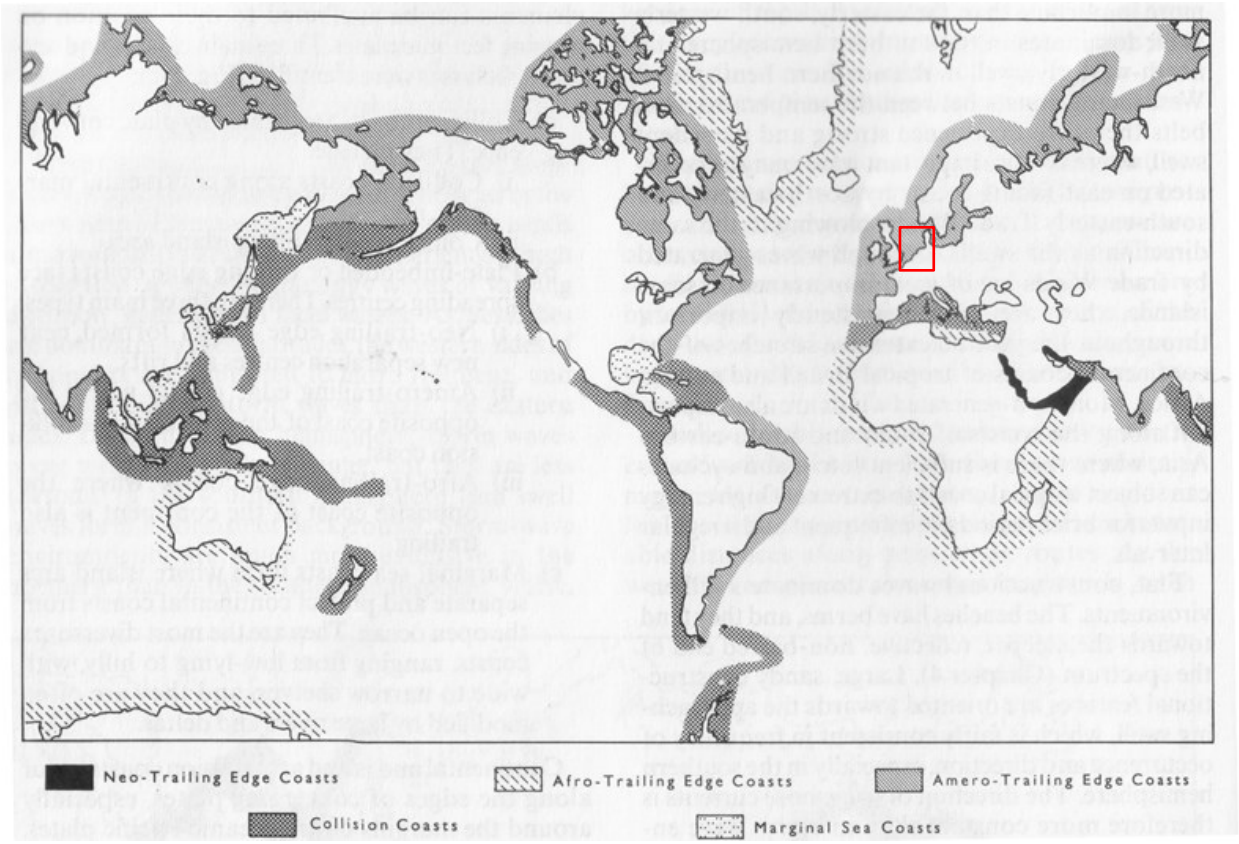

Figure 4.5: The tectonic classification of the coasts, red frame area is the Wadden Sea (modified from Inman and Nordstrom 1971).

4.1.3 Time Scales

Cowell and Thom (1994) classified the time scales and the coastal processes into four overlapping classes (Figure 4.6):

1. Instantaneous time scales: evolution of morphology during a single tidal cycle;

2. Event time scales: evolution of morphology over a time span from one wave/tide event (e.g. storm) or seasons;
3. Engineering time scales: the time scale of years to centuries. It includes the migration of the tidal flat and the deposition of the sediment to sandbars;
4. Geological time scales: the time scale over decades to millennia. It corresponds to the trend of the morphological development and the driving forces of the sea level, climate and tectonics.

The time range of interest here is the 14 years from 1996 to 2009, and the annual changes in this period. We will detect changes on the 'Engineering time scales', and it is also possible overlapped with 'Event time scale'.

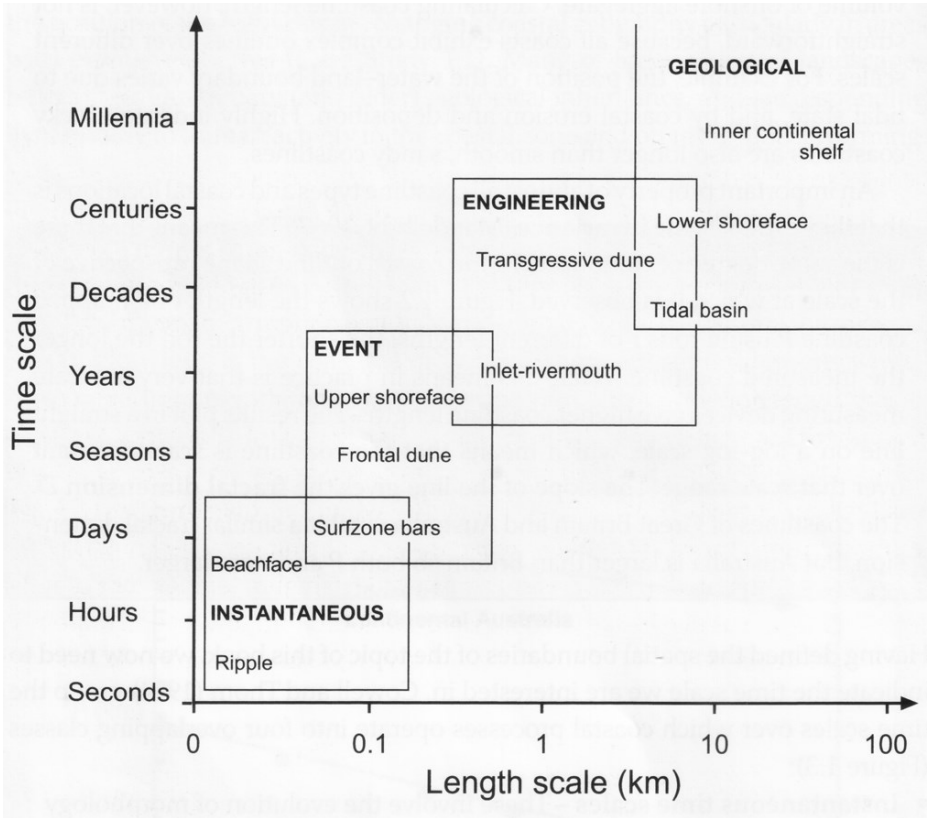

Figure 4.6: Definition of spatial and temporal scales involved in coastal evolution (Cowell and Thom, 1994).

4.2 Topographic Difference Maps of the German Wadden Sea

4.2.1 Motivation and Method

Difference maps are derived by subtracting two topographic maps that represent different years. It is the most straightforward way to illustrate the development and changes between different years and the difference maps give an overview of the research area. The outlines of the entire research area, -2 m isobaths, from 1996 to 2009 are also derived to show morphological development trends for the German Wadden Sea.

Bathymetric data can be used to produce topographic maps and compare the morphological evolution (Winter 2011) of the coastal area. However, because coverage of the bathymetric data is inconsistent within the tidal flat only areas covered by a subsequence of bathymetric data can be compared. Rivers and tidal channels are covered by more frequent surveys than other parts. The echo sounding devices used for this purpose are installed under the ship, so it is difficult to access shallow water areas, which are parts of the tidal flat. A complete survey for the Wadden Sea will typically take five to six years. As a consequence, it is difficult to analyze morphological development on engineering timescales (up to decades) and large spatial scale with echo sounding data.

The advantage of the topographic difference maps produced in this study is that the data consistently cover the whole research area throughout the period of investigation, so that different temporal stages can be compared and changes in space can be quantified.

4.2.2 Results and Discussion

The topographic difference maps presented here use the topographic map of year 1996, the earliest available yearly map in this study, as a reference. Topographic maps for subsequent years are compared to the map from 1996, which results in difference maps between 1996 and 2009, 1996 and 2008, 1996 and 2007, 1996 and 2006, 1996 and 2005, 1996 and 2004, 1996 and 1999, 1996 and 1998, 1996 and 1997, 1996 and 1997 (Figure 4.7: a to i). Different values represent the residual morphological changes between the two different years, in other words, the balance of erosion and sedimentation at each grid cell. Negative values correspond to net erosion, while positive values correspond to net sedimentation.

The most significant change occurred between the years 2009 and 1996 (Figure 4.7a), while morphological differences were smaller over shorter timespans. The greatest morphological change occurred at the outer part of the open tidal flat, in the river/tidal channels, and in the sandbars (as marked in Figure 4.7a). The extent of erosion (negative) towards the north of Medemrinne (tidal channel) was very pronounced, and sedimentation (positive) occurred towards the north of Medemgrund, corresponding to the outlines of the tidal flat (-2 m isobaths, Figure 4.8) with a large shift. Figure 4.8 gives an overview of the morphological development of the entire investigation area. The development occurred gradually year by year and the erosion or sedimentation direction varied locally. The tidal flats attached to the main land (e.g., Trischen, Eider, and Süderoogsand, marked in Figure 4.7a) and the sandbars located near to the open sea (e.g., Tertiussand, D-Steert, and Gelbsand) migrated toward east or southeast, while the sandbar in the Elbe estuary – Medemgrund has opposite development (Figure 4.8).

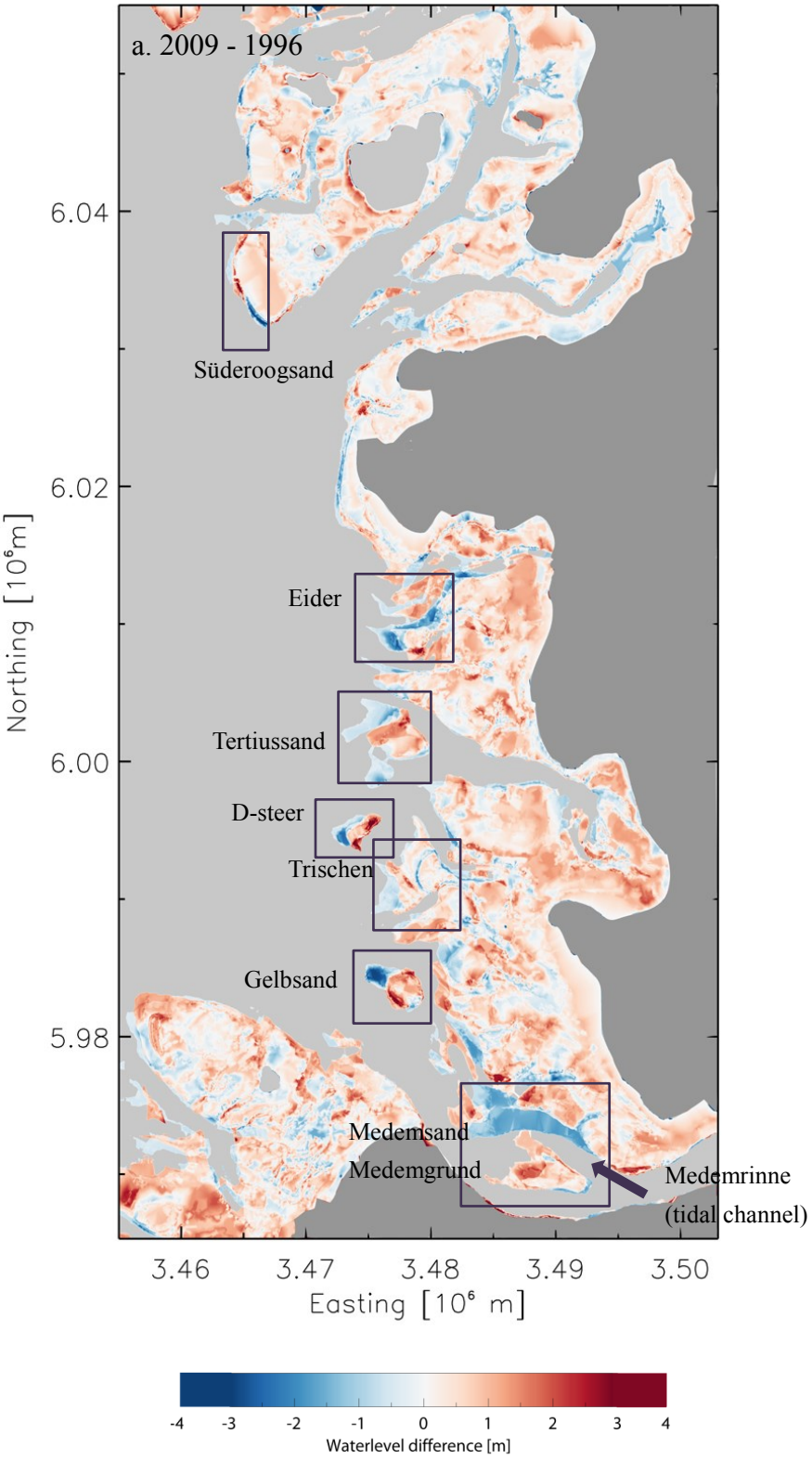

Figure 4.7: Topographic difference maps between the year 1996 and the subsequent years.

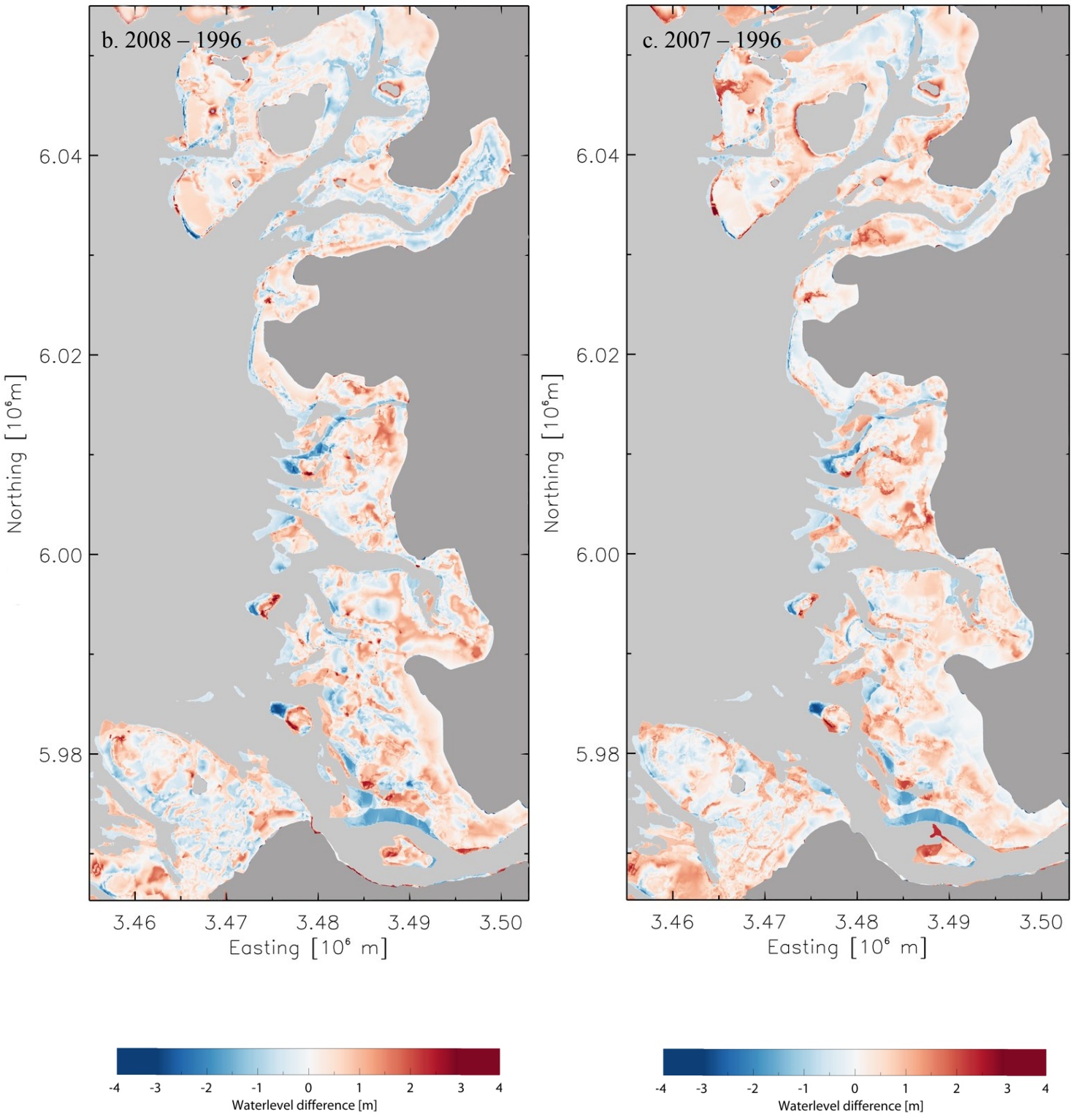

Figure 4.7: (Continued) b. 2008 – 1996; c. 2007 – 1996;

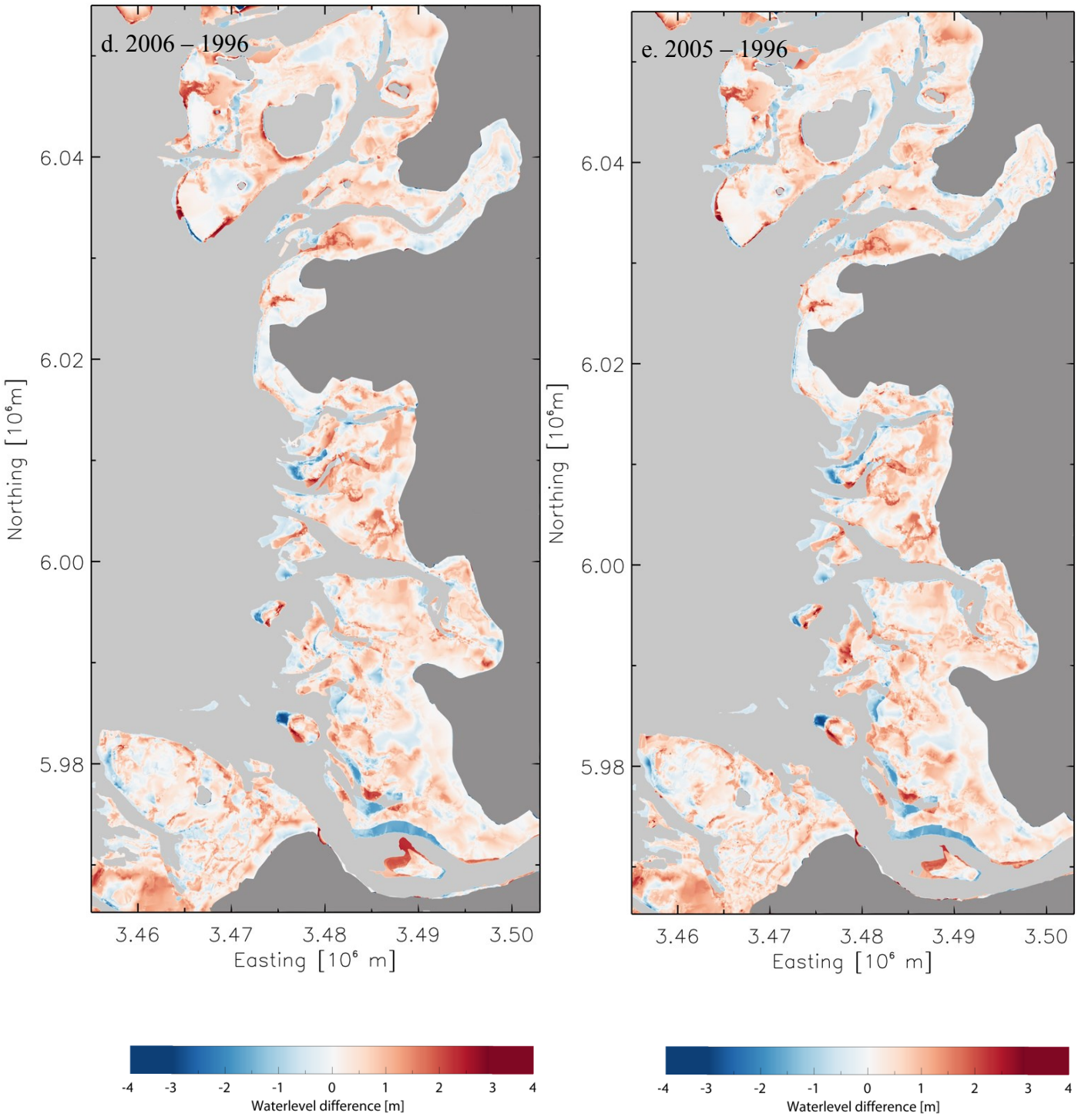

Figure 4.7: (Continued) d. 2006 – 1996; e. 2005 – 1996;

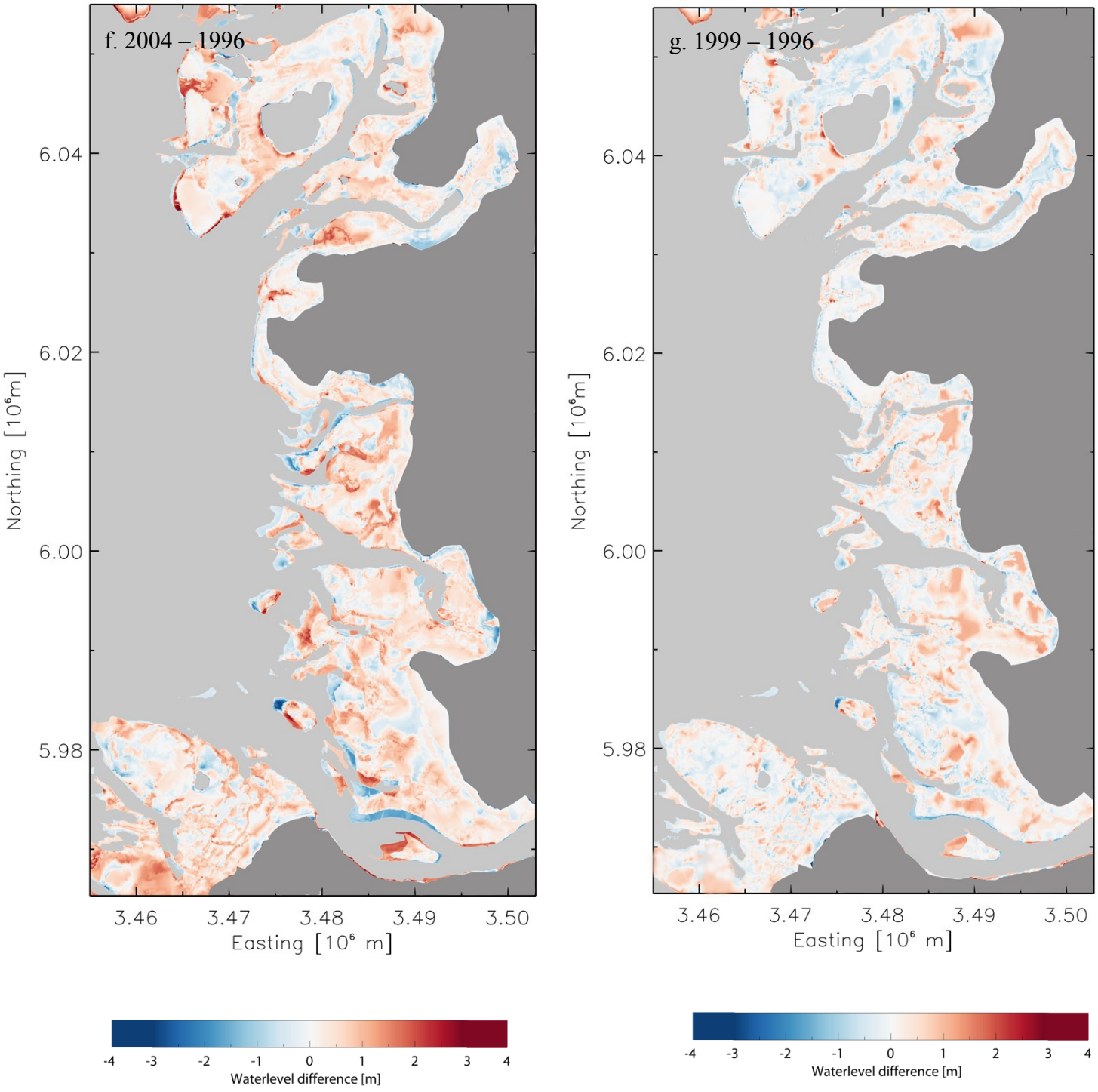

Figure 4.7: (Continued) f. 2004 – 1996; g. 1999 – 1996;

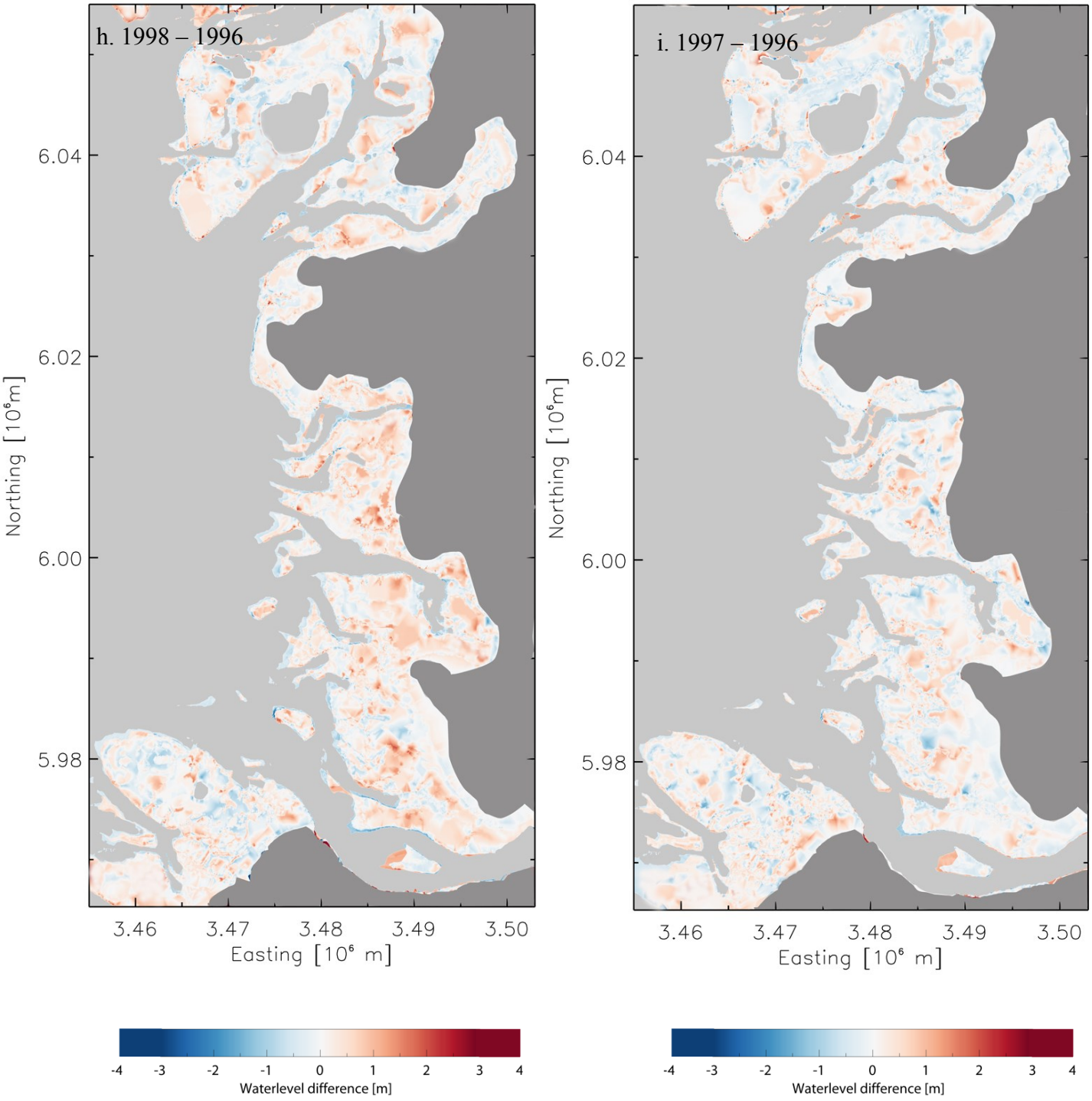

Figure 4.7: (Continued) i. h. 1998 – 1996; 1997 – 1996.

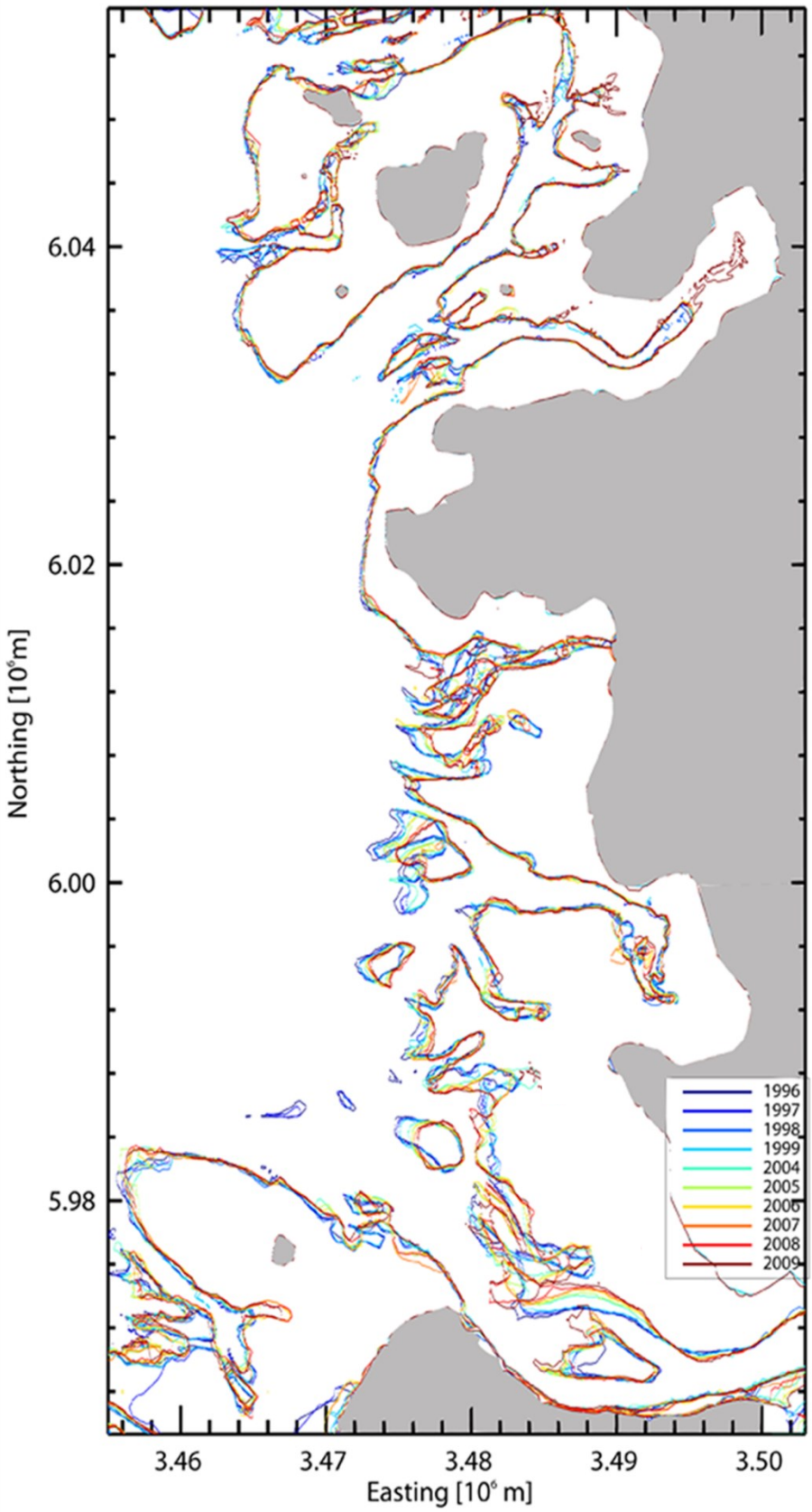

Figure 4.8: Outline of the tidal flat (-2 m isobaths).

4.2.3 Conclusion

The difference maps give an overview of the residual erosion and sedimentation of the German Wadden Sea between year 1996 and subsequent years. Difference maps are able to illustrate morphological development year by year. The most active regions are the outer parts of the tidal flats, the estuaries, and sandbars. Directions of migration can be identified by comparing the outlines of tidal flats (-2 m isobaths) from 1996 to 2009 (Figure 4.8). Sandbars near to the open sea and the outer parts of the open tidal flat were shrinking to the east or southeast (landward), while the Elbe region (Medemsand and Medemgrung) were migrating to north.

The difference maps compare the morphological development between two years, but do not account for all the information available for the period of investigation. Bed Elevation Range (BER) will be derived in the next section to account for information over the full duration of the period of investigation.

4.3 Morphodynamics of the German Wadden Sea

On-land and marine processes are continuously interacting to make tidal flats one of the most dynamic environments on the planet. It is crucial to understand and evaluate morphodynamics of tidal flats to discover their evolutionary trends under natural forcing and human influence. Coastal morphodynamics were described by Wright and Thom (1977) in terms of coastal processes and their associated morphological responses, which included mutual adjustment of the hydrodynamics, sediment transport, erosion, sedimentation, and coastal morphology.

Several studies have described the morphology and dynamics of the Wadden Sea tidal flat. Albers and von Lieberman (2010) used field measurements and modeling to investigate the morphodynamics of the Neufelder Watt in the Elbe estuary for selected days in the year 2006, 2007, and 2008. Niedermeier et al. (2005) studied the

topography and morphodynamics of the Elbe estuary with SAR and optical images, but it was not continuous annual covered data. Numerical modeling were applied to study the morphodynamics in the Wadden Sea as well (Lesser G.R. et al., 2004; Winter, 2004; Chu et al. 2013; Kösters and Winter, 2014), but in the absence of remote sensing data-based morphodynamics analysis over the large spatial scale of the German Wadden Sea. In this chapter, a data-based analysis will be presented and discussed to show the morphodynamics of the German Wadden Sea (North Frisian and the Cuxhaven-Neuwerk regions) on an 'engineering timescale' (from 1996 to 2009).

Morphological changes are defined as the temporal change in form or shape of the tidal flat by four parameters:

1. Bed Elevation Range (BER):

It is the difference between the maximum and the minimum of the bed elevation within the observation time frame (Winter, 2011).

$$BER_{i,j} = Max(z_{i,j}(t)) - Min(z_{i,j}(t))$$

$z_{i,j}(t)$ is the bed elevation at grid point (i, j) at time t. $Max(z_{i,j}(t))$ is the maximum elevation through time period t and $Min(z_{i,j}(t))$ is the minimum elevation through time period t. The BER map can provide the vertical extent of the morphodynamics, but cannot give information about the direction (erosion or sedimentation) of the morphodynamic process through the time period.

2. Vertical nodal linear regression:

It is the slope of the linear regression of all the bed elevation in the stacked time series (1996 to 1999, and 2004 to 2009) at each grid node.

Values quantify the speed and the sign of the morphologic evolution, whereby negative values represent a decreasing trend, and positive values represent an increasing trend. Higher absolute values indicate higher rates of change.

3. Turnover height and net balance height:

The turnover height is the mean of the absolute topographic height change within

a given time interval. It represents the total movement of the tidal flat elevation. The turnover height for the German Wadden Sea is calculated relative to the reference year, 1996. For example, the turnover height between 1996 and 1999 is calculated by first calculating the absolute height difference at each grid cell between 1996 and 1999. Second, the absolute values are summed and divided by the total grid cell number to represent the mean of the total elevation difference over the whole region. The result is the turnover height between 1996 and 1999. All the other years' turnover heights are derived using the same approach.

The net balance height is similar to the turnover height but with sign (not the absolute value of the change). Net balance height changes (i.e., sedimentation or erosion) are relative to the reference year, 1996.

4.3.1 Bed Elevation Range

4.3.1.1 Results

The BER at each grid point in the topographic map represents the residual of erosion and sedimentation over the 1996 to 2009 period of investigation. This parameter accounts for all elevation information obtained for the time of interest and represents the morphological evolution intensity over that timeframe.

Figure 4.9 shows the distribution of the parameter BER for the German Wadden Sea. The temporal coverage of the data used to calculate BER is from 1996 to 2009 with a data gap for the 2000 to 2003 time period. All data have the same spatial and temporal coverage with consistent methods. Because the topography of the tidal flat was between -2 m and 2 m, the BER ranged from 0 to 4 m.

Results show that BER with higher value (i.e., over 2 m) areas are mostly along the outer part of the tidal flat, especially in the regions: (a) outer part of Scharhörn; (b) Medemsand and Medemgrund; (c) Gelbsand; (d) Trischen; (e) D-Steert; (f) Tertiussand; (g) Eider; (h) Süderoogsand; (i) Norderoogsand; (j) Japsand.

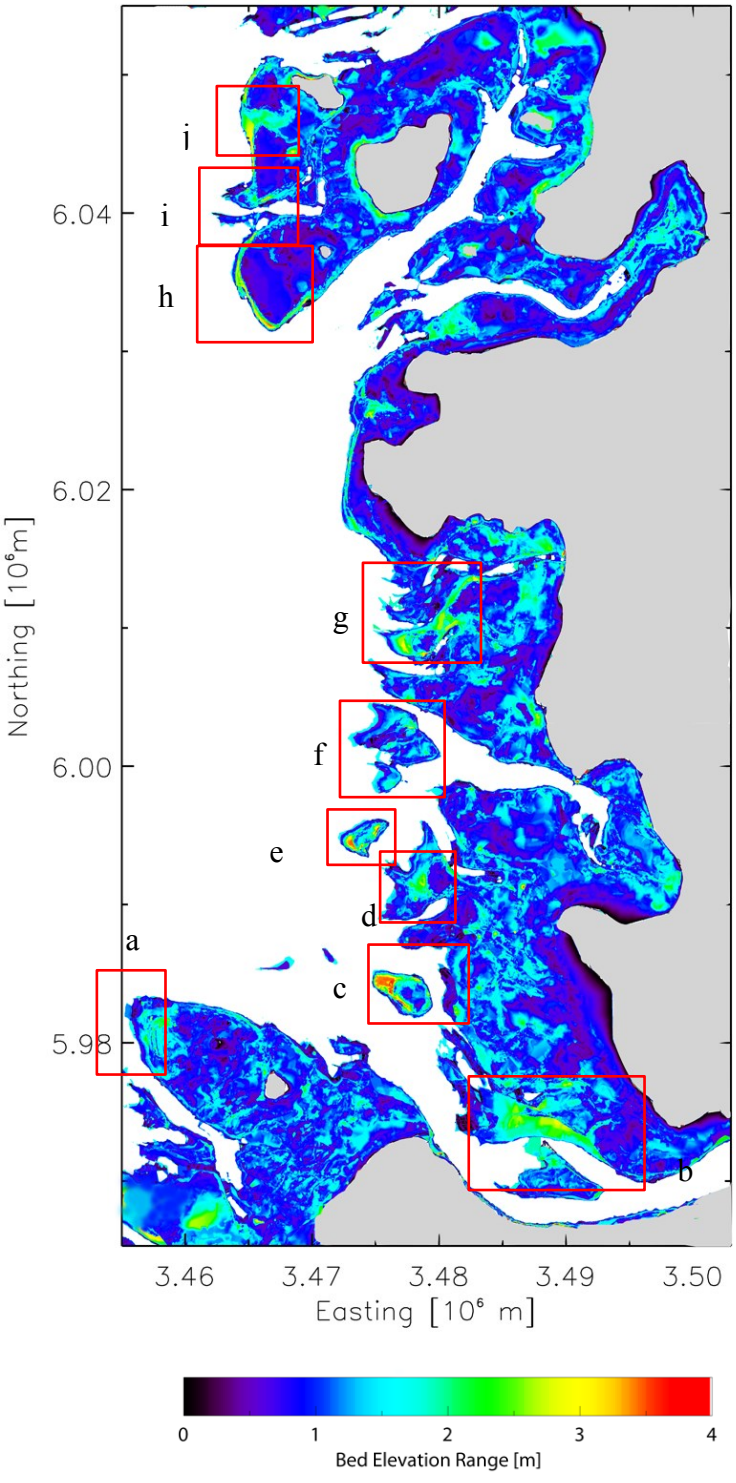

Figure 4.9: BER (Bed Elevation Range) of the German Wadden Sea (1996-2009). (a) outer part of Scharhörn; (b) Medemsand and Medemgrund; (c) Gelbsand; (d) Trischen; (e) D-Steert; (f) Tertiussand; (g) Eider; (h) Süderoogsand; (i) Norderoogsand; (j) Japsand.

Another way to calculate BER is using the bathymetric data mentioned in 1.4.1 provided by BSH. There are some restrictions of the bathymetric data discussed in 4.2.1. Some regions have more intensive surveys, such as the main shipping channels (for security reason), while other parts have less frequent data coverage. It is challenging to reach shallow water areas with ship-based measurements.

Bathymetric data are confined from -2 m to 2 m, the same range as the topography results of this work, to compare the results to the same standard. BER was calculated for the same time period (1996 to 2009), shown in Figure 4.9 and Figure 4.10, where the greatest morphological change occurs in the outer part of the tidal flat, the sandbars, and the river/tidal channels. Because of the restrictions of the bathymetry based map, the morphological changes in the tidal flat contain less detail compared to Figure 4.9.

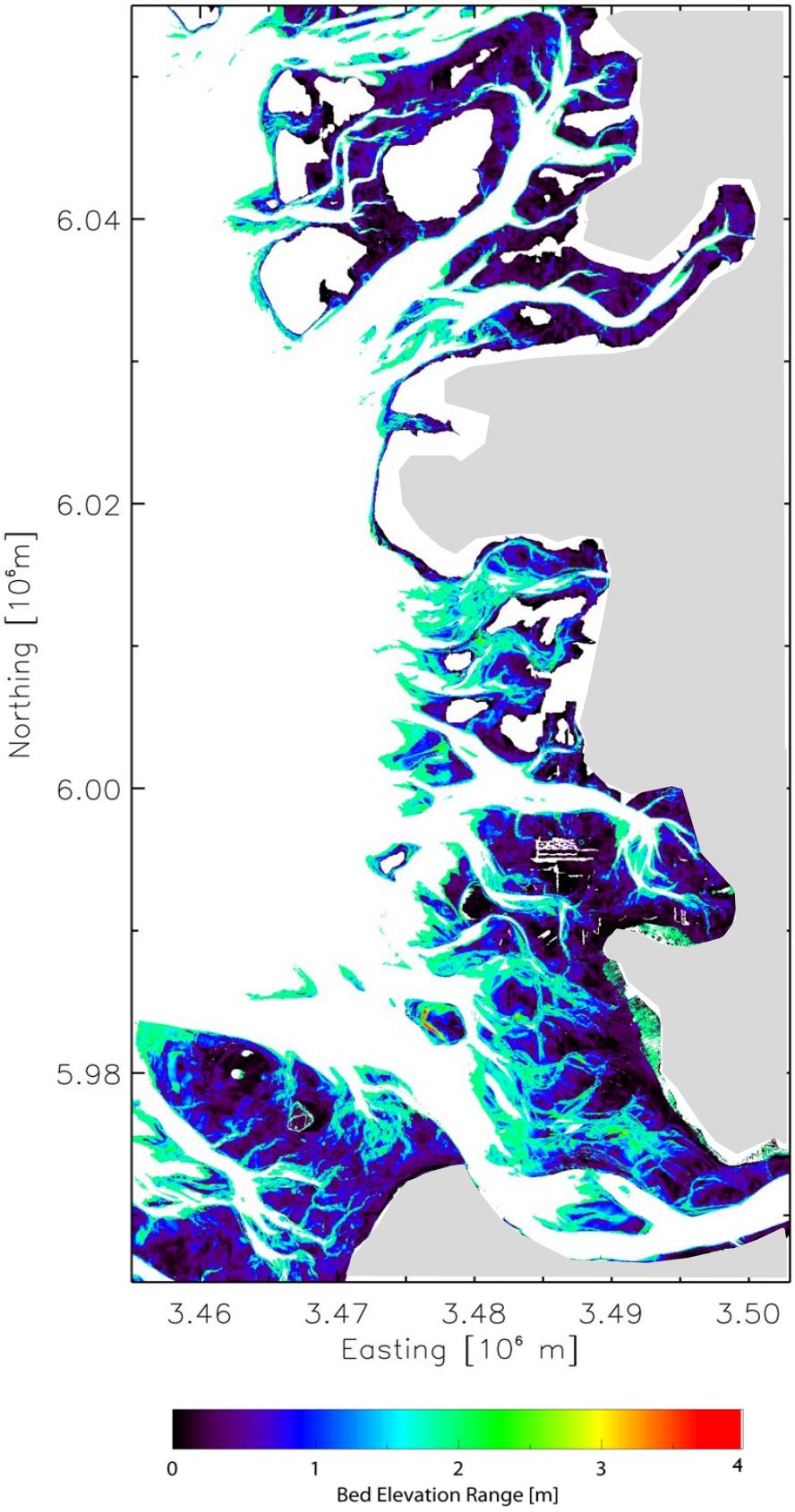

Figure 4.10: BER calculated from bathymetric data.

4.3.1.2 Discussion and Conclusion

Our study focuses on the morphodynamic activities within the tidal flat area. The BER map derived by bathymetric data (Winter, 2011) is not only for the tidal flat area, but also for the deeper water channels and includes part of the open sea. Due to the restriction of the data, the coverage is limited in the tidal flat area. The BER distribution map generated from the waterline method visualizes the morphodynamic activities in the German Wadden Sea by considering all the elevation information from 1996 to 2009, which cannot be captured by difference maps.

Morphology of the tidal flat is mainly controlled by two factors — tides and waves. Waves are mainly generated by wind with the predominant winds originating from the west in the German Wadden Sea. The outer part of the open tidal flats and the west part of the nearby sandbars are extensive breaker zones, which makes them morphodynamically active zones. Medemgrund and Medemsand are located in the Elbe estuary and dominated by tidal activity (Krösters and Winter, 2014) instead of energy in the wave breaking zone. They have strong morphodynamic activities at northwest part and south part, respectively.

BER includes all the available data during the timeframe and shows the intensity of morphological activity; however, BER does not describe how the evolution went through the time period. BER patterns in the German Wadden Sea capture where large morphological activities occur and where morphology stays relatively stable.

4.3.2 Vertical Nodal Linear Regression of the German Wadden Sea

Previous studies of the seabed dynamics are mainly focused on small scales with specific local conditions in the Wadden Sea (Knaapen, 2005; Buijsman and Ridderinkhof, 2008; Dorst et al., 2009; Albers and von Lieberman, 2010; Dorst et al., 2011). Although BER is capable to describe the intensity of the overall morphodynamics of the tidal flat, it cannot capture the morphological evolution trend (erosion or sedimentation) or rate of change. In this study, we derived the vertical nodal linear regression of the elevation within the period of investigation at each grid cell, give the quantified morphological evolution on a large scale, and increase our insight and understanding of the morphology evolution process. The description of the method is at the beginning of 4.3.

4.3.2.1 Results

Figure 4.11 shows an overview of the quantified vertical nodal linear regression in the German Wadden Sea. In this figure, erosion (negative value) is color coded as blue, while sedimentation (positive value) is color coded as red, whereas dark blue and dark red represent the most dynamic regions.

Overall, the vertical dynamic trend of the German Wadden Sea is typically from -0.1 m/yr to 0.1 m/yr, with extreme values of $\pm$0.4 m/yr. The averaged vertical dynamic trend of the whole study area is 6.02 mm/yr, which indicates that sedimentation is stronger than erosion during the period of investigation (1996 to 2009). The highly dynamic areas correspond well with high BER values (Figure 4.9). Medemsand had a large erosion rate of up to 0.2 m/yr toward the north, which changed from one long sand bank attached to the coast into two nearly separate sand banks.

The sandbars (Gelbsand, D-Steert, and Tertiussand) all have the same significant migration trend. Erosion occurred along the western part of the sandbars and sedimentation occurred on the eastern part. Gelbsand exhibits the greatest morphological change and highest rate of change, with erosion rate over -0.3 m/yr, and sedimentation rate is up to 0.36 m/yr.

The open tidal flat areas (Eider, Trischen) also eroded in the same direction (toward the east) as the sandbars, but at a lower rate (between 0.1 and 0.2 m/yr). The outer part of Süderoogsand has two patterns: sedimentation at the northern outer part with the highest rate up to 0.3 m/yr, and erosion at the southern outer part with the lowest rate up to -0.3 m/yr.

4.3.2.2 Discussion and Conclusion

The vertical nodal linear regression indicates a positive (sedimentation) or negative (erosion) trend, which is a further analysis comparing to BER. Van Dijk et al. (2012) analyzed vertical nodal linear regression, and mainly focused on the seabed dynamics of the large-scale continental shelf of the Dutch Wadden Sea. This study covered the coastal zone, but did not provide a detailed analysis of the Dutch tidal flat. Prior to our study, the vertical nodal linear regression in the German Wadden Sea was not examined. Our analysis gives an overview of the vertical dynamic trend at the large-scale of the German Wadden Sea (North Frisian and Cuxhaven, Neuwerk regions), and also gives a detail look of the high dynamic areas.

This vertical dynamic trend quantifies the erosion and sedimentation rate at a large scale over a period of 14 years. During this time, the morphodynamic trend of the German Wadden Sea varies from from -0.4 to 0.4 m/yr with average value 6.02 mm/yr, which indicates sedimentation over the period of investigation.

Overall patterns of the vertical dynamic trend strongly agree with the BER analysis. The outer part of the open tidal flats, sandbars, and tidal/river channels are

the most dynamic areas with high rates of erosion and sedimentation. The lowest vertical dynamic value occurs in the sandbars (Gelbsand, Trischen, and D-Steert), where western parts all suffered from erosion due to the wave energy breaking zones. Medemsand has large area that is dominated by erosion (negative value), while its adjacent sandbar Medemgrund has opposite evolution due to the influence of tide and Elbe River.

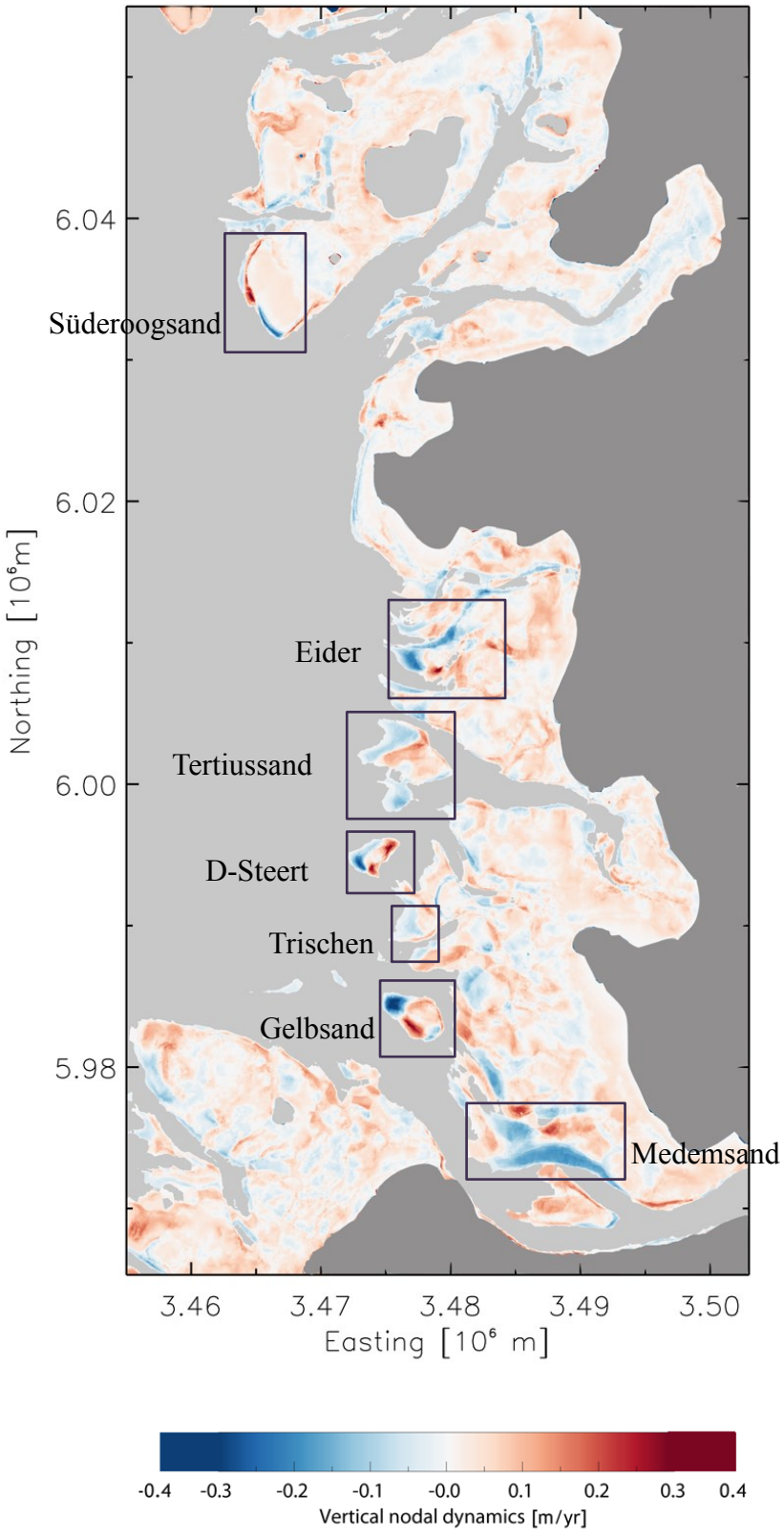

Figure 4.11: Vertical nodal linear regression at the German Wadden Sea.

4.3.3 Turnover Height and Net Balance Height

4.3.3.1 Motivation

A tidal flat will cause wave energy to dissipate and thus contribute to protect the coastline from erosion. Change of height in a tidal flat can be used to determine an overall increasing or decreasing trend. Decreasing height of the tidal flat will put the coast in danger of being eroded by wave and tide action.

4.3.3.2 Results

Figure 4.12 shows the turnover height and net balance height results from a linear fit and Pearson's correlation coefficient R. The turnover height has an obvious overall increasing trend from 1996 to 2009. The linear fit has a RMSD (Root Mean Square Different) of 38 mm and R value of 0.975 for a clear increasing fit at rate of 8.2 mm/yr. The net balance height is half of the turnover height due to erosion with RMSD of 34 mm. It also has an increasing trend of 6.8 mm/yr and R equals to 0.913.

These results represent the change in height for the whole research region, which may vary locally. The maximum turnover height is between 1996 and 2009 which is 0.22 m, while the maximum net balance height is between 1996 and 2006 which is 0.10 m. Positive values of the net balance height indicates that sedimentation is stronger than erosion over the 14 year period.

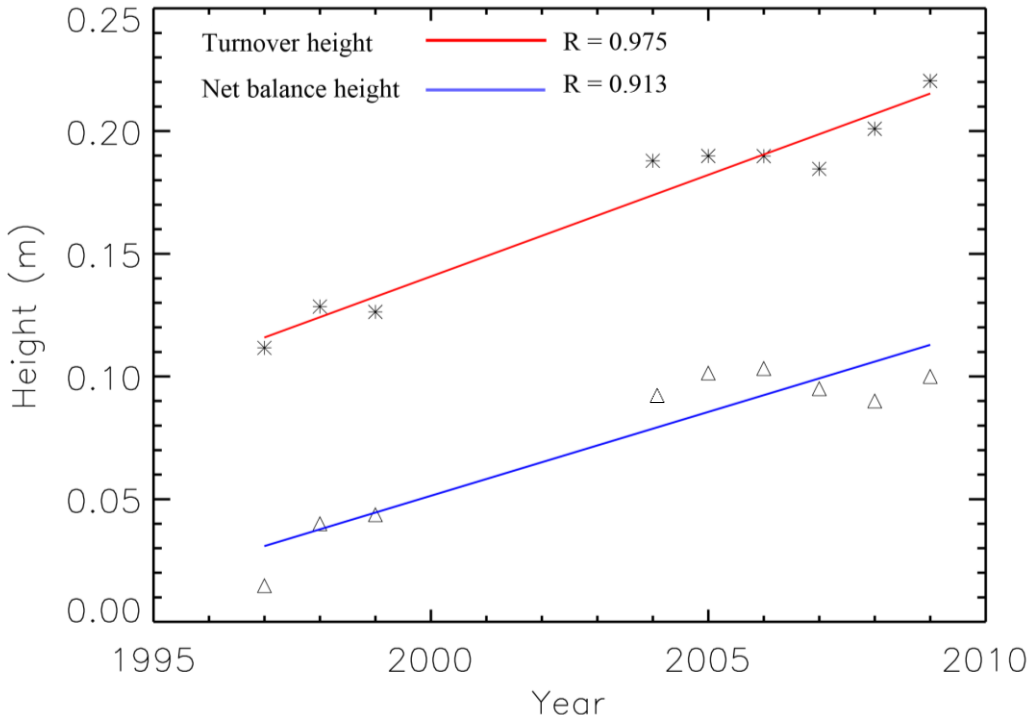

Figure 4.12: Turnover height of the German Wadden Sea.

4.3.4 Sandbars

Sandbars in the tidal flat are submerged or partly exposed ridges of sand near the shore line. Their development is strongly influenced by sediment transport, tides, waves, wind, extreme events, human intervention, and the interaction with other tidal flat areas. Tertiussand, Trischen, D-Steert, Gelbsand, and Medemsand/Medemgrund (Figure 4.9) show strong morphological development based on the difference maps, BER analysis, and vertical nodal linear regression.

4.3.4.1 Morphological Development Results

Figure 4.13 to Figure 4.16 display the topographic maps of the Tertiussand, Trischen, D-Steert, Gelbsand, and Medemsand/Medemgrund from the years 1996 to 1999 and 2004 to 2009. These maps illustrate the four most dynamic regions from 1996 – 1999 (year group A) and 2004 – 2009 (year group B).

Most of Tertiussand is below mean sea level, and sandbars (Figure 4.13) were clearly composed of two bars and a tail at the southern part (marked) from 1996 to 1999. The tail vanished in the maps of year group B, and could not be detected after 2007. The two parts of the sandbar gradually merged into one by 2009.

The shape of D-Steert was approximately an ellipse in year group A (Figure 4.14), but became thinner and a more curved in the middle with a pointing tip at the south end in year group B. Trischen did not change as strong as D-Steert. The fan shape remained intact during the period of investigation.

Gelbsand had a very clear ellipse shape in year group A with two relatively high value parts located at the west and east heads (Figure 4.15). The western head presented in year group A moved to the former center of Gelbsand, and the eastern head vanished by year group B.

Medemgrund (Figure 4.16) expanded northward. The south tidal flat line of Medemsand eroded northward, and Medemsand itself became thinner and thinner. The sandbar is also mostly below the sea level.

4.3.4.2 Discussion

Morphological development of the sandbars Tertiussand, Trischen, D-Steert, Gelbsand, and Medemsand/Medemgrund are shown as cold color tones for year group A (1996-1999) and warm color tones for year group B (2004-2009), which illustrates their -2 m isobaths outlines (Figure 4.17- Figure 4.20). All of the four sandbars developed significantly from 1996 to 2009. Four main features characterize this evolution for Tertiussand (Figur 4.17). First, the sandbar area decreased from 1996 to 2009, especially the southern part (marked) which could not be detected after 2007. Second, the west bank border of Tertiussand moved southeastward. Third, the east bank was relatively stable. Fourth, Tertiussand was composed of two sandbars that moved towards each other from 1996 to 2009, so that they are much closer to each other in year group B relative to year group A. The outlines of D-Steert (Figure 4.18)

relocated about 1.2 km toward the east, and the southern tip of Trischen (Figure 4.18, marked) moved about 1.6 km toward the east. The northern part of Trischen was relatively stationary. The outlines of Gelbsand (Figure 4.19) changed drastically during the period of investigation. The west bank border outlines of Gelbsand moved in a southeast direction (landward) about 1.6 km, and the east bank remained stationary. Tertiussand, Trischen, and Gelbsand show similar patterns of erosion on their west banks and relatively stable east banks.

In contrast, Medemsand/Medemgrund (Figure 4.20) developed differently. Medemgrund's west bank moved to the northwest instead of regressing to the southeast and its east bank remained stable. The outlines of Medemsand (Figure 4.20, arrow) moved about 2.2 km to the north from 1996 to 2009, which was verified by bathymetric data from BSH that showed the same trend (Chu et al., 2013). The morphologically changing of Medemgrund is also documented on historical maps from 1655 until 1910 (Figure 4.21). The historical maps illustrate that Medemgrund was composed of multiple sandbars in the years 1655, 1789 and 1811, which merged into one single sandbar after 19 century. Topographic maps generated from 1996 to 2009 fit the historical trend shown on the historical maps.

The environmental conditions (as discussed in 4.3.1) of Tertiussand, Trischen, D-Steert, Gelbsand and Medemsand/Medemgrund are quite different. Medemsand/Medemgrund is located in the Elbe estuary where the migration of tidal channels is strongly influenced by tidal asymmetry, which is the differences in magnitude and duration between ebb and flood tidal current and also associated with the development of adjacent sandbars. The Elbe estuary is dominated by tidal energy, while sandbars in Dithmarschen Bight are mainly controlled by waves and a mixture with tidal and wind energy. Thus, the sandbars except Medemgrund/Medemsand are located at the outer parts of the open tidal flat; they face most of the high energy wave and tide arriving from west side. These explains the opposite development directions.

Figure 4.22 illustrates the calculated areas of sandbars in the study area. Sandbar area in Tertiussand and Gelbsand decrease, while in Medemgrund increases. All these

three sandbars have a linear fit with absolute value R above 0.81, which indicates a strong relationship. However, sandbar areas of Trischen and D-Steert have no clear increasing or decreasing trend. They did not continually reduce or increase. If only considering the earliest year 1996 and the latest year 2009, the area of D-Steert and Trischen both have reduced about 0.732 km^2 and 4.49 km^2, respectively.

Three cross sections were chosen to investigate the elevation changes of Tertiussand, Gelbsand and Medemgrund (see the dash lines in Figure 4.17, Figure 4.19, Figure 4.20). The elevations were averaged for year group A and year group B and illustrated with thicker lines in Figure 4.23, Figure 4.24, and Figure 4.25. Average elevation lines of year group A and B keep similar shape at these three sandbars, and year group B is higher than year group A. Table 4.1 gives detail numbers of the average elevation and its changes. Elevation of Gelbsand increased most, by 0.44 m, while Medemgrund increased least, by 0.13 m. Their increasing fits into the overall elevation rising discussed in 4.3.3. However, all three sandbars rise between 2.1 and 7.2 times faster than the overall Wadden Sea elevation (6.8 mm/yr). The increasing elevation of the sandbars might relate to the sea level rising. The concept model (Flemming and Bartholomä, 1994) indicated that the elevation of the tidal flat follows the sea level rising. The sediment supply for the increasing elevation has two kinds of income — internal and external. Tertiussand and Gelbsand locate in the open sea and both of them have reducing tidal flat area through the investigation period. Their elevation increasing could relate to their internal sediment redistribution. Medemgrund has increasing tidal flat area, but Medemsand has significant erosion (Figure 4.20) and the Elbe River is also able to bring in extra sediment. These could be the compensated external source for Medemgrund's elevation rising.

4.3.4.3 Conclusion

Sandbars are the most dynamic regions in the research area and they can be quantified in our study. Tertiussand, Trischen, D-Steert, and Gelbsand are located in the outer parts of the main tidal flat, so similar development trends and directions are exhibited such as southeast migration from 1996 to 2009. Tertiussand and Gelbsand show clear

decreasing area. Medemsand/Medemgrund are located in the Elbe estuary and have a contrasting development when compared to the other sandbars. Medemgrund expanded toward the northwest, while Medemsand eroded largely to the north. The elevation of each sandbar in Tertiussand, Gelbsand and Medemgrund increased increased from year group A to year group B based on cross sections. Internal sediment redistribution may explain the increasing elevation and decreasing area of Tertiussand and Gelbsand. External sediment compensation may explain the increasing in both area and elevation of Medemgrund. Differences in migration are due to location and dominant mechanisms for erosion and sedimentation.

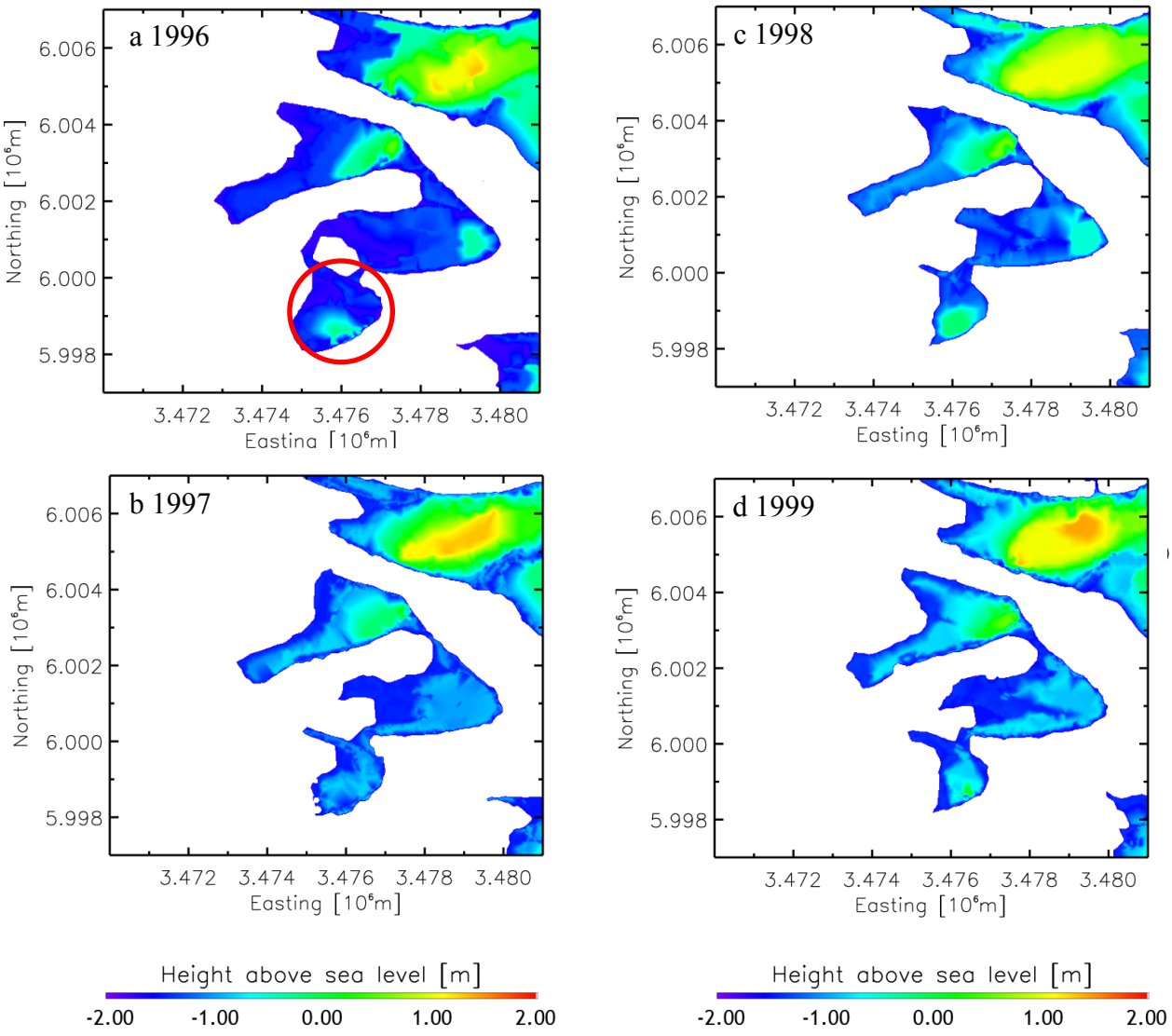

Figure 4.13: Tertiussand from 1996-1999 and 2004-2009 (a: 1996; b: 1997; c: 1998; d: 1999; e: 2004; f: 2005; g: 2006; h: 2007; i: 2008; j: 2009).

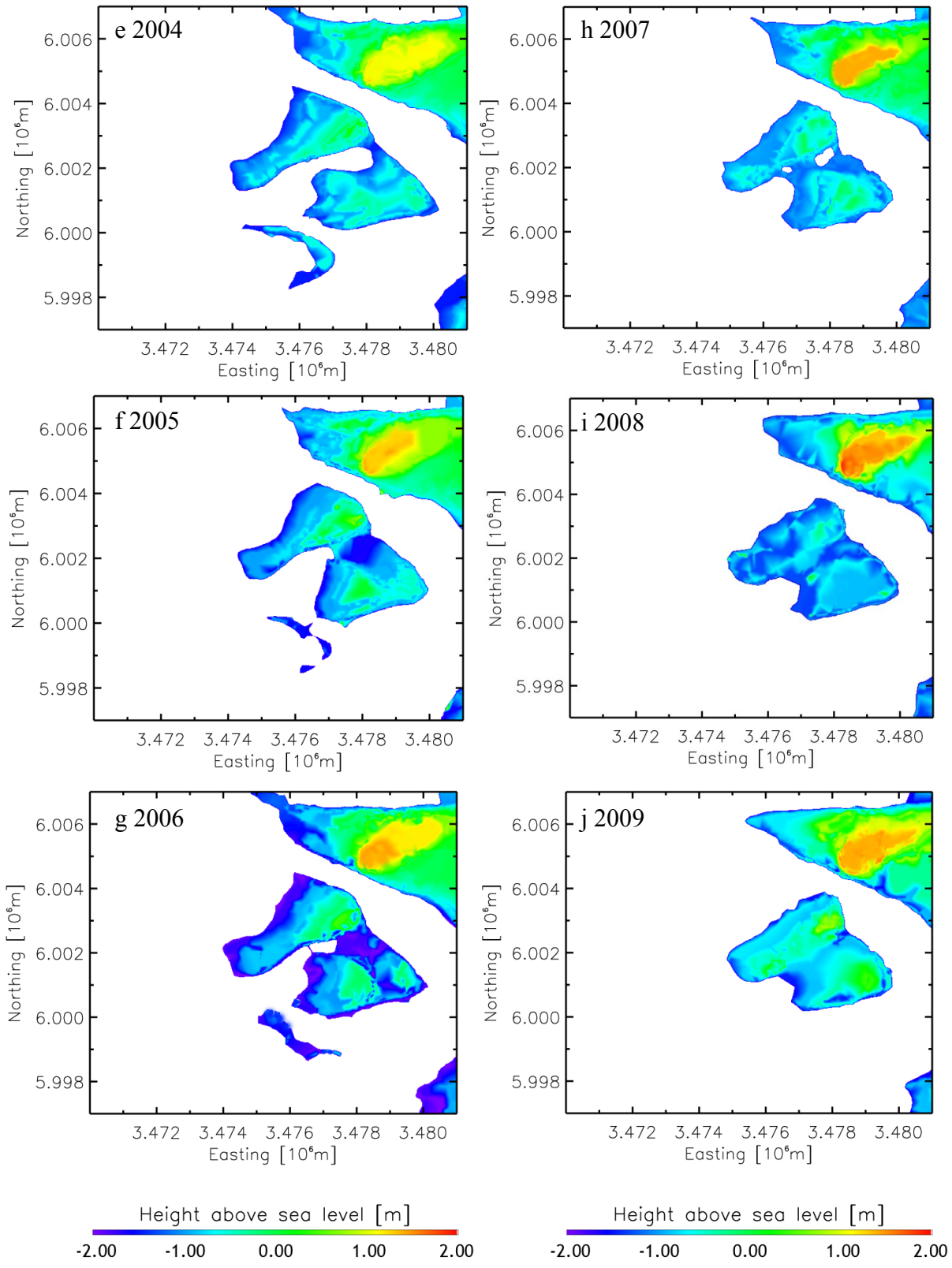

Figure 4.13: (Continued).

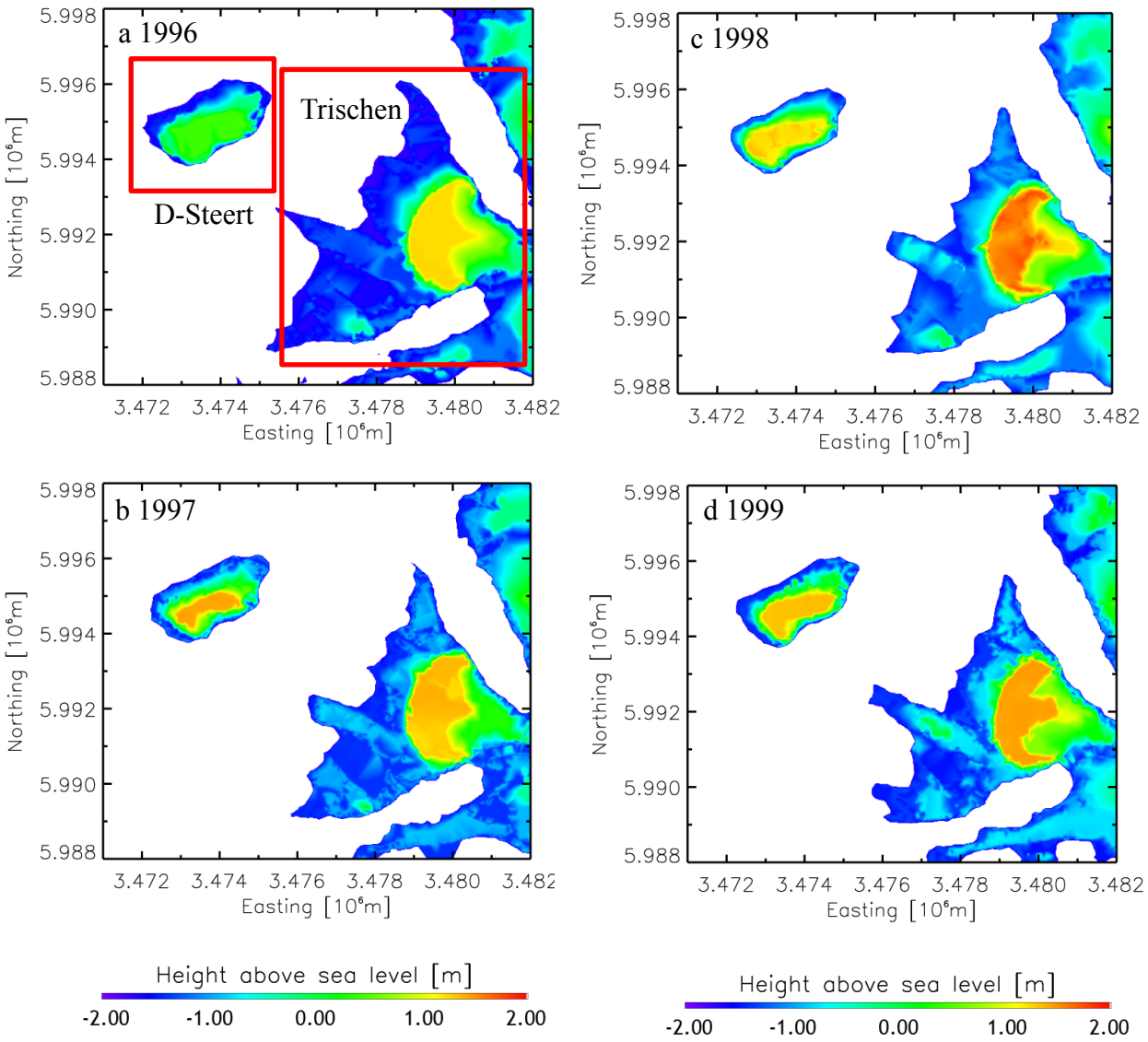

Figure 4.14: Trischen and D-Steert from 1996-1999 and 2004-2009 (a: 1996; b: 1997; c: 1998; d: 1999; e: 2004; f: 2005; g: 2006; h: 2007; i: 2008; j: 2009).

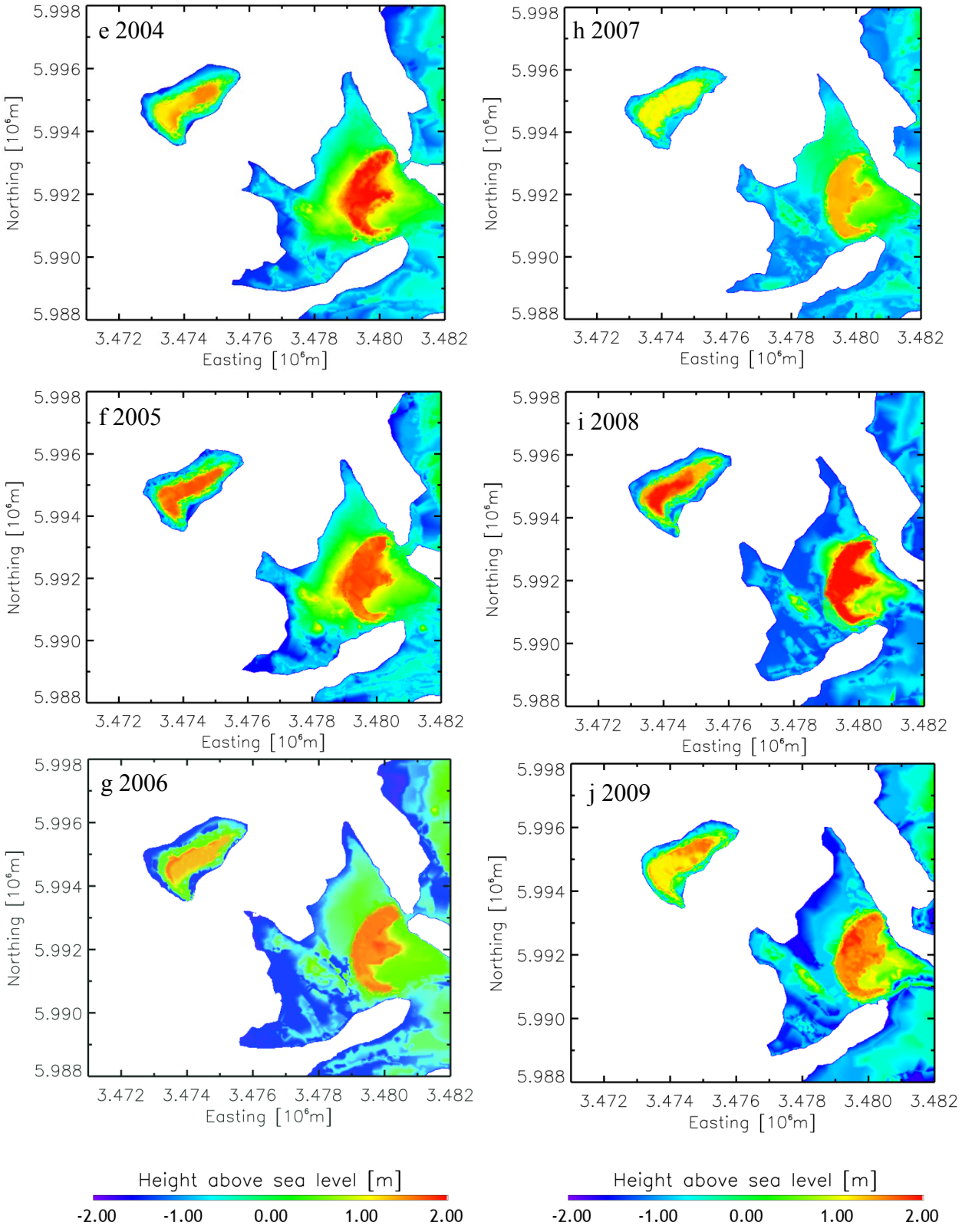

Figure 4.14: (Continued).

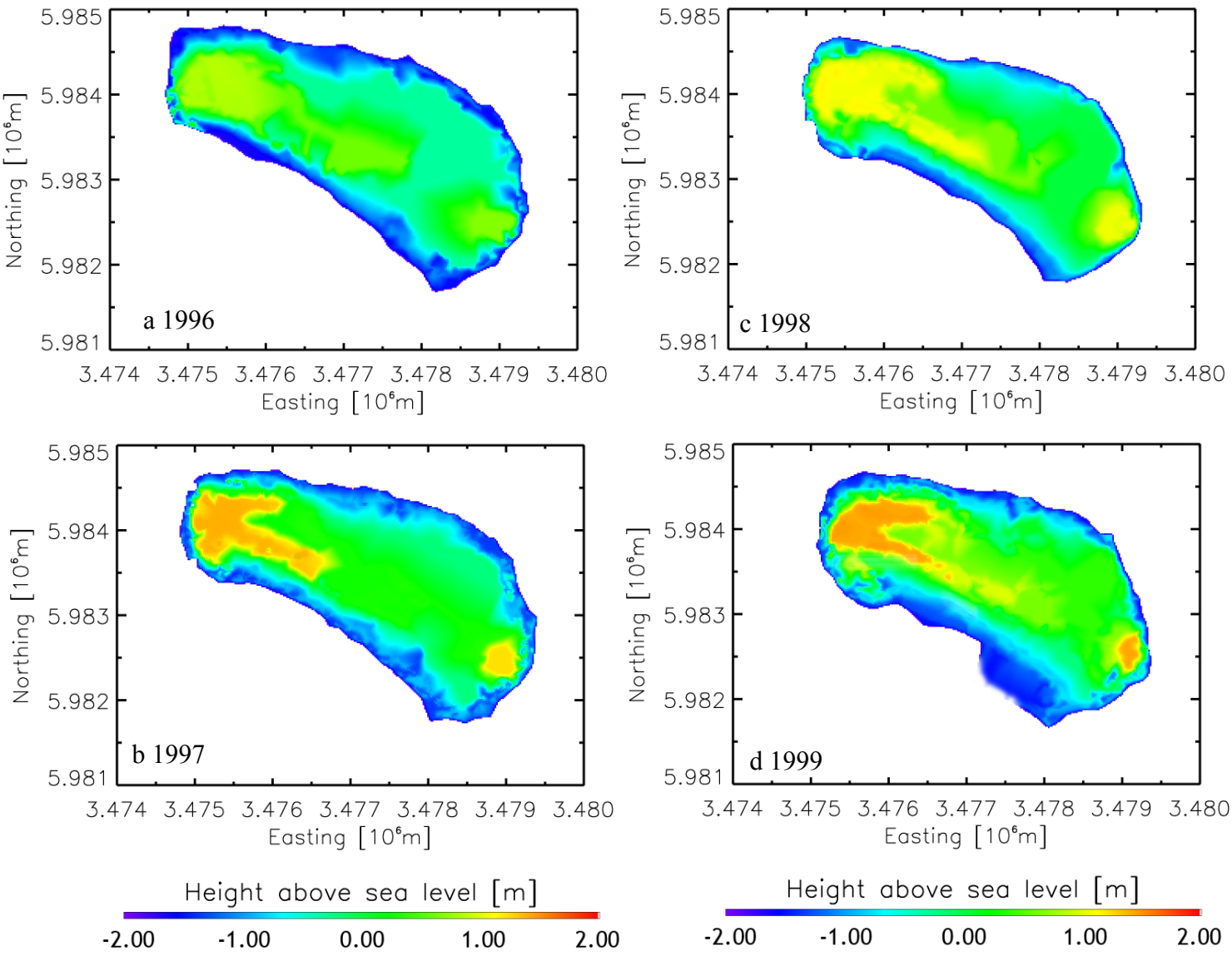

Figure 4.15: Gelbsand from 1996-1999 and 2004-2009 (a: 1996; b: 1997; c: 1998; d: 1999; e: 2004; f: 2005; g: 2006; h: 2007; i: 2008; j: 2009).

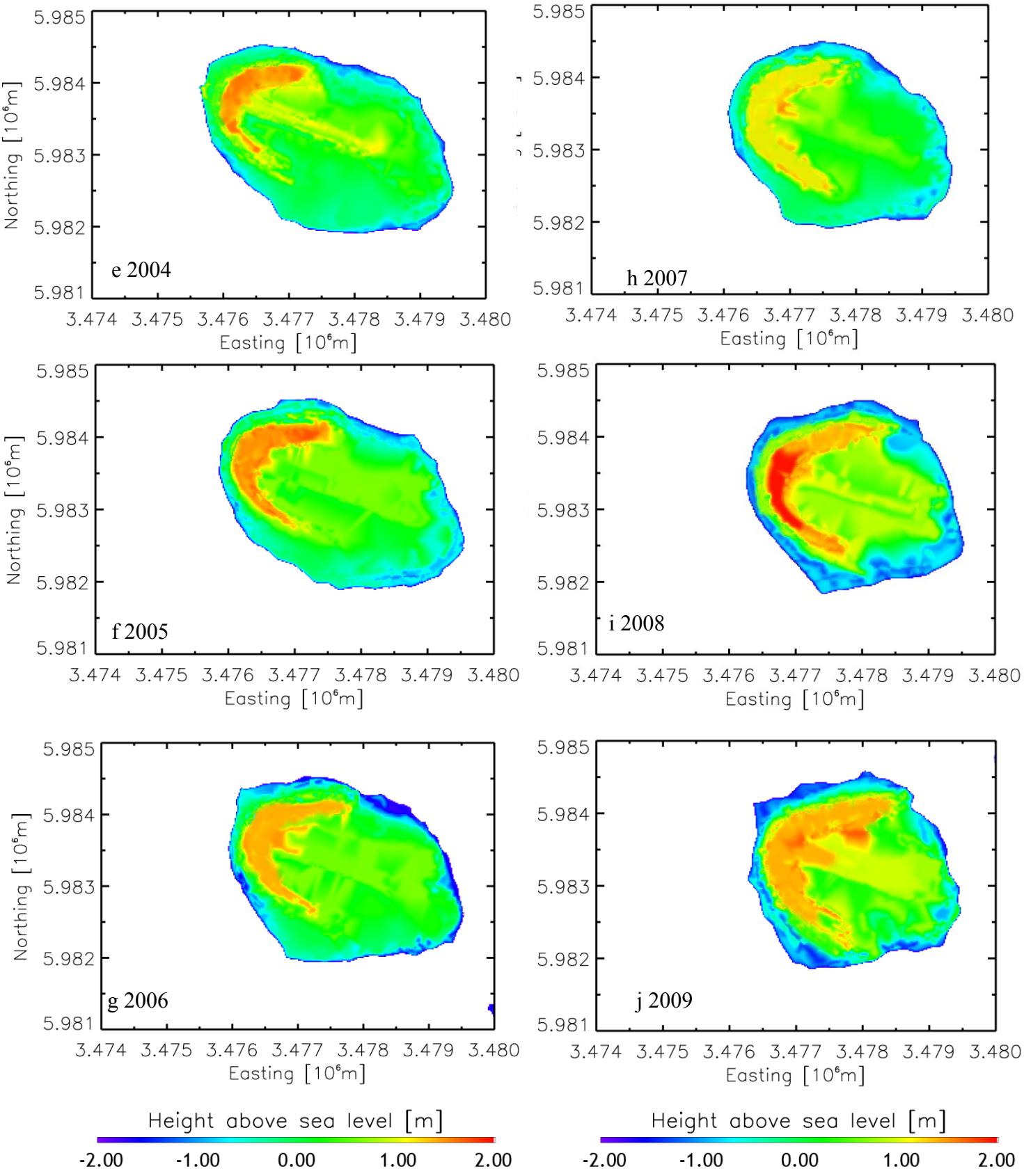

Figure 4.15: (Continued).

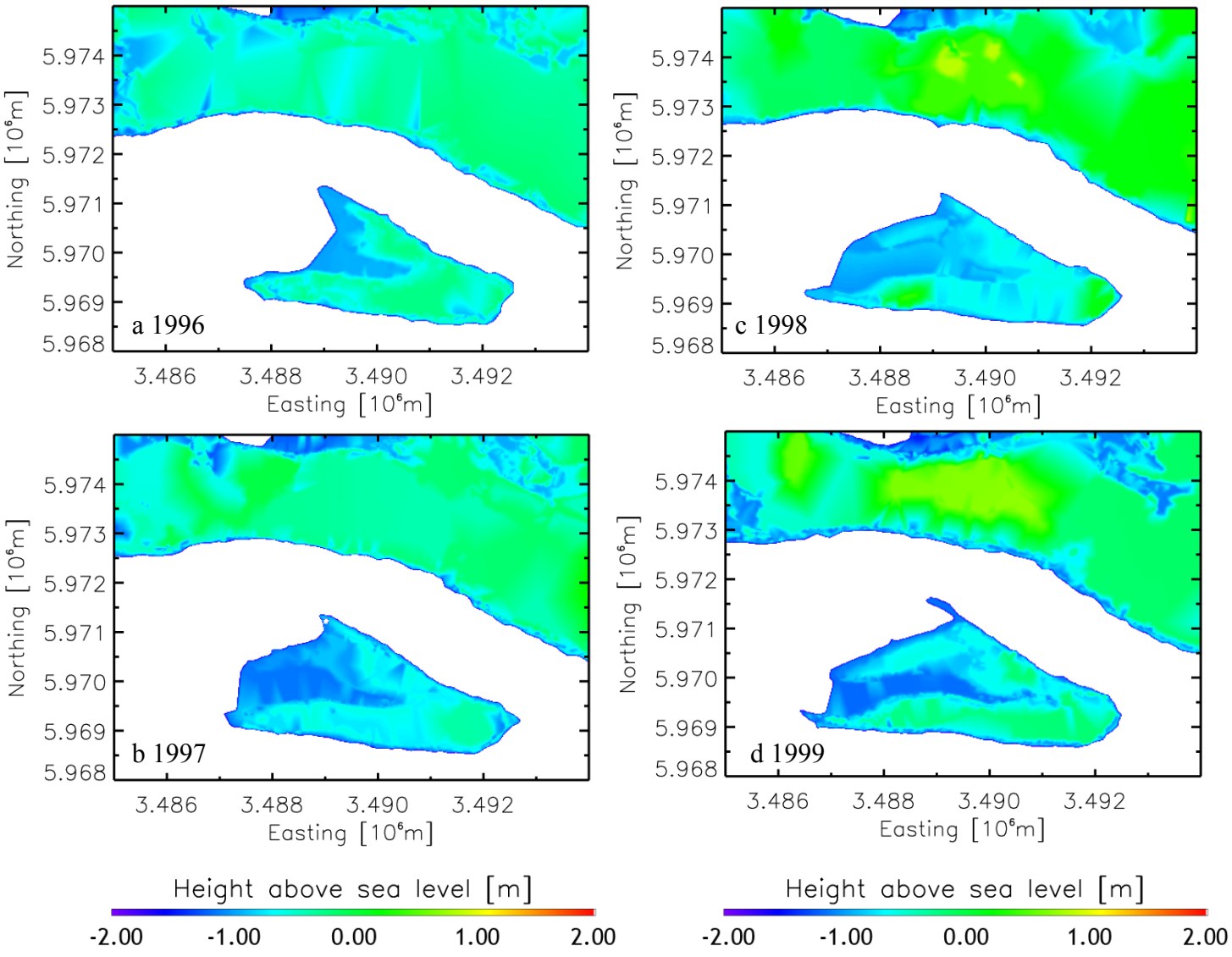

Figure 4.16: Medemsand/Medemgrung from 1996-1999 and 2004-2009 (a: 1996; b: 1997; c: 1998; d: 1999; e: 2004; f: 2005; g: 2006; h: 2007; i: 2008; j: 2009).

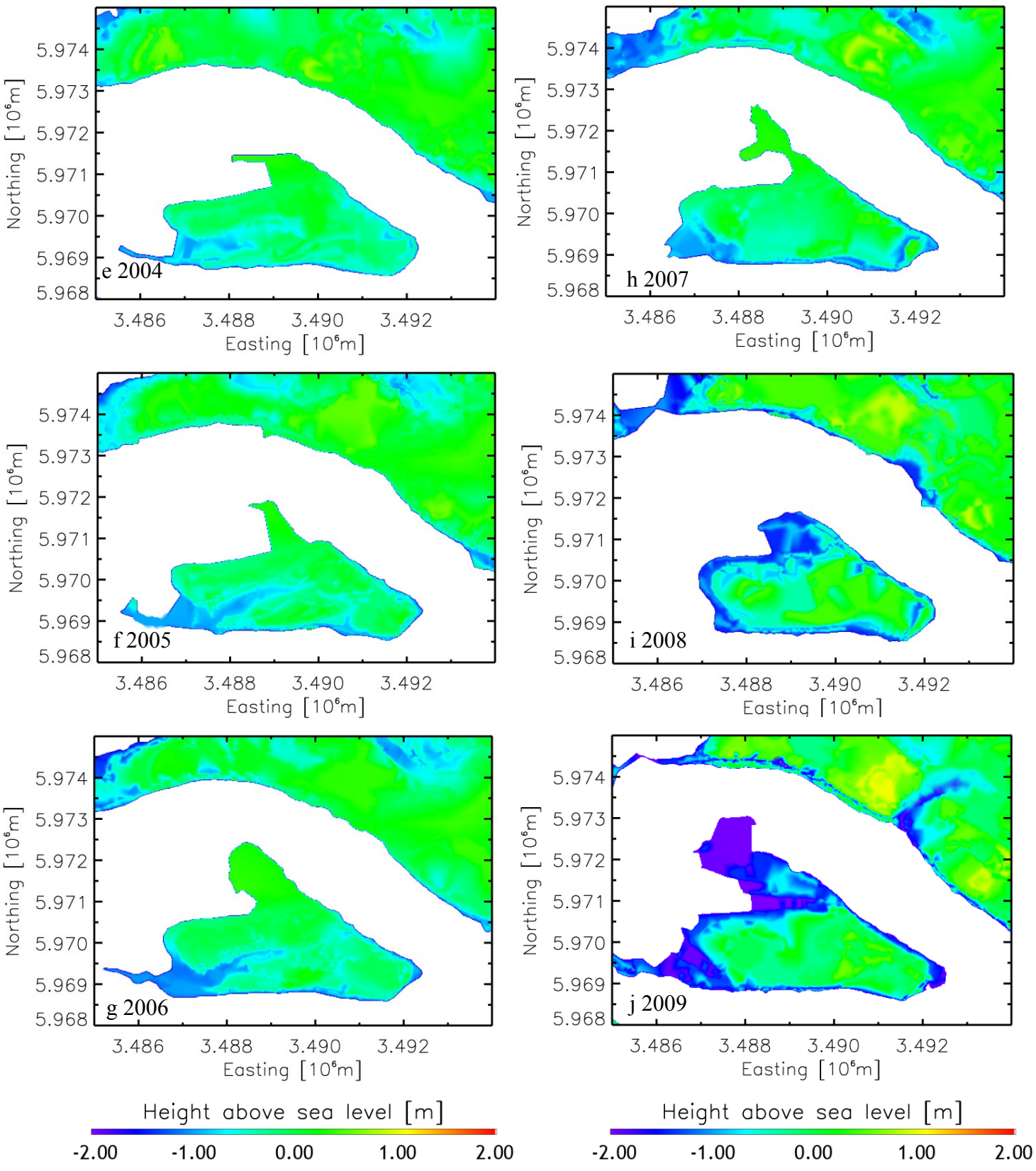

Figure 4.16: (Continued).

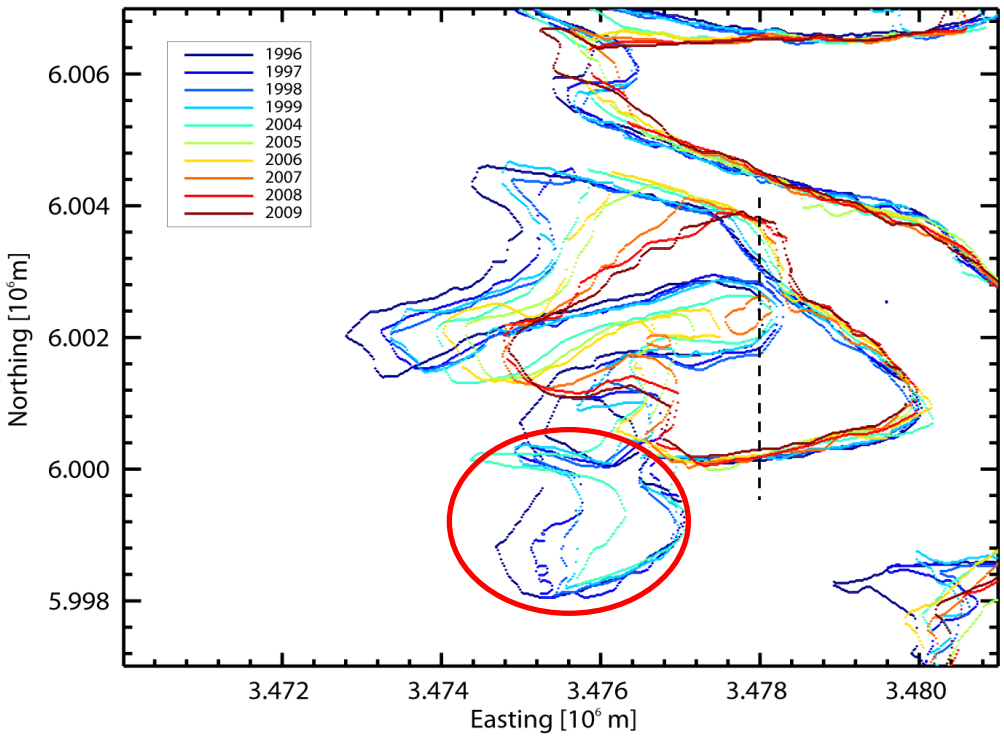

Figure 4.17: Outlines of Tertiussand (-2 m isobaths, dash line indicates the cross section).

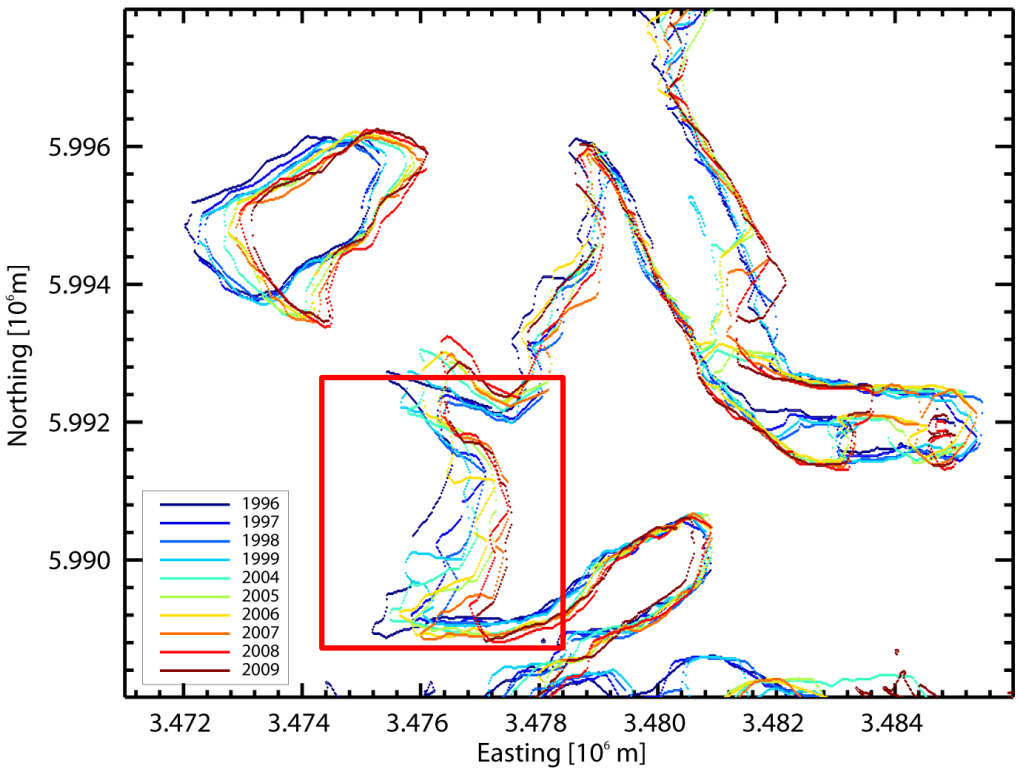

Figure 4.18: Outlines of Trischen and D-Steert (-2 m isobaths).

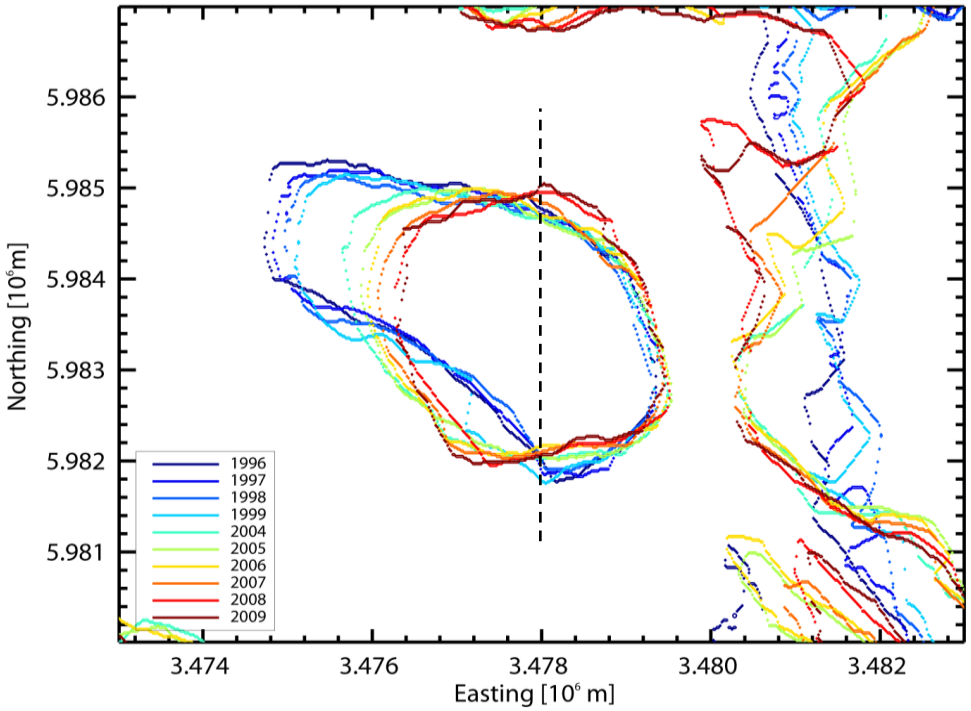

Figure 4.19: Outlines of Gelbsand (-2 m isobaths, dash line indicates the cross section).

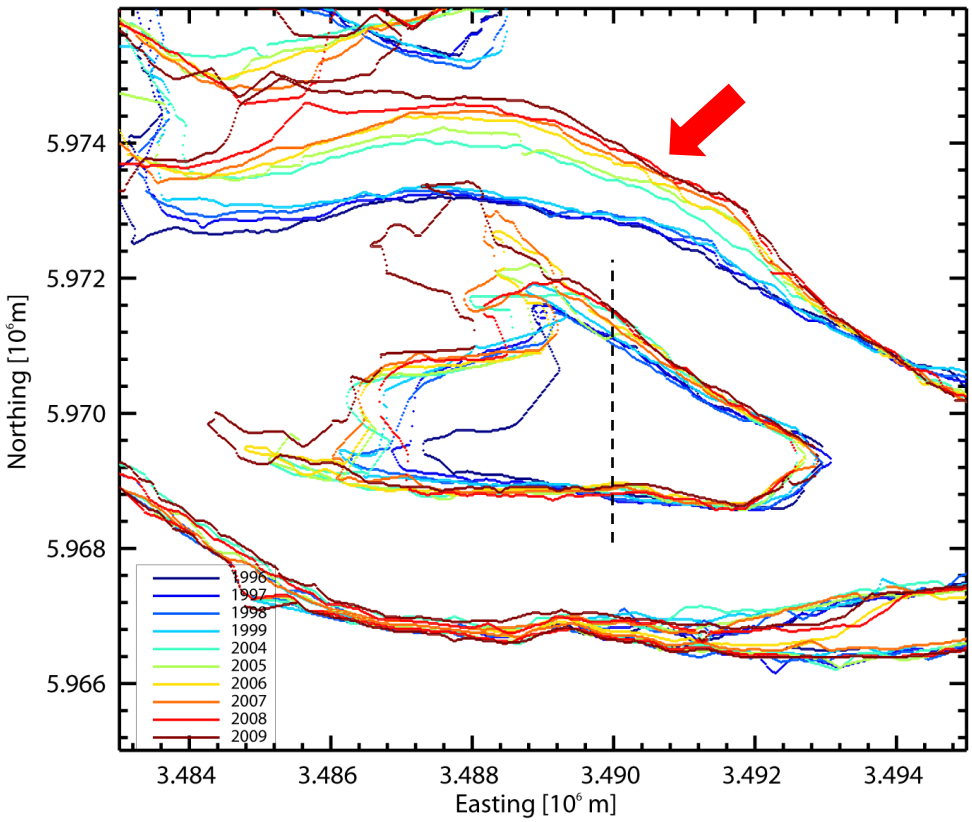

Figure 4.20: Outlines of Medemsand/Medemgrund (-2 m isobaths, dash line indicates the cross section).

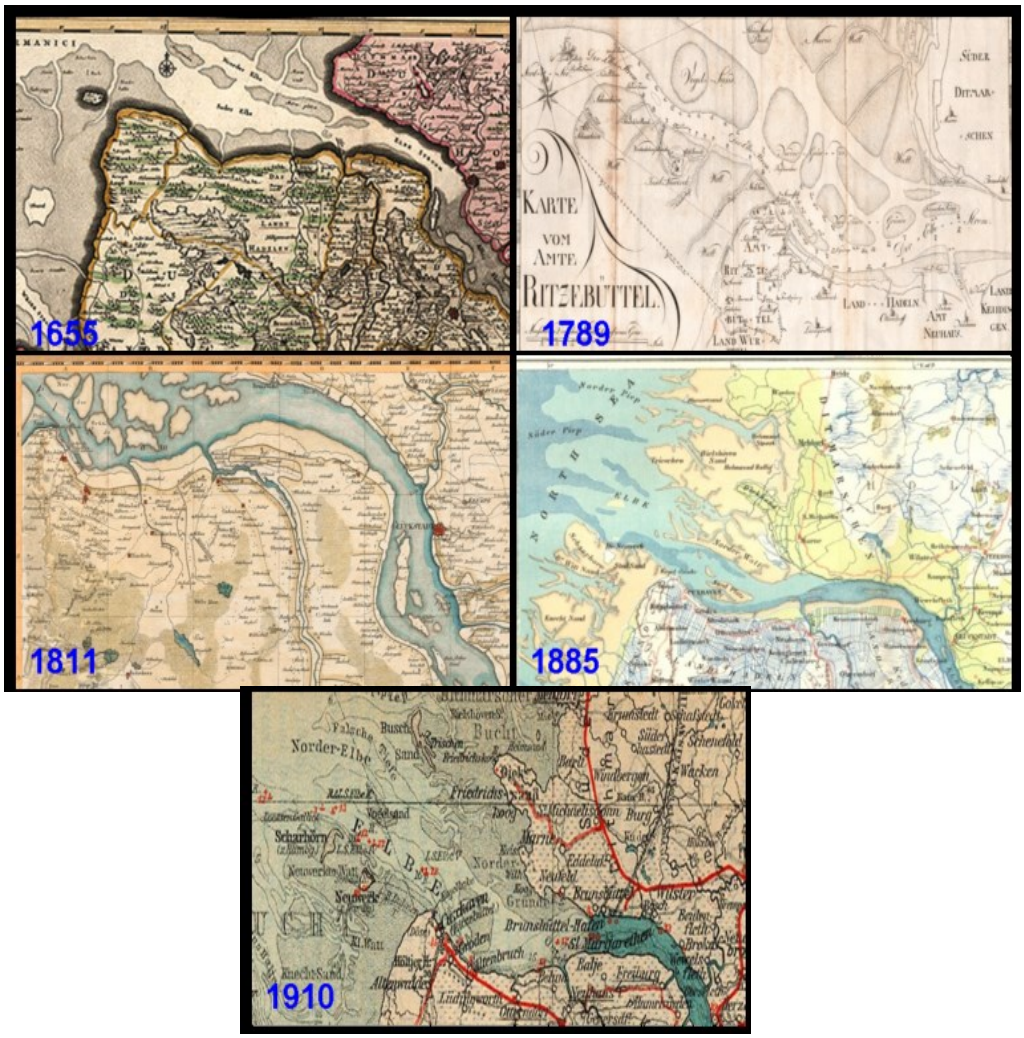

Figure 4.21: Historical maps of Medemsand and Medemgrund from 1655 to 1910, Dashed and solid lines and orange patches represent land boundaries, channel banks and sandbars, respectively (de Wit, 1665; von Hess, 1789; Streit, 1811; Vuillemin 1885; Wagner and Debes, 1910).

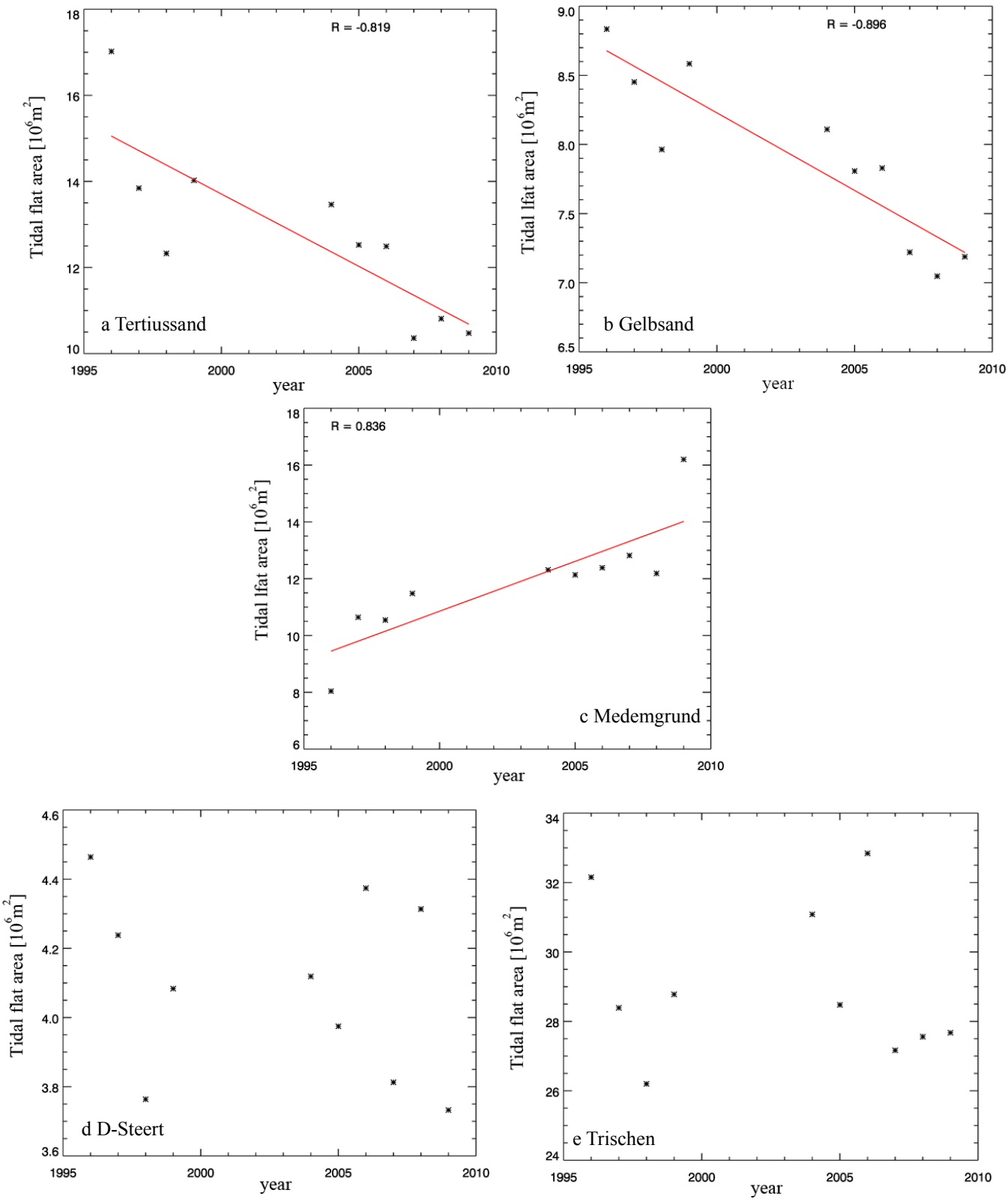

Figure 4.22: Tidal flat area from 1996 to 1999 and 2004 to 2009 (a: Tertiussand; b: Gelbsand; c: Medemgrund; d: D-Steert; e: Trischen).

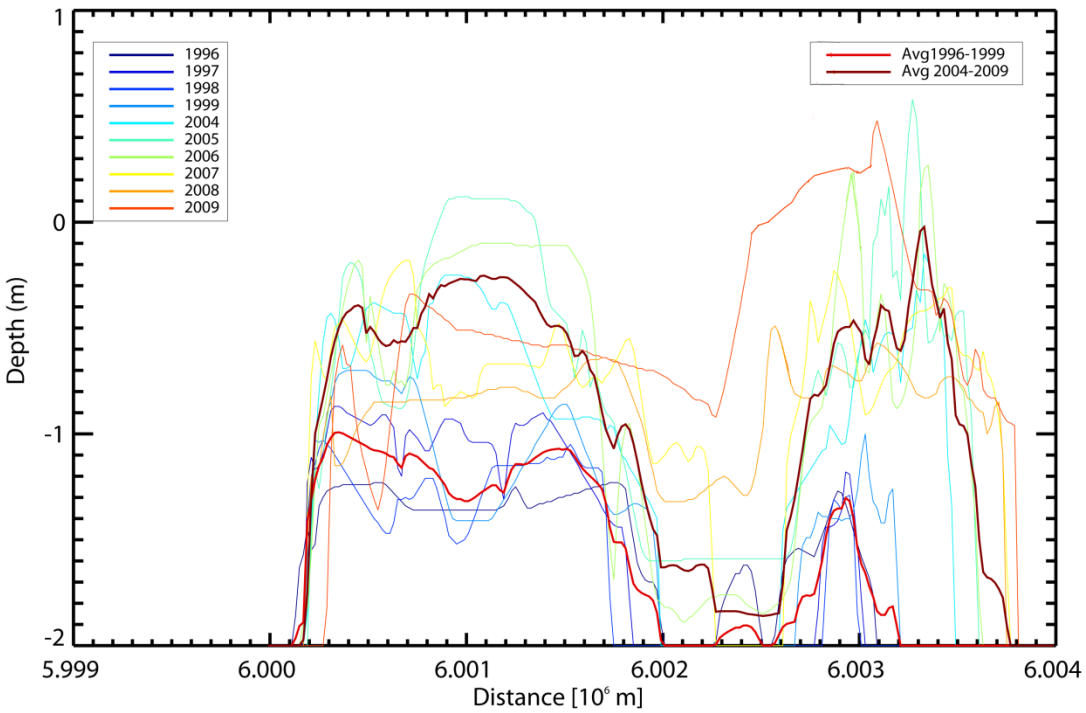

Figure 4.23: Cross section of Tertiussand.

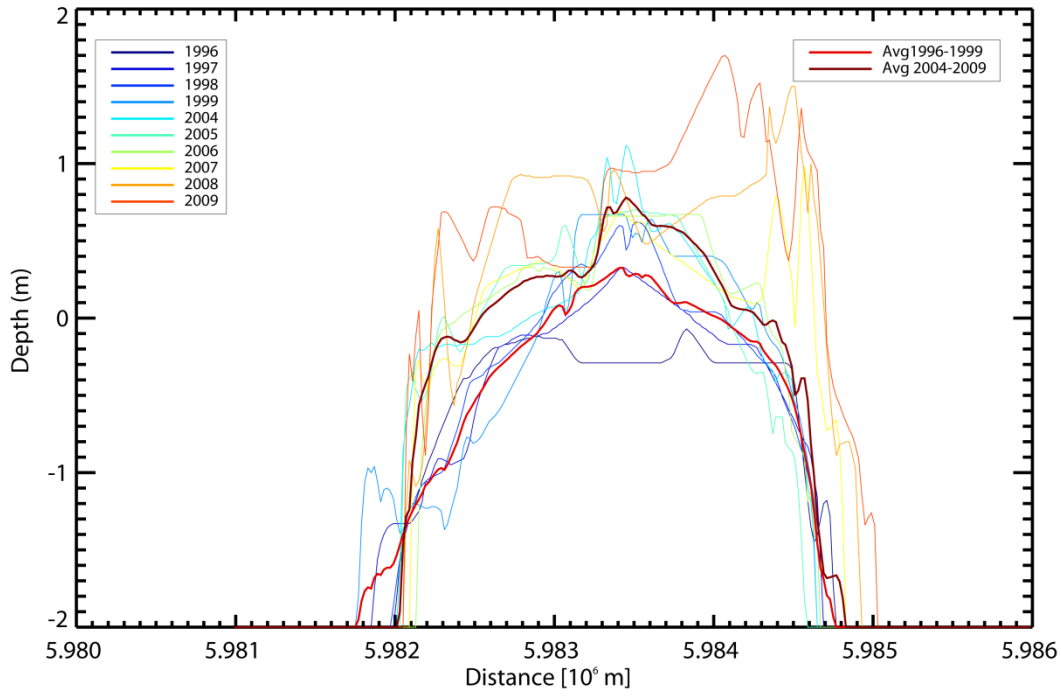

Figure 4.24: Cross section of Gelbsand.

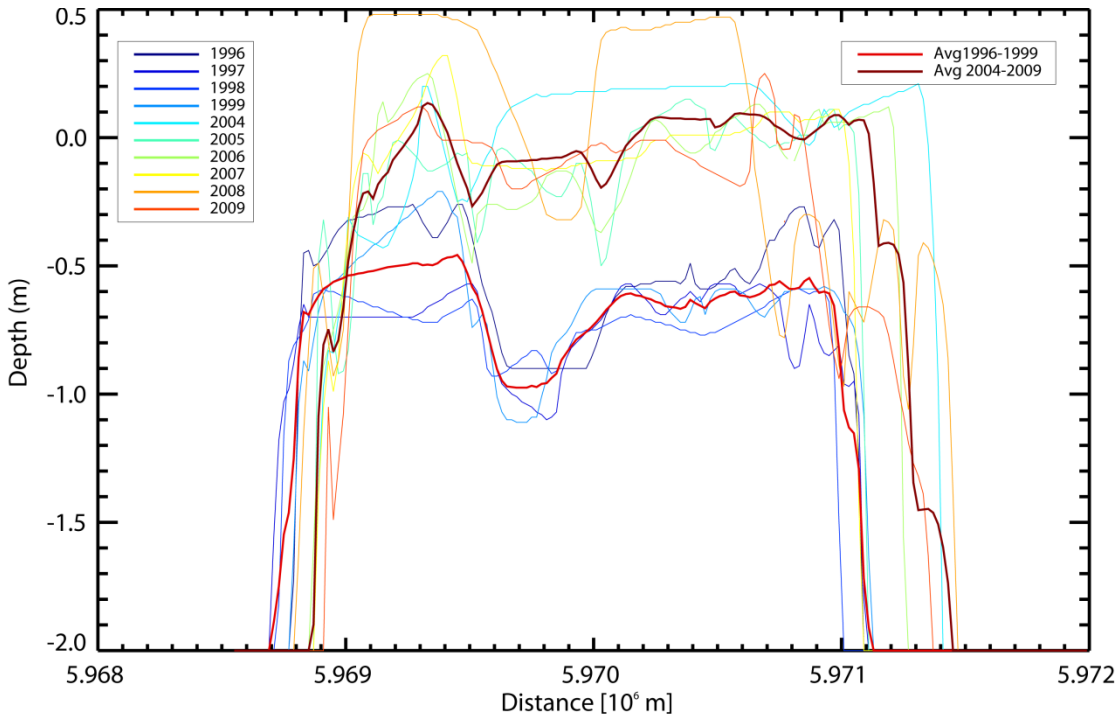

Figure 4.25: Cross section of Medemgrund.

Table 4.1: Average elevation for the sandbars.

Sandbars	Average elevation (m)		Elevation difference (m)	Averaged increasing per year (m)
	year group A (1996-1999)	year group B (2004-2009)		
Tertiussand	-1.09	-0.84	0.25	0.028
Gelbsand	-0.16	0.28	0.44	0.049
Medemgrund	-0.48	-0.35	0.13	0.014

Chapter 5 Summary and Outlook

Topographic maps from 1996 to 1999 and 2004 to 2009 were derived using the waterline method and satellite images from ERS, Enivsat ASAR, and Landsat TM 5. Geocoding and data coverage were improved, hence increasing the accuracy of the results. Morphological development was investigated within the engineering timescale (1996 to 2009) on a large spatial scale of 90 km (from the North Frisian to the Neuwerk, and Cuxhaven area). Difference maps with respect to the reference year 1996 were generated as the first step of the analysis. They show that the strongest change was between 2009 and 1996. The -2 m isobaths outline map gives an overview of the morphological development over the engineering timescale, which shows that the most frequent isobaths relocation are in the outer parts of the open tidal flats, river channels, and the sandbars.

Bed Elevation Range (BER) was calculated to analyze the intensity of morphological changes. BER visualizes the morphodynamics by accounting for elevation information from the entire period of investigation. The outer parts of the tidal flat and the nearby sandbars are impacted by extensive wave and tidal energy, which explains the high BER. Vertical nodal linear regression illustrates the rates of erosion and sedimentation. Overall, the vertical dynamic trend of the German Wadden Sea is mostly between -0.1 and 0.1 m/yr with extreme values over $\pm$0.3 m/yr, and the average is 6.02 mm/yr, which indicates that sedimentation is stronger than erosion at the large scale. However, smaller scale variations occur in features such as sandbars or

tidal channels. Turnover height and net balance height derived for the tidal flats within the study area showed good linear fit with R being above 0.9. Turnover height considers sedimentation and erosion as absolute values, while net balance height takes sign into account. The maximum turnover height was 0.22 m between 1996 and 2009, while the maximum net balance height was 0.10 m between 1996 and 2006. The increasing trend of turnover height and net balance height are 8.2 mm/yr and 6.8 mm/yr, respectively.

The sandbars (Tertiussand, D-Steert, Trischen, Gelbsand, and Medemgrund/Medemsand) in the tidal flat show the strongest morphodynamics. Tertiussand, D-Steert, Trischen, and Gelbsand migrated landward (southeast), while Medemgrund expanded to the northwest and Medemsand largely eroded to north. Varying environmental conditions caused the differences in the development of the sandbars. Tertiussand, D-Steert, Trischen, and Gelbsand are located at the outer parts of open tidal flats; therefore, they receive most of the strong wave and tide energy from the west side. Their western parts, in the breaking zone, eroded towards the east. Medemgrund and Medemsand are located in the Elbe estuary, which is dominated by tidal energy and lead to different morphological development. The area of Medemgrund showed increasing trend, while the area of Tertiussand and Gelbsand showed decreasing trends. D-Steert and Trischen had no clear trend, but showed a reduction of 0.732 km^2 and 4.4 km^2, respectively between 1996 and 2009. Three cross sections were chosen in Tertiussand, Gelbsand, and Medemgrund for elevation analysis. Average elevations of year group A (1996-1999) and year group B (2004-2009) from these three cross sections showed similar shapes and all increased. They rose between 2.1 and 7.2 times faster than the overall German Wadden Sea elevation. Sediment for the increasing elevations may have been derived from internal and external sources. Tertiussand and Gelbsand lie at the outer part of the open tidal flat and had decreasing areas; therefore, increases in elevation could relate to their internal sediment redistribution. The area of Medemgrund increased, but its adjacent tidal flat Medemsand showed significant erosion and it is located in the Elbe River. The elevation increase of Medemgrund can be compensated by the erosion at Medemsand and the sediment from Elbe River (external).

Our work gives detailed morphological development analysis with consistent data coverage, and quality on a large spatial scale and engineering timescale. In future work, the investigation area could be extended to the Weser and Ems area (east Frisian), where exist extensive investigations, important water channels and more gauge station data. Moreover the waterline method results can be compared with morphodynamic model data. The waterline method still requires adjustment by human intervention at the edge detection, the most time consuming step of the procedure, which could be developed into a nearly automatic procedure in the future.

Bibliography

Ahrendt K., ‘Ein Beitrag zur holozänen Entwicklung Nordfrieslands’, in Die Küste, H. 71, 2006.

Albers T. and von Lieberman N., ‘Morphodynamics of Wadden Sea areas – field measurements and modeling’, The International Journal of Ocean and Climate Systems, vol. 1, pp. 123-132, 2010.

Brzank A., Heipke C., Goepfert J., Soergel U., ‘Aspects of generating precise digital terrain models in Wadden Sea from lidar-water classification and structure line extraction’, ISPRS Journal of Photogrammetry & Remote Sensing vol. 63, pp. 510-528, 2008.

BSH, Bundesamt fuer Seeschifffahrt und Hydrographie. http://www.bsh.de/en

Buijsman M.C. and Ridderinkhof H., ‘Long-term evolution of sand waves in the Mardiep inlet, II: relation to hydrodynamics’, Continental Shelf Research, vol. 28, pp. 1202-1215, 2008.

Buziek G., ‘Neure Untersuchungen zur Dreiecksvermaschung’, Nachriten aus dem Karten- und Vermessungswesen, vol. 105, 1990.

Chu, K., Winter C., Hebbeln D., Schulz M., ‘Improvement of morphodynamic modelling of tidal channel migration by nudging’, Journal of Coastal Engineering vol. 77, pp. 1-13, 2013.

Cotton C.A., ‘Deductive morphology and genetic classification of coasts’, Sc. Monthly, vol. 78 (3), pp. 163-181, 1995.

Cowell P.J., and Thom B.G., ‘Morphodynamics of coastal eveolution’, in R.W.G. Carter and C.D. Wooderoffe (eds) Costal Evolution, Cambridge University Press, Cambridge, pp. 33-86, 1994.

Curlander J. C. and McDonough R. N., Synthetic Aperture Radar: Systems and Signal Processing, Jon Wiley & Sons, Inc., Canada, pp. 1 -31, 1991.

Cutrona L. J., Vivian E. N., Leith E. N. and Hall G. O., ‘A high resolution radar combat surveillance system’, IRE Trans. Military Elec., MIL-5, pp. 127-131, 1961.

Dannenberg J., ‘Ableitung der Topographie des Wattenmeeres aus ERS- SAR Daten’, Ph.D. dissertation, Univ. Bremen, Bremen, Germany, 2004.

Davies J.L., Geographical variation in coastal development, Oliver & Boyd, Edinburgh, 1972.

Davies J.L., Geographical variation in coastal development (2nd edn), Longman, New York, 1980.

Davis L.S., ‘A survey of edge detection techniques’, Computer Graphics and Im. Process., No. 4, pp. 248-270, 1975.

Davis R.A. and Hayes M.O., ‘What is a wave-dominated coast?’, Marine Geology, vol. 60, pp. 313-329, 1984.

De Wit F., ‘Ducatus Bremae & Ferdae’, Publisher Witte Pascaert, Amsterdam, 1665.

Deronde B., Houthuys R., Debruyn W., Fransaer D., Lancker V. V., Henriet J. P., ‘Use of airborne hyperspectral data and laser scan data to study beach morphodynamics along the Belgian Coast’, Journal of Coastal Research vol. 22, pp. 1108–1117, 2006.

Dick S., ‚Operationelles Modellsystem für Nord- und Ostsee', FORUM, Proc. Der Fachtagung 'EDV im Seeverkehr und maritimen Umweltschutz'. GAUSS, Bremen, pp. 22–25, 1997.

Dick S., Kleine E., Müller-Navarra S.H., Klein H., Komo H., 'The operational circula- tion model of BSH (BSHcmod) model description and validation', Berichte des BSH, 2001.

Dorst L.L., Roos P.C., Hulscher S.J.M.H., 'Spatial differences in sand wave dynamics between the Amsterdam and the Rotterdam region in the Southern North Sea', Continental Shelf Research, vol. 31, pp. 1096-1105, 2011.

Dorst L.L., Roos P.C., Hulscher S.J.M.H., Lindenbergh R.C., 'The estimation of sea floor dynamics from bathymetric surveys of a sand wave area', Journal of Applied Geodesy, vol. 3, pp. 97-120, 2009.

Esbjerg Declaration, Ministerial Declaration of the Sixth Trilateral Governmental Conference on the Protection of the Wadden Sea, Esbjerg, November 1991.

Ehlers J., The morphodynamics of the Wadden Sea, pp. 33-40, 211-220, A.A. Balkema Publishers, Rotterdam, the Neterlands, 1988.

Flemming B.W. and Bartholomä A. 'Holocene evolution, morphodynamics and sedimentology of the Spiekerkoog barrier island system (southern North Sea)', Senckenbergiana maritima, vol. 24, pp. 117-155, 1994.

Flood M., Gutelius B., 'Commercial implications of topographic terrain mapping using scanning airborne laser radar', Photogrammetric Engineering and Remote Sensing, vol. 63, pp. 327–366, 1997.

Frost V.S., Shanmugan K.S., and Holtzman J.C., 'Edge detection for synthetic aperture radar and other noisy images', in Proc. IGARSS, sec. FA2, pp. 4.1-4.9, 1982.

Goehren H., Triftstroemungen im Wattenmeer. Mitteilungen des Franzius-Instituts fuer Grund- und Wasserbau der Technischen Universitaet Hannover 30: 142-270, 1968.

Heygster G., Dannenberg J., Notholt J., 'Topographic Mapping of the German Tidal Flats Analyzing SAR Images With the Waterline Method', IEEE Geoscience and Remote Sensing, vol. 48, No. 3, pp. 1019 – 1030, 2010.

Inman D.L. and Brush B.M., 'The coastal challenge', Science, vol. 181, pp. 20-32, 1973.

Inman D.L. and Nordstrom C.E., 'On the tectonic and morphologic classification of coasts', the Journal of Geology, vol. 79, pp. 1-21, 1971.

Kleine E., Das operationelle Modell des BSH für Nordsee und Ostsee, Hamburg, Germany: Bundesamt für Seeschifffahrt und Hydrographie, 1994

Kleine E., 'A class of hybrid vertical co-ordinates for ocean circulation modelling', Proceedings of the 6th HIROMB Scientific Workshop. ISBN: 5-86813-0, Morzaschita, St. Petersburg, pp. 7–15, 2003.

Klein H. and Frohse A. 'Oceanographic processes in the German Bight', in Die Küste, Bozen Medien GmbH & Co. KG, Heidei. Holstein, pp. 60-63, 2008.

Klocke B., 'Topographische Karte des Wattenmeeres aus ERS-1 SAR- und Modelldaten', PhD dissertation: Bd. 7 von Berichte aus dem Institut für Umweltphsik, Berlin, 2001.

Knaapen M.A.F., 'Sandwave migration predictor based on shape information', Journal of Geophysical Research, vol. 110, pp. 9, 2005.

Kohlus J., 'Elemente des Wattenmeeres', In: Umweltatlas Wattenmeer, Ulmer, 1998.

Kruse I., Topographisches Auswerte-System Hannover: Inst. für Kartographie Geoinf.

der Univ. Hannover, [Online]. Available: http://www.ikg.uni-hannover.de/forschung tash/, 2003.

Kösters F. and Winter C., 'Exploring German Bight coastal morphodynamics based on modeled bed shear stress', Geo-Marine Letters, vol. 34, pp. 21-36, 2014.

Landsat Project Factsheet, Landsat—A Global Land-Imaging Mission, https://landsat.usgs.gov/about_project_descriptions.php, 2012.

Lee J. -S., 'Digital image enhancemant and noise filtering by Use of Local Statistics', IEEE Transactions on Pattern Analysis and Maching Intelligence, vol. pami-(No. 2), pp. 1978–1981, 1980.

Lee J.-S., 'Speckle analysis and smoothing of synthetic aperture radar images', Computer Graphics and Image Processing, vol. 17, pp. 24–32, 1981.

Lee, J.-S., 'A simple speckle smoothing algorithm for synthetic aperture radar images', IEEE Transactions on Systems, Man, and Cybernetics, vol. smc-1(No. 1), pp. 85–89, 1983.

Lee, J. -S., 'Coastline detection and tracing in SAR images', IEEE Transaction on Geoscience and Remote Sensing, vol. 4, pp. 662-668, 1990.

Lesser G.R., Roelvink J.A., Van Kester J.A.T.M., Stelling G.S., 'Development and validation of a three-dimensional model', Coast. Eng., vol. 51, pp. 883-915, 2004.

Liu Y., Li M., Cheng L., Li F., and Chen K., 'Topographic Mapping of Offshore Sandbank Tidal Flats Using the Waterline Detection Method: A Case Study on the Dongsha Sandbank of Jiangsu Radial Tidal Sand Ridges, China', Marine Geodesy, vol. 35(4), pp. 362–378, 2012.

Liu Y., Li M., Mao L., Cheng L., and Li F., 'Toward a Method of Constructing Tidal Flat Digital Elevation Models with MODIS and Medium-Resolution Satellite Images', Journal of Coastal Research, vol. 287, pp. 438–448, 2013.

Mallat S., A Wavelet Tour of Signal Processing. London: Academic Press, 1997.

Marencic H. (Ed.), 'The Wadden Sea protection and management', in Wadden Sea Ecosystem, No. 25, pp. 3-24, 2009

Masselink G., Huges M., Knight J., Coastal processes & geomorphology, Hodder Education, An Hachette UK Company, London. pp. 1, 2011.

Mason D. C., Davenport I. J. and Robinson G. J., 'Construction of an intertidal digital elevation model by the 'waterline' method', Geophysical Research Letters, vol. 22, No. 23, pp. 3178-3190, Dec 1995.

Mason D.C. and Davenport I.J., 'Accurate and efficient determination of the shoreline in ERS-1 SAR images', IEEE Transactions on Geoscience and Remote Sensing, vol. 34, No. 5, pp. 1243-1253, 1996.

Mason D. C., Davenport I.J. and R. A. Flather R.A., 'Interpolation of an intertidal digital elevation model from heighted shorelines: a case study in the Western Wash', Estuaries, Coastal and Shelf Science, vol. 45, pp. 559-612, 1997.

Mason D. C., Amin M., Davenport I. J., Flather R. A., Robinson and J. A. Smith, 'Measurement of Recent Intertidal Sediment Transport in Morecambe Bay using the Waterline Method', Estuaries, Coastal and Shelf Science, vol. 49, pp. 427-456, 1999.

Mason D. C., Scott T. R., Dance S. L., 'Remote sensing of intertidal morphological change in Morecambe Bay, U.K., between 1991 and 2007', Estuaries, Coastal and Shelf Science, vol. 87, pp. 487-496, 2010.

McCandless S.W., and Jackson C.R., 'Principles of Synthetic Aperture Radar', in SAR Marine User's Manual, U.S. department of commerce, Washington DC., pp. 1-24, 2004.

Niedermeier A., Romaneeßen E and Lehner S., 'Detection of Coastlines in SAR

Images using Wavelet Methods', IEEE Transactions on Geoscience and Remote Sensing, vol. 38, No. 5, pp. 2270-2281, Sep 2000.

Niedermeier A., Romaneeßen E and Lehner S., 'Topography and morphodynamics in the German Bight using SAR and optical remote sensing data', Ocean Dynamics, vol. 55, pp. 100-109, 2005.

Official Topographic Maps of Schleswig-Holstein/Hamburg, National Survey Agency and EADS Germany GmbH, 2009.

Petersen M. and Rohde H., 'Sturmflut – Die großen Fluten an den Küsten Schleswig-Holstein und in der Elbe', Karl Wachholtz Verlag, Neumünster, 1977.

Rhodes W.F., 'Classification of coasts', Journal of Coastal research, vol. 20, pp. 155-165, 2004.

Ricklefs K. and Neto N.E.A., 'Geology and morphodynamics of a tidal flat area along the German North Sea coast', Die Küste, 69 Promorph, pp. 93-127, 2005.

Roberts L.G., 'Machine Perception Of Three-Dimensional Solids', PhD dissertation: Massachusetts Instiued of Technology, June, 1963.

Stockdon H.F., Sallenger Jr A.H., List J.H., Holman R.A., 'Estimation of shoreline position and change using airborne topographic lidar data', Journal of Coastal Research, vol. 18, pp. 502–513, 2002.

Streit F.W., 'Unterelbe, Sect 16 und Sect 17', Weimar, Germany: Geographisches Institut Weimar, 1811.

Tanner W.F., 'Bases for coastal classificaiton', Southeastern Geol., vol. 2, pp. 13-22, 1960.

Touzi R., Lopes A., and Bousqut P., 'A statistical and geometrical edge detector for SAR images', IEEE Transactions on Geoscience and Remote Sensing, vol. 26, No.

6, pp. 764-773, 1988.

Trenhaile A.S., ‘Introduction’, in Coastal Dynamics and Landforms, Oxford University Press, New York, 1997.

Ulaby F.T., Moore R.K., and Fung A.K., Microwave Remote Sensing, vol. 3, Dedham, MA: Artech Haouse, 1986.

Ulrich J., ‘Der Gelbsand Entwicklung einer Sandbank in der Elbmündung von 1905 bis 1990’, Die Schriften des Naturwissenschaftlichen Vereins für Schleswig-Holstein, vol 61, pp. 19-24, Dec, 1991.

UNESO world heritage list, http://whc.unesco.org/en/list/1314

Valerius J., Feldmann J., van Zoest M., Milbradt P., and Zeiler M., ‘Documentation of morphological products from the AufMod project functional seabed model, data fromt: Text files (CSV, XYZ)’, Federal Maritime and Hydrographic Agency (BSH) and smile consult GmbH, available online: ftp://ftp.bsh.de/outgoing/AufMod-Data/ CSV_XYZ_files/, 2013.

Van Dijk T. A.G.P., Kleuskens M.H.P., Dorst L.L., van der Tak C., Doornenbal P.J., van der Spek A.J.F., Hoogendoorn R.M., Rodriguez Aguilera D., Menninga P.J., Noorlandt R.P., ‘Quantified and applied sea-bed dynamics of the Netherlands continental shelf and the Wadden Sea’, Jubilee Conference Proceedings, pp. 223-227, 2012.

Von Hess J.L., ‘Hamburg Topographisch, Politisch und Historisch Beschrieben’, the second part, Luebeck, 1789.

Vuillemin A., ‘The universal geography, the Earth and its inhabitants’, London, U.K.: Virtue & Co Ltd, 1885.

Wadden Sea World Heritage Site, http://www.waddensea-worldheritage.org/ taxonomy/ term/17

Wagner and Debes, ‘Mouth of Elbe’, in Geographic Establishment, Leipzig, Germany, 1910.

Wang Y. and Koopmans B. N., ‘The topographic mapping of the tidal flats using remote sensing and GIS techniques – a case study in the Wadden Sea area, north Netherlands’, International Symposium of operationalization of Remote Sensing, J.L.v.Genderen et. Al. Enschede, The Netherlands, vol. 7, pp. 193-203, 1993.

Wang Y. and Koopmans B. N., ‘Monitoring tidal flat changes using ERS-1 SAR images and GIS in the Western Wadden Sea area, the Netherlands’, EARSeL Advances in Remote Sensing, vol. 4, No. 1 - IX, 1995.

Wang Y., Koopmans B.N. and Pohl C., ‘The 1995 flood in the Netherlands monitored from space – a multi-sensor approach’, Int. J. Remote Sensing, vol. 16, No. 15, pp. 2735-2739, 1995.

Wiley C. A., ‘Pulsed Doppler radar methods and apparatus’, United States Patent, No. 3,196,436, Filed August, 1954.

Wimmer C., Siegmund R., Schwabisch M., Moreira J., ‘Generation of high precision DEMs of the Wadden Sea with airborne interferometric SAR’, IEEE Transactions on GeoScience and Remote Sensing, vol. 38, pp. 2234–2245, 2000

Winter C., ‘Meso-scale morphodynamics of the Eider estuary: analysis and numerical modelling’, Journal of Coastal Research, SI 39, pp. 498-503, 2004.

Winter C., ‘Macro scale morphodynamic of the German North Sea coast’, Journal of Coastal Research, SI. 64, pp. 706-710, 2011.

Wright L.D. and Thom B.G., ‘Coastal depositional landforms: a morphodynamic approach’, Progress in Physical Geography, vol. 1, pp. 412-459, 1977.

WSA Cuxhaven, 2002: Wasser und Schifffahrtsamt Cuxhaven, UVU und Beiweissicherungsdatenbank. http://www.wsa-cuxhaven.de/

Zee D.v.d., ‘Water line, 1980’, internal report, ITC, Enschede, the Netherlands, pp. 38, 1980.

Zeiler M., Schwarzer K. and Ricklefs K., ‘Seabed morphology and sediment dynamics’, in Die Küste, pp. 31-35, 2008.

Abbreviation

AufMod: Aufbau integrierter Modellsysteme zur Analyse der langfristigen Morphodynamik in der Deutschen Bucht; Development of integrated model systems for the analysis of long-term morphodynamics in the German Bight.

BER: Bed Elevation Range.

BSH: Bundesamt fuer Seeschifffahrt und Hydrographie; German Federal Maritime and Hydrographic Agency.

CFAR: Constant False Alarm Rate.

DEMs: Digital Elevation Models.

DWD: Deutscher Wetterdienst; German Weather Service.

Landsat 5 TM: Landsat 5 Thematic Mapper.

MMSE: Maximum Mean Square Error.

MSL: Mean Sea Level.

m/yr: meter/year.

NASA: National Aeronautics and Space Administration.

near-IR: near Inferred.

RMSD : Root Mean Square Different.

SAR: Synthetic Aperture Radar.

VMR: Variance to Mean Value.

WSV: der Wasser und Schifffahrtsverwaltung des Bundes; the Waterways and Shipping Administration in Germany.

WTMM: Wavelet Transform Modulus Maxima.

Acknowledgements

In the end, I would like to express my sincere gratitude to all the people who have ever worked with me, helped me, and supported me:

My supervisor Dr. Georg Heygster for supporting my work and many discussions; Prof. Justus Notholt for giving me the opportunity to do my PhD at the Institute of Environmental Physics; Dr. Christian Winter for the new ideas he brought, the interest and time to review my thesis.

The colleagues of my working group: Gopika Suresh, Dr. Alexandra Cherkasheva, Yufang Wang, Marcus Huntemann, Junshen Lu, Dr. Christian Melsheimer, Dr. Maria Hoerhold, Dr. Larysa Istomina, and Rauls. It was an enjoyable time to work with you all.

Polmar PhD School gave the opportunities of all the nice seminars, soft skill courses and the communication between PhD students. Founding of CSC (Chinese Scholarship Council) supported for my PhD project.

Personally thank to my family and my friends for bringing love and support to me. New journey will get started.